EFFECT OF BLOOD TRANSIENTS ON CARDIOVASCULAR SYSTEM

Submitted in fulfilment of the requirements of

the degree of

DOCTOR OF PHILOSOPHY

by

BLESSY THOMAS

Supervisor: Dr Sumam K S

Department of Civil Engineering

GOVERNEMENT ENGINEEERING COLLEGE THRISSUR

UNIVERSITY OF CALICUT

(February 2022)

UNIVERSITY OF CALICUT

BONAFIDE CERTIFICATE

Certified that this thesis titled **"EFFECT OF BLOOD TRANSIENTS ON CARDIOVASCULAR SYSTEM",** is the bonafide work of Mrs. BLESSY THOMAS. who carried out the research under my supervision. Certified further that to the best of my knowledge the work reported herein does not form part of any other thesis or dissertation on the basis of which a degree or award was conferred on an earlier occasion of this or any other candidate.

Dr SUMAM K S
(Supervisor)
Professor (Retd)
Department of Civil Engineering
Government Engineering College, Thrissur

Place: Thrissur
Date: 23.02.2022

Certified that the corrections/suggestions, recommended by the adjudicators as per Ref. No. 51167/RESEARCH-E-ASST-3/2022/Admn, dated 06.09.2022 from the Director of Research, University of Calicut, have been incorporated in the thesis and that the contents in the thesis and the soft copy are one and the same.

Dr SUMAM K S
(Supervisor)
Professor (Retd)
Department of Civil Engineering
Government Engineering College, Thrissur

Place: Thrissur
Date: 15.11.2022

DECLARATION

I hereby declare that this submission is my own work and that, to the best of my knowledge and belief, it contains no material previously published or written by another person nor material which has been accepted for the award of any other degree or diploma of the university or other institute of higher learning, except where due acknowledgement has been made in the text.

Place: Thrissur

Date:

Signature:

Name: BLESSY THOMAS

Registration No. 2777/2015/Admn Dated 20.03.2015

ACKNOWLEDGEMENT

First of all, I thank God Almighty for giving me the strength throughout the period of my research work and completion of this task.

I wish to express my sincere gratitude to my research supervisors Dr Sumam K.S., for motivating, guiding and supporting me during the course of my research work. Madam has taken a lot of pain for me, and have become a beacon of guidance during the course of my work. I also extend my sincere gratitude to Dr N. Sajikumar, Professor (Retd), Department of Civil Engineering, GEC Thrissur for the technical support given to me during my research.

I would like to express my gratitude to my doctoral committee members Dr B.S.Murty (Professor, IIT Madras), Dr C. V. Lal (Professor, Department of Civil Engineering, GEC Thrissur), Dr N. Sajikumar (Retd Professor, Department of Civil Engineering, GEC Thrissur), Dr Manju .M.S. (Associate Professor, Department of Chemical Engineering, GEC Thrissur), Dr P.T. Nowshaja (Associate Professor, Department of Civil Engineering, GEC Thrissur) for their valuable suggestions during my research work. I am also grateful to the Head of Civil Engineering Department Anilkumar P.S. and former heads of department Dr P. Vijayan, Prof. K.S. Dinesh Kumar, Dr N. Sajikumar, Dr P. Vinod and Dr C. V. Lal for their support during my research.

I am grateful to Dr Ranjini Bhattathiripad T Principal, Government Engineering College Thrissur, for providing all the facilities of this college for the conduct of this research work. At this moment I also acknowledge former principals Dr V. S. Sheeba, Dr B. Jayanand and Dr K. P. Indiradevi, for providing all the facilities of this college for the conduct of this research work during those periods.

I am grateful to Dr Abdul Samad P.A. and Dr Miji Cherian R. for their help and constant mental support given during this research period. I also thank Dr Jabir E. and Mr. Roopesh Kaimal. I also thank my fellow research scholars of Civil Engineering Department for their timely help extended always.

Above all I would like to thank my spouse Mr. Jose Varghese, my daughter Isabella Jose and my parents for their compassionate consolations, timely mental support and encouragement given, to make this research a reality.

BLESSY THOMAS

CONTENTS

LIST OF FIGURES

LIST OF TABLES

NOTATIONS

A	Area of cross section, m^2
a	Amplitude of pulsation, m
a_p	Diagonal matrix
Co	Courant number
D	Diameter of the tube, m
D_ω	Cross diffusion
e_a	Approximate relative error
e_{ext}	Extrapolated relative error
f_e	Face value
f_x, f_y, f_z	Body force per unit mass in X, Y, Z directions
G_k	Generation term of turbulent kinetic energy
G_ω	Generation term of specific rate of dissipation
H	Residual matrix after extraction of diagonal matrix
h	Grid size
L	Length of the stenosis, m
$J_0()$	Bessel function of order zero
k	Turbulent kinetic energy
N	Total Number of cells in the domain
n	Power index, Unit vector

P_d	Pressure after stenosis, Pa
P_a	Pressure before stenosis, Pa
p	Pressure, Pa
$\bar{p}$	mean pressure, Pa
p̈	Apparent order
Q	Flow rate, m^3/s
$\bar{Q}$	mean volumetric flow rate, m^3/s
R	Radius of artery, m
Re	Reynolds number
R̈	Convergence ratio
r	radial distance from the central axis, m
r̈	Grid refinement factor
S̈	Error
S_0	Stenosis severity fraction
t	Time, s
u, v, w	Fluid velocity components in x, y and z directions
U	Velocity, m/s
u_m	Mean velocity, m/s
u_c	cycle-averaged centreline velocity, m/s

x_o	Location of the centre of the stenosis
Y_k	Diffusion term of turbulent kinetic energy
Y_ω	Diffusion term of specific rate of dissipation
V	Cell volume
Z	axial distance
x, *y*, *z*	Cartesian co-ordinates, m
α	Womersley number
$\alpha_j^Q, \beta_j^Q, \alpha_j^p, \beta_j^P$	Fourier constants
ω	Specific rate of dissipation
ε	Rate of dissipation
ώ	Angular frequency, rad/s
Γ_k	effective diffusivity of k
Γ_ω	effective diffusivity of ω
Δx	mesh size
Δt	time step, s
$\dot{\gamma}$	Shear rate
τ	Wall shear stress
$\bar{\bar{\tau}}$	viscous stress tensor
λ	Relaxation time, s

ρ	Density of flowing fluid, kg/m^3
μ	Dynamic viscosity, Pa.s
ν	Kinematic viscosity, m^2/s
μ_0	Viscosity at zero shear rate, Pa.s
μ_{inf}	Viscosity at infinite shear rate, Pa.s
ϕ	Scalar quantity
$\ddot{\Phi}$	Key variable

ABBREVATIONS

CAD	Coronary Artery Disease
CFD	Computational Fluid Dynamics
CT	Computed Tomography
CVD	Cardiovascular disease
DM	Diabetes mellitus
DNS	Direct Numerical Simulation
DICOM	Digital Imaging and Communications in Medicine
DSA	Digital Subtraction Angiography
FFR	Fractional Flow Reserve
FSI	Fluid Structure Interaction
FVM	Finite Volume Method
GCI	Grid Convergence Index
HDL	High density lipoprotein
ICA	Invasive coronary angiography
LAD	Left Anterior Descending artery
LDA	Laser Doppler Anemometry
LDL	Low-density lipoprotein
LDV	Laser Doppler Velocimeter

LES	Large Eddy Simulation
OSI	Oscillatory shear index
PCI	Percutaneous coronary intervention
PISO	Pressure Implicit Splitting of Operators
RANS	Reynolds-Averaged Navier-Stokes
RMS	Root Mean Square
RNG	Re-Normalisation Group
RSM	Reynolds stress model
SAS	scale adaptive simulation
SST	Shear Stress Transport
STL	Stereolithography
VMTK	Vascular Toolkit Modelling
WSS	Wall Shear Stress

ABSTRACT

Blood flow in the cardiovascular system is a transient phenomenon, driven by the rhythmic contraction and expansion of the heart. Heart muscles receive oxygen and nutrients through coronary arteries. Physiological and psychological activities in the body influence the heart rate and consequently the blood flow in the coronary artery. When the physical and psychological activities become intense, coronary vessels have to carry a higher volume of blood by self-expansion. Such a condition of blood vessels carrying a higher volume of blood is known as hyperaemia. Hyperaemia can be a life-threatening condition for persons with coronary artery diseases (CAD). CAD is one of the leading causes of death worldwide. The major CAD causing millions of deaths across the world is atherosclerosis. It is developed due to the accumulation of plaques in coronary arteries known as stenosis. Plaque deposition reduces the vessel cross-sectional area, making vessel wall rigid and limiting its ability to carry higher volume of blood during hyperaemia. This will lead to reduction in supply of oxygen and nutrients to heart muscles causing ischemia. The dynamics of blood flow (hemodynamics) has a major role in the initiation and propagation of atherosclerosis.

A better understanding of local flow dynamics is very useful to estimate and forecast the complexity of heart disease and thus help the medical community in the planning of treatment. These are normally carried out by invasive diagnostic techniques like angiogram and are risky. In this study, flow through the coronary artery with stenosis is analysed for normal and hyperaemic condition with the help of images received from a non-invasive technique viz., the CT scan of the stenosed artery and the Computational Fluid Dynamics (CFD). Blood flow through idealized geometry and patient-specific geometries (extracted from CT scan with 33%, 66% and 85% stenosis) are analysed numerically by using the ANSYS FLUENT, commercial CFD software. An ideal 75% axisymmetric stenosed geometry is used for the identification and validation of methodology. The blood is modelled as a non-Newtonian fluid by using the Carreau viscosity model. The study considered blood flow as pulsatile in nature. Transition Shear Stress Transport k-ω model is used to represent the flow transition from laminar to

turbulent and vice versa. All three asymmetric stenosis cases are analysed for normal and hyperaemic conditions. The results show large variation in hemodynamic characteristics, viz., Wall Shear Stress (WSS), pressure drop, velocity, and turbulence and re-laminarization of flow in the post stenotic region.

When the stenosis level is near critical level, cardiologists use an index called Fractional Flow Reserve (FFR) for evaluating the criticality of stenosis which is obtained by using an invasive method. The study proposes a methodology for evaluating the FFR by using non-invasive method viz., CT scan of the stenosed artery and CFD. The methodology reveals that stenosis at the order of 47% can be critical under hyperaemic conditions. The WSS values exceed the lower and upper ranges by a large margin, subsequently damaging the endothelial cells leading to development of secondary stenosis. Even though, medical practitioners normally assume that the stenosis range less than 50% is not critical, the current study reveals that FFR can become critical even when the percentage of stenosis is as low as 47%. Recent statistical studies observe that people with diabetes at a younger age tend to develop cardiovascular disease at an early age compared to the people without diabetes. The present study reveals that the FFR value in the case of diabetic patients reaches the critical value even when the stenosis is at the order of 40%. The devised methodology can evaluate the criticality of the stenosis and hence avoid the need for using angiography or other invasive methods just for evaluation purposes.

Keywords: Coronary artery, Stenosis, Wall shear stress, Flow rate - Pressure relation, Fractional Flow Reserve.

CHAPTER 1

INTRODUCTION

1.1. Background

Blood flow in human body (cardiovascular system) is a transient phenomenon, maintained by the rhythmic pumping action of heart. At many times heart cannot pump enough blood to various organs including heart muscles by itself due to dysfunctions/ heart diseases, leading to heart failures. Any dysfunction in cardiovascular system leads to cardiovascular diseases like Coronary Artery Disease (CAD), stroke, congenital heart disease, aneurysms, valvular heart disease, etc. Among them CAD is the major cause of millions of deaths worldwide since more than a decade. CAD is commonly a result of atherosclerosis, a disease in which the wall of the artery develops abnormalities/ lesions leading to narrowing of the flow area due to the build-up of atheromatous plaque, causing stenosis (McDonald, 1974; Maton, 1997) (Fig. 1.1). CAD during the transient flow behaviour of blood makes the patient more vulnerable to heart failures. Stenosis (narrowing of blood vessel) in a coronary artery hardens the vessel wall and the wall loses its normal elastic behaviour due to plaque depositions. Atherosclerosis remains asymptomatic for decades in many patients due to elastic property of arteries and significant blood flow reduction does not happen at early stages.

Hemodynamics plays a major role in the origin and progression of atherosclerosis and hence, it is important in the diagnosis and evaluation of CAD (Manuck et al., 1986; Zeiher et al., 1993). The hemodynamics in coronary artery varies mainly with variation in heart rate as it increases with physical activities, emotional surges, etc. and decreases while resting, sleeping, confusion, dizziness, etc. During the active condition of heart, coronary vessels carry higher volume of blood by self-expansion. Such condition of blood vessel having high volume of blood is known as hyperaemia (Bliss, 1998). In the recent past, stenosis and CAD cases in younger age group are seen increasing and the statistics reveal

that these cases are related to patients with early diabetes. The studies and statistics show that, a person with diabetes has an increased level of blood viscosity, Low-density lipoprotein (LDL) and triglyceride (Sloop and Garber, 1997; Weinstock et al., 1995; Rosenson et al., 2002; Takiwaki et al., 2014). The increase in osmolarity causes increased capillary permeability and consequently, increased haematocrit and viscosity. Blood viscosity is a measure of resistance to flow, and high viscosity level increases the criticality of CAD (Jeong et al., 2010; Cowan et al., 2012).

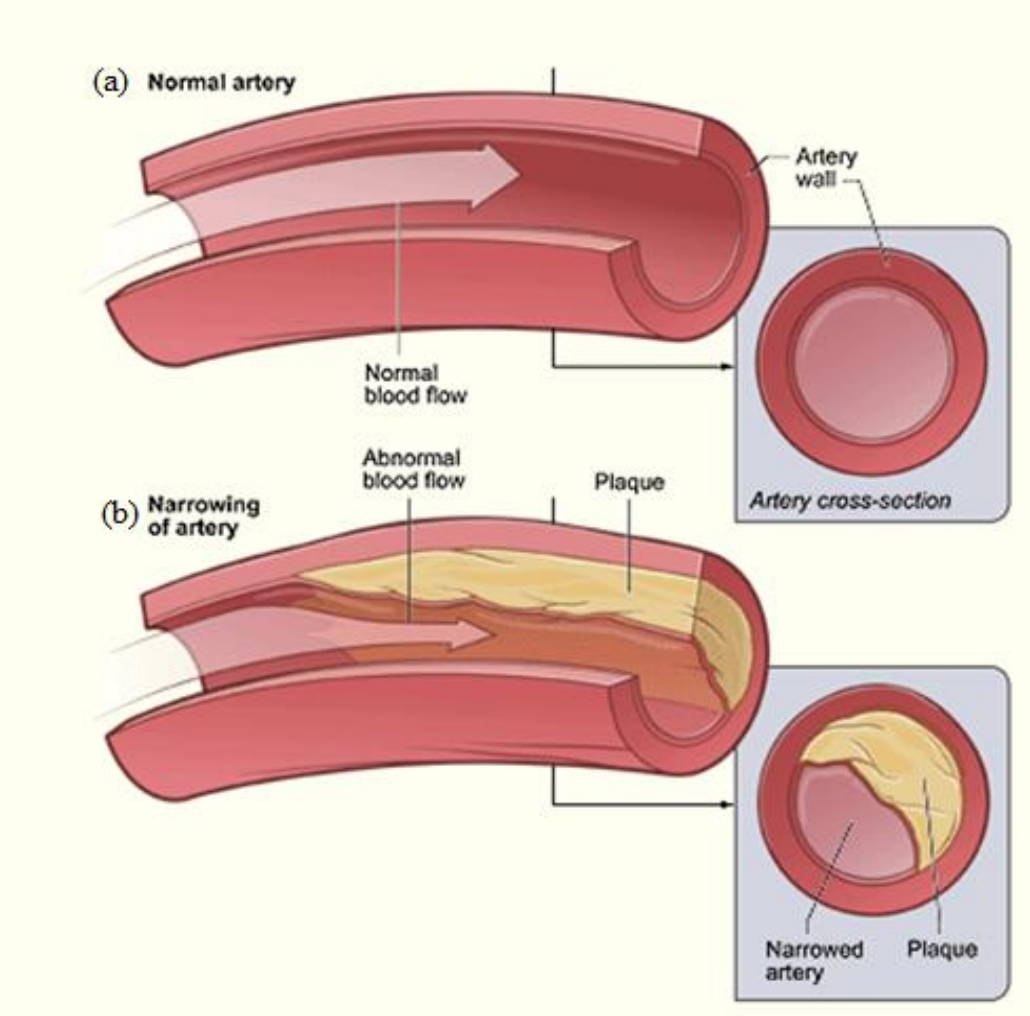

Fig. 1.1 Schematic of arteries (a) Normal artery; (b) Narrowing of artery (Carreras et al., 2014)

Several experimental research works has been conducted to study the blood flow dynamics (hemodynamics) in diseased blood vessels (Cassanova and Giddens, 1978;

Deshpande and Giddens, 1980; Ahmed and Giddens, 1983a, 1983b, 1984). Experimental investigations of blood flow dynamics in arteries are highly complicated due to small size and complex branching structure of arterial network. Mathematical modelling and computational simulations can play significant role in overcoming such limitations and difficulties of experimental studies. Computational Fluid Dynamics (CFD) is a powerful tool in such cases for evaluation of complex geometries and its analysis (Ku, 1997). In cardiovascular studies, the major applications of CFD is the investigation and analysis of blood flow in diseased vessels (like in case of atherosclerosis). CFD also plays an important role in development of medical aids and equipment (Ku,1997). CFD can equip the medical practitioners with solutions to decide the type of equipment and method of treatment to be used for each case of atherosclerosis. One of the major advantages of CFD in hemodynamics is that it offers various chances for simulation before a real obligation is undertaken for executing any medical design alterations and helps in providing the correct direction to develop medical interventions.

Several researchers (Ghalichi et al.,1998; Bluestein et al.,1999; Varghese and Frankel, 2003; Ryval et al., 2004) studied hemodynamics of stenosed coronary artery using CFD under various conditions. In order to bring down the complexity of hemodynamic problem, various assumptions were adopted by the researchers. They are as follows.

Ideal geometry

Laminar flow

Ideal boundary conditions

Blood as a Newtonian fluid

Constant density

In real case, the blood flow is laminar and the presence of stenosis (disease case) create turbulence. This encouraged many researchers to use Reynolds Averaged Navier-Stokes (RANS) models to accommodate the effect of turbulence in blood flow. RANS models include one equation and two equation models and the performance of each model varies from problem to problem (Ghalichi et al.,1998; Bluestein et al.,1999; Varghese and Frankel, 2003; Ryval et al., 2004). Large Eddy Simulation (LES) is another technique in

which small eddies can be modelled using fine grid size and predict turbulence effectively (Jabir and Lal, 2016). Even though smaller eddies can be modelled by using LES, it required large computational power and time. However, the transition SST (Shear Stress Transport) k-ω model of RANS model, is observed to capture the flow transitions and turbulence effectively and predict the Wall Shear Stress (WSS) accurately (Ryval et al., 2004; Tan et al., 2008; Mahalingam et al., 2016). In this study transition SST k-ω model is used for blood flow simulations to accommodate the effect of transitions and turbulence of flow in stenosed artery.

In clinical cardiology, severity of stenosis is generally determined by the measurement of pressure before and after the stenosis, using pressure transducer catheters. The measurement is expressed in terms of an index called Fractional Flow Reserve (FFR), which is the ratio of pressure after stenosis to pressure before stenosis. In clinical cardiology, FFR value of 0.8 is identified as the threshold limit to decide between medication and revascularisation procedures (De Bruyne et al., 2012; Muller et al., 2011; Nørgaard et al., 2014). FFR value below 0.8 will initiate revascularisation therapy for a patient and FFR above 0.8 may confine the treatment to medications. When the value of FFR lies in between 0.8 to 0.75 (commonly referred as grey zone) a detailed clinical evaluation is conducted to decide upon the treatment procedures (Kern et al., 2006; Van de Hoef et al., 2014). The above practices in the medical field register the importance of FFR in diagnosis and treatment of CAD. FFR measurements are generally obtained using invasive techniques (by inserting catheter with sensors) in specific arteries. The invasive method involves procedures which require expertise and pose high risk to the patients with CAD. Introduction of non-invasive techniques for the assessment of FFR will nullify the procedural difficulties and reduce the risk for patients. CFD can be used as a tool for identifying FFR along with scanning techniques in diagnosing criticality of CAD patients.

1.2. The relevance of the topic

From World Health Organisation data, the world's biggest killer is ischaemic heart disease, responsible for 16% of the world's total death (WHO, 2019). Since 2000, the largest increase in deaths has been due to this disease, rising by more than 2 million to 8.9 million deaths in 2019. The reason behind this should be investigated in detail. Ischemic

heart disease - atherosclerosis usually does not show up any symptoms until it severely narrows an artery or totally blocks an artery. Atherosclerosis/ stenosis decrease the blood flow to the distal part, reducing the supply of oxygen and nutrients to the heart muscles. The blood flow reduction stimulates the heart to work harder to supply sufficient volume of blood to every part and leads to unstable angina or heart attack in future. It has been proved in the literature that, (Fry, 1968 and 1969; Caro et al., 1971) various biomechanical and hemodynamic factors like WSS, viscosity of blood, blood pressure etc. play an important role in the localization of such dysfunctions. These diseases are found to be critical; life threatening and occurs at certain branches and bends. In most of the cases, atherosclerotic lesions have been found to develop at the inner wall of curved segments and outer walls of bifurcations where WSS is low (Zarins et al., 1983; Friedman et al., 1986; Asakura and Karino, 1990; He and Ku, 1996). Recent statistical studies on the occurrence of ischemic cases in younger people reveal direct relation with diabetes. A number of studies by various researchers analysed the effect of diabetic mellitus on whole blood viscosity. All these studies point towards the strong impact of diabetes on the early occurrence of CAD in such patients. The studies reveal that the increase in blood viscosity due to diabetes aggravates the damages to endothelial layer of blood vessels. Hence the study of variation in blood viscosity on CAD patients is also significant to analyse the risk while conducting CFD analysis (Mayer, 1964; Rosenblatt et al., 1965; Lowe et al., 1980).

1.3. The motivation for the research work

Ischemic heart disease stands first as the world's biggest killer since decades, it retains its position in all continents. The most terrifying point in this regard is its year-on-year increase in the mortality rate. The statistical and other studies bring up many reasons for the increase, but the solution to bring it down or stopping the rise in cases is still a mirage for the medical fraternity. The major reason for high death rate is that it remains asymptomatic till critical stage and the patient suffers a heart attack; many a time becoming fatal at the first instant itself. Earlier days the ischemic heart diseases were observed in aged people say above 50 or 60 years. The present-day statistics shows that even people in their early twenties are hit by the heart disease-stenosis/ atherosclerosis. Many statistical studies point towards increase in viscosity due to diabetes as the reason for such early cases

of heart attacks. The development of atherosclerotic blocks and its propagation is directly depended on the hemodynamics. Detailed study of blood flow dynamics using conventional techniques like direct measurements and experimental setup is limited due to narrow size of blood vessels and its complex structure. In such situations non-invasive method like CFD shows its significance, which can be used for the analysis and evaluation of the risk.

1.4. Objectives of the research work

The geometry of the artery and irregularities in the thrombus plays important role in generation and propagation of stenosis. Even though many researchers studied the topic related to CAD and thrombus formation in arteries, the studies are concentrated on using ideal geometries. The experimental setups even cannot replicate the real environments in an artery, employed ideal geometries. Further studies considered axisymmetric stenosis cases for the analysis, were as in practical case it is eccentric and have irregular shapes. The studies which investigated patient specific geometries seldom considered flow characteristics in detail for hyperaemic flow condition. The post stenotic flow characteristics and its flow transitions were not evaluated completely in these studies. So far, the studies did not consider to bring a relation with the practical medical diagnosis parameter, viz., FFR. Hence the objective for the research work is identified and fixed as mentioned below.

Objective:

To device a non-invasive risk assessment tool in diagnosis of CAD using CFD model of patient specific stenosed coronary artery under normal and hyperaemic blood flow conditions.

Specific objectives

1. To investigate the blood flow characteristics in a stenosed coronary artery for patient specific cases by using transition SST k-ω model.

2. To provide an aid (numerical tool) to doctors in assessing the criticality of stenosis in terms of FFR by analysing hemodynamic characteristics for patient specific geometry.

3. To devise a tool in evaluating the severity of stenosis and its risk in diabetic patients, where variation in blood viscosity is critical.

1.5. Organization of the thesis

The thesis work is organised into six chapters under following headings.

- Chapter 1: The section provides an overview of the blood flow in cardiovascular system, significance of CAD and stenosis, effect of variation in blood viscosity and the relevance of modelling of hemodyamic variables using CFD model. The scope and objective of work are also given at the end of this chapter.

- Chapter 2: The Literature Review provides historical background of the studies and research works relevant to the present research area. It is divided into following subsections, viz., Experimental, and Numerical studies, Newtonian and non-Newtonian models, Fractional Flow Reserve (FFR), Wall Shear Stress (WSS) and effect of blood viscosity on hemodynamic properties. properties. Research gap is also mentioned at the end.

- Chapter 3: Materials and Methods discusses governing equations of fluid dynamics, theory involved in Computational Fluid Dynamics, application of various boundary conditions and describes various procedures involved in modelling the fluid and the geometry.

- Chapter 4: Verification and Validation of the Selected Model: Simulation of flow through circular stenosed pipes is carried out with published data for the selection and the validation of numerical model.

- Chapter 5: Results and Discussions: Numerical investigation of coronary artery under various percentage stenosis levels and blood viscosities are carried out. FFR index under each case is studied and developed a methodology to evaluate FFR numerically for unknown percentage stenosis from the available clinical data.

- Chapter 6: Summary and conclusion of the research.

1.6. Summary

The chapter gives an introduction about atherosclerosis (CAD) and its effect on hemodynamic properties. It points out the importance of studying blood flow characteristics through patient specific stenosed coronary artery by using non-invasive methods and its application in medical field. It also explains the importance of FFR for the diagnosis of CAD, its treatment decisions and effect of blood viscosity on hemodynamic properties in stenosed coronary artery. Further, it details the relevance of the topic, scope and objectives of the present study and the outline of the thesis.

CHAPTER 2

REVIEW OF LITERATURE

2.1. General

The analysis of blood flow in arteries, especially in coronary, carotid and similar arteries became important and interesting among researchers due to exponential increase in diagnosing dysfunctions and complications related to stenosis, atherosclerosis etc. in 20^{th} century. Early days witnessed the research works using experimental setups with the help of mammalian samples (from dogs). The experimental setups have many limitations like; difficulties in obtaining the samples, measurement of parameters, mimicking the real flow conditions etc. With the advancements in numerical techniques and application of CFD, much research is happening in this field. Early experimental studies in the field could give a path for these researchers to decide on the fluid properties and setting the boundary conditions. In the initial stages, numerical studies considered laminar flow models. Prediction of turbulence in the post stenotic region is obtained by using models like LES, Direct Numerical Simulation (DNS) and RANS. Initial studies considered blood as a Newtonian one, however latest research works identified the non-Newtonian behaviour of blood in smaller arteries like coronary and carotid arteries. Most relevant parameters discussed by the researchers in their studies are WSS and pressure. Further many statistical and experimental studies regarding the change in blood viscosity of patients with diabetic mellitus observe correlation with CAD and blood viscosity. Following sections details the above-mentioned studies and their results.

The literature review illustrates the experimental and numerical studies of blood flow in stenosed coronary artery by considering blood as Newtonian and non-Newtonian fluid during steady and transient flow. The review also includes the study on impact of high blood viscosity on hemodynamic parameters.

2.2. Experimental studies

The experimental study in human arteries especially in coronary artery is complex and involves large risk. In the early days, researchers used rigid pipes, materials mimicking arteries or biological specimen from any mammal, such as dog, for conducting experimental studies related to stenosis. Reul et al. (1972) conducted experiments in pipes fitted with orifice plates to model stenosis constrictions. The study observed small losses in pressure when the cross-sectional area is reduced beyond 25%.

Young and Tsai (1973a, 1973b) conducted experiments in axisymmetric stenosis under steady and unsteady flow. The experiments were conducted in a tube casted out of polyester resin with axisymmetric stenosis. A Cosine curve shape is used to cast the axisymmetric stenosis. The study analysed various factors like pressure drop, flow separation and turbulence in both cases. Hot-film probes were used to map and measure the Re at which transition to turbulent flow occurs. Under steady flow, the study considered Re values in the range of 100-5000. Blood was modelled as a Newtonian fluid in their studies. Experiment used piezometer for measuring pressure drop across the stenosis. The primary interest of this work was to identify the specific Re values at which the flow separation and reattachment occur, and to spot the starting point of this phenomenon. At higher Re values, the pressure drop observed was considerably high. It was noted that pressure falls sharply near the constriction zone and recovers after certain distance. At Re value of 1000, pressure drop of 89% stenosis was 23 times higher than the pressure drop of 56% stenosis. Flow separation occurs at 0.8D to 0.9D (D - diameter of the tube) distance from the throat of stenosis and turbulence was observed in 56% stenosis case at critical Re value 500. In 89% stenosis case flow separation was difficult to capture and turbulence was observed at critical Re 200. The same stenosis percentage is used for transient flow analysis. To generate pulsatile flow, a piston cylinder (rotary pump) is used at the inlet. During transient flow capturing the flow separation was difficult due to the limitations in instrument capabilities. Turbulence was observed for 56% stenosis at Re value 3500 and for 89% stenosis, at Re, value of 173. They also observed that pulsatile flow is less stable compared to steady flow in severe stenosis case (89% stenosis). Due to limitations of

measuring instruments used, the experiment could not capture the flow separation phenomenon satisfactorily in both stenosis case.

Giddens et al. (1976) conducted their experimental study in descending thoracic aorta of anesthetized dogs at different stenosis percentages (25%, 36%, 50%, 69%) and measured instantaneous velocity distribution using hot film anemometer. Specific occlusion levels were created by inserting several precisely tailored plastic strips at pre-designed locations of the blood vessel. Study used magnetic flow meter for the flow measurements, observed localized velocity disturbance and turbulence fields in the post stenotic region. Turbulence regions were observed from the velocity profiles and energy spectrum. The turbulence was first observed at deceleration phase of flow for 69% stenosis case.

Khalifa and Giddens (1978) conducted experimental study in dog's aorta, the study used digital measurement techniques to analyse turbulence under pulsatile flow conditions. Following stenosis percentage cases: 20%, 40%, 58% and 74%, were selected for the study. They observed turbulence at higher level of stenosis in the deceleration phase of waveform in a pulsatile flow. As the degree of stenosis increase, one could observe flow disorders in acceleration phase also. In mild stenosis case flow disorders are observed immediately at the downstream of constriction zone. The disturbance noted in energy spectra option is similar to that of velocity profiles. Cassanova and Giddens (1978) conducted stenosis experiments in a rigid tube under pulsatile water flow with Reynolds number in the range of 318 to 2540. Velocity was measured using anemometers. The study selected two sets of axisymmetric stenosis with 50% and 75% occlusion level, one set is sharp edged and the other, with a smooth shape. The study observed significant flow disorders for mild stenosis under pulsatile condition. At sharp edged stenosis the vortex rings were observed in the post stenotic region. For sharp edged stenosis case, the vortex rings were observed within one tube diameter downstream of occlusion at Re, 2540. But in smooth shape stenosis, vortex and recirculation were observed in three tube diameter distance. At Re value of 2540, the vortex rings were observed in x/D = 1.125 (D - diameter of the tube) and completely disappear at x/D = 3.25 in 50% sharp edge case. The experiment could visualise the flow patterns in the post stenotic region, describing the

turbulent and recirculation zones. The magnitude of fluctuations in velocity profile is seen increasing with increase in stenosis percentage, irrespective of the shape of the stenosis. Compared to sharp edge stenosis in 50% and 75% cases, smooth edge stenosis creates more instabilities in flow and lengthy recirculation zone in post stenotic region. The sharp edge stenosis shows higher velocity magnitude than smooth contoured geometry in both 50% and 75% stenosis.

Deshpande and Giddens (1980) analysed turbulent flow through a constricted tube with 75% block using Laser Doppler Anemometry (LDA) with dye. The researchers plotted velocity profiles corresponding to Re values; 5000, 10000 and 15000. The study recorded the velocity profiles, RMS (Root Mean Square) turbulence velocities and energy spectra. Wall pressure variations and length of recirculation region were determined from the above data. The result portrays extremely high levels of turbulence in recirculation region. The methodology could not catch the recirculation happening at the post stenotic region. Velocity profile forms a plug-like profile at the throat of the stenosis. The study observed negative velocity at an axial distance of 1D to 4D in velocity profile, representing recirculation zone. The velocity returns to its primary upstream profile after recovery from turbulence.

Khalifa and Giddens (1981) conducted experimental studies on stenosis using plexiglass tube having dimensions of dog's aorta. LDA was used to measure velocity. They applied velocity waveform at inlet with Re values 500 and 2400 (minimum and maximum). They studied axisymmetric stenosis cases with 25%, 50% and 75% blocks and observed the following results. Zero turbulence was observed in the post stenotic region for 25% stenosis case. In 50% stenosis case, disturbances in velocity profiles were observed at a distance of 2.7 to 20 cm from the throat. At 26.5 cm, waveform returned to the shape close to upstream profile. The study observed that the intensity of disturbance in post stenotic region is high for 75% stenosis case compared to that of 50% case. In 75% case velocity disturbance were observed from 2.7 cm to 30 cm from the throat of the stenosis in post stenotic region.

Ahmed and Giddens (1983a, 1983b) measured the velocity fields in a stenosed tube with rigid wall (similar to the dimensions of carotid artery) and with steady flow at inlet.

They used LDA for velocity measurements at varying stenosis cases (25%, 50% and 75%) and Reynolds number in the range of 250 to 2000. Axisymmetric models were constructed from plexiglass with smooth cosine curve shapes. A centrifugal pump with flow control valve is used for regulating the flow. Mixture of water and glycerol maintained at 33^0C was used as fluid. The flow field in post stenotic region were visualized using hydrogen bubbles, which is formed when sodium sulphate is added to the flow mixture. Following conclusions were derived from the flow visualization study:

a) Flow field is observed to be laminar and stable for 25% stenosis at Re $\leq$ 1000.

b) For 50% stenosis case at Re value of 1000, vortex rings were generated but transition to turbulence was not observed. At Re value of 2000, turbulence was formed at 3D to 4D distance, distal to the throat.

c) For 75% stenosis case, flow is observed to be completely laminar at Re value of 250. At Re value of 500 oscillations were observed in the post stenotic region, position is not specified. When Re was made 1000 and 2000 turbulence were observed at 5D and 6D distances from stenosis throat respectively.

The velocity profiles were plotted for different locations of 50% case at different values of Re (500, 1000 and 2000) and following observations were made. Velocity profile analysis depicts that, velocity profile becomes blunt shaped at stenosis region for Re values 1000 and 2000. Negative velocity is observed near the wall at all values of Re, creating flow separation zone in post stenotic region. Length of flow separation region is observed to vary with varying Re values and seen increasing with increase in Re value. In case of 75% case, flow separation was observed at lower Re value of 500. At Re value of 1000 flow separation zone was observed between 5D and 6D distance from stenosis throat. The centre line velocity tends to accelerate until 3D distance after stenosis and decelerates thereafter.

Ahmed and Giddens (1983b) extended their previous study to investigate more about flow transitions and turbulence in post stenotic region at varying stenosis case of 25%, 50% and 75% with Reynolds number in the range of 250 to 2000. The energy spectra show disturbances in post stenotic region, which is a clear sign of turbulence. Compared

to the previous study, at Re value of 2000 high intensity turbulences were observed in post stenotic region for 50% stenosis. In case of 75% stenosis the spectra show vortex rings in post stenotic region for all Re values. When Re was 1000, the separation was observed between 5D and 6D distance from stenosis throat, it diminishes thereafter. For Re value of 2000, turbulence was formed very early at a distance of 1.5D. In centreline velocity profiles of 50% stenosis, magnitude of velocity is less compared to 75% stenosis at both Re values (1000 and 2000). The velocity attains its maximum value at stenosis throat thereafter decreases and merges to the upstream value.

Ahmed and Giddens (1984) work was an extension of their previous studies (Ahmed and Giddens, 1983 a, b). The study conducted pulsatile flow experiments in ideal geometry with an average Re of 600, resembling to flow conditions in human carotid artery with 25%, 50% and 75% occlusions. A smooth cosine curve shaped stenosis was selected for the study. Pulsating pump was designed to produce pulsatile flow profile at the inlet. Hydrogen bubbles were used for visualising the flow. The study observed that, turbulence gets developed when stenosis blockage exceeds 50%. In 25% stenosis case, flow is stable throughout the length of geometry with no flow disturbance. For 50% stenosis case, flow disturbances were observed in the post stenotic region during the acceleration phase. For 75% stenosis case, turbulence and flow transitions were clearly observed in post stenotic region. Intense turbulence was observed in the velocity profiles at flow reattachment zones during deceleration phase of the cardiac cycle.

Ojha et al. (1989) conducted experiments in mild (45% axisymmetric and 38% asymmetric) to moderate degrees of stenosis constriction (65% and 75% axisymmetric) using photo chromic tracer method for flow visualization. At inlet, a pulsatile velocity profile was applied. The study used a fluid with density of 0.755 g/cm^3 having viscosity 1.43 cP at 20^{0}C. The internal diameter of the tube was 5 mm and constrictions (stenosis) were made by inserting machined acrylic rods. The study observed that, the axial velocity fluctuations in 45% axisymmetric stenosis case were less than that in 38% asymmetric case. Transition to turbulence occurs in post stenotic region for both 65% and 75% stenoses cases. These transitions were clearly visible from velocity profiles. The flow gets

relaminarized in case of 65% stenosis at each phase. While in 75% case the flow could not get relaminarized completely during the acceleration phase.

Lieber and Giddens (1990) conducted experiments in plexiglass having dimension similar to aorta of monkey. The study examined the post stenotic flow in 75% and 90% stenosis under pulsatile flow (sinusoidal pulse). A mixture of glycerine and water with kinematic viscosity 0.07 stokes maintained at 26.5^{o} C was used as the fluid. The average Re is 300 and the velocity was measured using Laser Doppler Velocimeter (LDV). In case of 75% stenosis, vortexes were observed at 5D distance from throat of the stenosis at peak flow. In 90% case these disturbances were observed at 2.5D and 3D distances at acceleration and deceleration phase. In 90% stenosis, velocity drop was observed at 5D from throat. A strong jet is formed at throat of 90% stenosis case creating a separation region, which extends up to 5D distance from throat. From observations of the study, it is concluded that, complex behaviour of flow is more in 90% case compared to 75% case.

The importance of selection of inlet boundary conditions was tested by Siouffi et al. (1997). The experiment was carried out in a mould of axisymmetric stenosis (75%) made of plexiglass with different inlet boundary conditions like, oscillatory, pulsatile (sine wave) and physiological flow waveforms. The selected fluid is a mixture of water, glycerol, starch, and sodium chloride. Velocity in post stenotic region is measured using Ultrasonic Doppler Velocimeter. Fan shaped velocity profiles were generated at 1D and 2D distances from throat of the stenosis during the early acceleration phase and under oscillatory condition. At peak flow, vortical structures were observed between 2D and 5D. Fan shaped velocity profiles were observed at 1D and 2D distances in pulsatile condition also. Compared to velocity profiles of oscillatory condition, the pulsatile velocity profiles are asymmetric in nature. The study observed vortices at 1D distance during peak flow phase of the physiological inlet waveform case. During deceleration phase of the pulse, vortex structures were formed between 4D and 7D distance. It is also observed that in axisymmetric stenosis case, the velocity profiles were symmetric in nature for physiological waveform. The study concluded that velocity field is strongly dependent on the flow waveform at inlet.

Beratlis et al. (2005) conducted an experimental study in an axisymmetric 50% stenosis. Experiments were conducted in closed loop set up, test section dimension was 1830 x 150 x 12.5 mm and velocity was measured using LDV. The study used water, maintained at a constant temperature of 25^0 C, as fluid for experiment. From velocity profiles, reverse flow is observed near the wall during minimum flow phase of the pulse. In acceleration phase, some background noises were noted. Two peaks were observed in the velocity profiles close to wall during the deceleration phase caused by disturbance in post stenotic region. To know more about the turbulent transition numerical study was also conducted. Both the experimental and numerical results were in good agreement with each other.

All the above researchers used idealised geometries such as circular tubes to model stenosis in arteries. Experimental studies were limited to the use of pathological samples or studies in other mammals due to the difficulties in the measurement of haemodynamic parameters. Further it is practically difficult to replicate the properties of blood vessels and blood flow characteristics in an experimental setup. The experimental conditions adopted in studies were mainly not representing the specific segment of human body, it replicates the thoracic aortas of dogs and monkeys with induced blockage(stenosis). The usage of patient specific geometry for the study is important in obtaining and understanding the actual hemodynamics of each stenosis geometry. However, during early days, the studies and research were much limited in this area. Because of the above limitations in experimental studies, mathematical modelling of arterial blood flow started gaining popularity. The research studies in the field became active in the late half of 19^{th} century with the advancements in numerical techniques and CFD. The numerical model could overcome other limitations in experimental studies like replicating the features of patient specific model; curvature of the vessel axis, stenosis eccentricity, realistic boundary condition like pulsatile flow and selection of turbulence models, discussed in the next section.

2.3. Numerical studies

Numerical studies in the field of blood flow through artery with stenosis are playing an important role in understanding the blood flow dynamics. It attained new dimension in

the final decade of twentieth century lead by the developments in CFD and numerical techniques. CFD studies analysed effects of blood flow in small stenosed arteries by selecting suitable geometry, boundary conditions, fluid, and flow models. The studies in this area can be classified in to two major sections based on the flow assumptions (laminar and turbulent) and fluid properties (Newtonian and Non-Newtonian). The numerical studies of blood flow dynamics focused on the medical aspects shall evaluate the hemodynamic parameters relevant to diagnosis also (Varghese et al. 2007a; Tan et al. 2008).

2.3.1. Laminar and Turbulence model

Numerical studies during the initial days modelled the blood flow in arteries as laminar one (Nosovitsky et al., 1997; Long et al., 2001; Boutsianis et al., 2004; Su et al., 2014; Wu et al., 2015). With the advancements in numerical modelling techniques and CFD software, flow transition (laminar to turbulence and vice versa) in post stenotic region is effectively captured (Jabir and Lal, 2016; Mahalingam et al., 2016). Researchers employed RANS, LES and DNS models for flow studies in post stenotic region. The review of numerical studies conducted in this area are discussed below.

Tu et al. (1992) used Galerkin finite element method for blood flow studies in rigid stenosed artery with 25%, 50% and 75% area reductions for steady and physiological pulsatile flows. The study considered Re values of 100, 200 and 500 for steady flow. Flow separation was noted in 50% and 75% stenosis at Re values of 500. They observed maximum value of WSS at throat of the stenosis and its value drops drastically after stenosis in all the cases. Velocity profiles were parabolic in nature under steady flow case, and it became blunt shaped at maximum area reduction part. Further they observed that the length of recirculation zones increases with Re. The study could not find any recirculation zone in 25% stenosis even at Re value 500. The recirculation length in 75% stenosis is greater than 50% stenosis. Under steady condition, the method gives results which agree with the experimental findings of Young and Tsai (1973a). Under pulsatile flow the study analysed 50% and 75% stenosis cases with Re value 337 and Womersley number 6.27. The study observed that the vortex becomes bigger during the accelerating phase and continues to grow even at the decelerating phase of flow in both 50% and 75% cases. The

vortex structures formed in post stenotic region are not stable and develop small vortices again in the deceleration phase. Under pulsatile flow study, velocity profile at throat forms plug profile. The velocity profile at post stenotic region changes its shape at different phase of the flow.

Nosovitsky et al. (1997) used laminar flow assumption to determine the velocity and WSS distributions in an artery with 25%, 56% and 75% stenosis near a 90^0 bend. Steady and transient velocity profiles were applied at inlet. They used Reynolds number 500 for steady flow and 700 during the peak of pulsatile flow respectively. Velocity profiles were plotted at different axial location. Due to curvature in artery, flow was skewed towards outside of the curve. As stenosis increases, the velocity profiles shift more towards outer wall and forms M-like shape. They also mentioned that flow separation may occur at 75% stenosis with 90^0 curvatures, under steady flow. The value of peak WSS, increases with increase in stenosis occlusion level. WSS gradually return to its upstream values at downstream side of stenosis. Under transient case, velocity profile is applied at inlet with maximum Re value of 700. Velocity profiles were plotted at different locations corresponding to five specific phases (End of diastole, Local systolic maximum, Local systolic minimum, Reversed flow in early systole and Maximum flow at the beginning of diastole) of the pulse. It is observed that, the flow skew towards outer surface of the bend and forms recirculation zones in every phase of the pulse. At 75% stenosis recirculation zone is large compared to 50% stenosis. Under transient flow, WSS value increases with increase in stenosis percentage.

Wilcox low-Re RANS turbulence model was used by Ghalichi et al. (1998) for the simulation of 50%, 75% and 86% axisymmetric stenosis cases. The study considered steady flow and the blood was modelled as Newtonian fluid. At the inlet, parabolic velocity was applied. Re values varying from 400-1500 were used for the study. The study observed that the length of vortex ring increases with increase in Re value. The study found that for 50% stenosis, flow transition occurs in post stenotic region for Re values above 1100. In 75% stenosis case, the critical value of Re at which flow transition occurred was 400 and it was 230 for 85% stenosis case. They compared vortex length using laminar and Wilcox model and observed that laminar model overestimates the vortex length in transition-

turbulent region. Pressure distribution obtained from Wilcox model was compared with experimental result of Deshpande and Giddens (1980) and got similar result. WSS results of both laminar and Wilcox model were compared and observed that, Wilcox model gives better results when transition or turbulence flows coexist. They also compared centre line turbulence intensity and observed similar result between Wilcox and experimental results. Deplano and Siouffi (1999) conducted both experimental and numerical study for 75% stenosis case, using finite element method for the transient numerical simulations. Velocity is measured using Doppler ultrasonic velocimetry. As reported earlier, high WSS values were observed at the stenosis throat. Velocity and WSS values of numerical and experimental studies were found to be in good agreement.

Long et al. (2001) applied pulsatile blood flow in straight tube with axisymmetric stenosis models having area reduction of 25%, 50% and 75% to investigate the post-stenotic flow phenomena. Pulsatile blood flow waveform was used as the upstream flow condition which had a mean Reynold's number of 300. The study was focused on the flow separation and secondary motion in post stenotic region. No disturbances were observed in post stenotic region of 25% stenosis case. But observed a permanent flow separation throughout the cardiac cycle in 50% stenosis case. The length of flow separation varies at different phase of the cardiac cycle in both 75% and 50% cases. In 75% stenosis case the flow separation size was higher than the 50% stenosis case. Further under 75% case, the flow disturbances were observed for the entire downstream length. The study observed formation and development of complex free separation zones in the post stenotic region, especially in the flow deceleration phase. It was found that the oscillations in WSS values were high in the post stenotic region and the maximum value depends on the degree of stenosis.

The experimental studies of Ahmed and Giddens (1984) and Ojha et al. (1989) clearly observed the presence of transitional or turbulent flows, distal to the stenosis. Therefore, Varghese and Frankel (2003) carried out numerical simulation studies in stenotic vessel to address the issue of turbulence. Their study selected pulsatile flow (Womersley profile) through sharp-edged stenosis. Low Reynolds number k-ω, low Reynolds number Re-Normalisation Group (RNG) k-ε, RNG k-ε and standard k-ε models

were selected for study. Velocity profiles at different phases of cardiac cycles were plotted. Low Reynolds number k-ω model gives similar results as experimental result and predicts jet like flow at immediate downstream of the stenosis. The centreline velocity predicted by all models show deviation from experimental results. Streamlines computed by the low Reynolds number RNG k-ε, RNG k-ε and standard k-ε model were same. From the streamline plot, it is observed that, reverse flow region gets developed immediately after the stenosis throat at peak flow. The reverse flow region continued to grow at deceleration phase and at early phase of acceleration. This reverse flow completely disappears in the middle of acceleration phase. In low Reynolds number k-ω model, recirculation zone is observed at distance of 0.35R to 0.4R (R- radius of vessel) from throat of stenosis. The experimental studies also got recirculation zone at same points. But for k-ε model and its variants, the recirculation zones were at different points. The turbulence intensity and WSS predicted by k-ω model is compliant with experimental results than k-ε model and its variants. The study concluded that k-ω model produces better results which are in good agreement with experimental results and can be used to represent transitional or turbulent flows.

Ryval et al. (2004) analysed the capability of two equation turbulence model to capture laminar, transition and turbulence regimes in a stenosed artery. They used Wilcox's standard k- ω model and a transitional variant of the same model was employed for 75% and 90% stenosed vessels with a sinusoidal pulsatile flow inlet. The rigid wall concept and Newtonian assumptions were used for the study. For 90% stenosis case, standard k-ω model predicted turbulence in post stenotic region. Turbulent fluctuations were observed beyond Z = 2.5 (Z - axial distance) from throat of stenosis in 90% case during peak flow. At Z = 4, the fluctuations were very high and thereafter it gets reduced. In transitional k-ω model of 90% case, the computed results closely resemble the experimental results. In 75% case, standard k-ω model predicts turbulence in post stenotic region. On the other hand, transitional k- ω model predicts very low turbulence in post stenotic region of 75% case. The results of 75% stenosis case were compared with the experimental results of Ahmed and Giddens (1983a, 1983b, 1984). It is observed that transitional k- ω model gives better results of axial velocity profiles in each section of 75% stenosis case. Hence the study concluded that, the transitional version of the k- ω model showcases an overall better

representation of pulsatile flow. The standard model consistently over predicts turbulence at downstream of the stenosis. It was found that a relatively simple two-equation turbulence model can be used for simulating physiological pulsatile flows.

Numerical investigation of pulsatile flow in a stenotic artery (50% axisymmetric stenosis) is presented by Beratlis et al. (2005). DNS method was used for the numerical studies. No slip condition was applied at wall. The axial velocity of both experimental and numerical methods were compared and observed good agreement with each other. A reverse flow near the wall was observed at minimum flow phase of the pulse. The results clearly show sequential flow transition to turbulence and relaminarization in post stenotic region. In simulation, they observed that the stenosis becomes unstable due to the formation of strong jet just after the stenosis at the peak mass flow rate, developing a role-up and subsequent breakdown of the shear layer.

The steady and pulsatile flow through concentric and eccentric configurations having different severity levels of stenosis were studied using DNS method by Varghese et al. (2007a, 2007b). The stenosis geometry (75% stenosis) selected in this study is similar to the geometry used by Ahmed and Giddens (1983a, 1983b, 1984). Blood was modelled as Newtonian fluid. Under steady flow, Poiseuille flow profile was applied at the inlet. The vessel wall was assumed as rigid one and no-slip conditions were applied at wall. The study selected Re values of 500 and 1000. The velocity profile changed from parabolic to plug-like profile at the throat of 75% stenosis, when Re value was 500. The peak velocity at downstream section increases four or more times of the inlet mean velocity. Up to a distance z = 2.5D (D - diameter of the tube), the velocity profiles from DNS method exactly match with experimental results (Ahmed and Giddens, 1983a, 1983b, 1984). After 2.5D distance, the results showed variations from experimental results. An eccentricity of 5% was created in stenosis geometry and simulations were carried out at Re values 500 and 1000. The velocity profile shows same plug profile at stenosis region and found that peak velocity is four times more than inlet mean velocity. From velocity vector diagram, cross flow velocities were observed due to geometric eccentricity. The accelerating jet formed at the stenosis causes flow separation along the side of the vessel. Recirculation regions were created up to a distance of z = 2D. The recirculation region is seen extended up to 8D

and flow relaminarization take place after 14D. In case of Re value 1000, the transition to turbulence occurred at z = D. At this place the peak velocity is 50% of mean inlet velocity. Further in case of Re value 1000, the stenotic jet starts to break down at x = 6D. In post stenotic region the recirculation region is seen extended up to 11D and after this, axial velocity profile forms uniform shape with peak velocity 1.5 times of the mean inlet velocity. The study observed transitions stages in post stenotic region.

Varghese et al. (2007b), extended their studies to pulsatile inlet condition from steady inlet condition. Same geometry (75% stenosis) as explained in previous study was used for the pulsatile study. Womersley pulsatile profile was applied at inlet. Minimum and maximum value of Re were approximately 200 and 1000, Womersley number selected was 7.5. The recirculation region is observed to be extended up to 7D, in axisymmetric 75% stenosis case under maximum flow. During maximum flow the velocity at stenosis throat reaches 4.65 times the mean inlet velocity. During minimum flow, the peak velocity at throat is 3.1 times the inlet mean-velocity and the flow separation zone gets extended up to 12D. Comparing both experimental and DNS results of velocity profile, differences were observed in recirculation region. Similar conditions were applied in 5% eccentric case. From velocity profiles, it is observed that, the profile shape gets changed to plug profile from parabolic shape and recirculation region is observed just after the stenosis. The study observed following conclusion in 5% eccentric case;

a) periodic and localized transition to turbulence is observed in post stenotic region,

b) at early and mid-acceleration phase no turbulence is observed in post stenotic region.

c) But the vortexes were formed at early acceleration stage.

Varghese et al. (2008) conducted a detailed comparison of popular two-equation turbulence models (low Reynolds number k–ω model, low Reynolds number RNG k-ε and realizable k-ε model) to predict their ability to represent flow through an eccentric stenosis. The eccentric geometry considered by Varghese et al. in their previous studies (2007a, 2007b) was used for this study as well. Poiseuille parabolic profile was applied at inlet and

Re value of 1000 is selected for the study. The low Reynolds number k- ω model predicts jet extended up to 5D only, but in DNS simulation jet was observed up to 11D. Similar differences were observed in other two models (low Reynolds number RNG k-ε and realizable k-ε model) as well, when compared with DNS results. In both the models, jet was extended only up to 3D distance. The study also conducted LES simulation in eccentric stenosis, their velocity profiles were compared with DNS results. Both results were in good agreement up to 4D distance from throat of the stenosis. The study concluded that RANS based approach is unable to give satisfactory solutions or represent the turbulence effect. The study concluded that LES based approach is more reliable and promising.

Tan et al. (2008) used magnetic-resonance image-based model of carotid bifurcation with 70% stenosis. The study engaged transitional version of shear stress transport (SST) and its scale adaptive simulation (SAS) variant with pulsatile inlet flow as boundary condition. In case of carotid artery blood was modelled as Newtonian fluid with density of 1176 kg/m^3 and viscosity of 3.34 mPa s. At inlet, pulsatile flow profile was applied. For validation of above models, geometry similar to the one used by Ahmed and Giddens (1983a, 1983b, 1984) was selected and the simulations were carried out. The results were compared with experimental results of Ahmed and Giddens and found that transitional SST gives better results than other models. The peak WSS observed in laminar flow is 16.3 Pa and transitional SST 1.5 and its SAS variant predicted 18.7 Pa. Axial WSS analysis showed no difference in results between the transitional model and its SAS variant. At an axial distance (Z) of 4D the turbulence fluctuations were very high in both transitional SST 1.5 and its SAS model. The study concluded that the transitional version of SST and its SAS variant has given better results with experimental data for pulsatile flow in an axisymmetric stenosed tube than laminar and their standard models.

A comparison of LES and RANS turbulence models for the prediction of transitional flow is done by Tan et al. (2011), using the same geometrical configuration (75% stenosis) of Ahmed and Giddens (1984). Transient inlet flow with Re value, 1000 is selected for the study. Vorticity, velocity profiles and turbulence intensity profiles were compared with already existing DNS results and experimental results. The results were in

good agreement with each other. The study observed flow transition to turbulence in post stenotic region which is clearly indicated in vorticity contours. The reattachment point predicted by Transition SST model is similar to the prediction made by LES and experimental results. It was reported that LES model gives better results compared with other models. However, LES simulations were computationally costly when it comes in patient specific models. But the Transition SST model managed to capture important flow features like flow separation, reattachment, and velocity profiles like experimental data. Hence Transition SST model can be used effectively for patient specific models to analyse transient flow.

Guleren (2013) simulated pulsatile flow in triangular wedge-shaped stenosis using LES model. The study observed significant pressure drop across the stenosis and noted that the flow separates from the diseased wall at the throat and quickly re-attaches at X/D ~ 3 (D - tube diameter, X - axial distance). Vortex dynamics and coherent structures were significantly altered by the inflow variations. WSS is found to change not only by the high shear rate but also by the turbulence effects, especially at post-stenotic region. Wu et al. (2015) analysed transient flow through partially occluded elastic arteries to study the effect of stenosis on hemodynamic parameters like WSS, wall pressure gradient and pressure drops by using Fluid Structure Interaction (FSI) model. Blood was modelled as Newtonian fluid with density 1050 kg/m^3 and viscosity as 0.0034 Pa s. In FSI simulation the vessel wall was modelled as elastic material. The study observed maximum WSS at stenotic region. The study suggests that to get more accurate details on deformations and WSS, the vessel wall should be modelled as viscoelastic in nature.

Jabir and Lal (2016) investigated the steady and pulsatile flow past an elliptic-vertically shifted stenosis in carotid artery using LES model. No slip condition was applied at vessel wall. Initially in the first part of validation, LES is carried out in an ideal geometry, selected from the experimental work of Ahmed and Giddens. In second part of the study, elliptical stenosis is selected and applied parabolic steady profile and carotid pulsatile flow at inlet. In steady case Re values in the range of 500 to 1000 were selected and studied the velocity profiles and recirculation region in detail. In post stenotic region, the velocity profile is deflected towards the one side of the pipe. Strong recirculation zones

were observed in post stenotic region. The recirculation zone length at Re value 500 is 8.5D from throat. For Re value 1000, it is only 3.5D. The contour plots of vorticity gave much clear picture about the turbulence zone in the post stenotic region. The study concluded that at steady flow, for all Re values (500 to 1000), flow undergoes transition to turbulence. Under pulsatile flow recirculation zones are observed between 3D and 7D in post stenotic region. The flow disturbances were observed up to 10D and these disturbances were high in deceleration phase. The study observed high level of randomness in WSS distribution due to turbulence effect.

Mahalingam et al. (2016) quantitatively analysed turbulent transition during pulsatile flow through coronary arteries for varying degree of stenosis (i.e., 0%, 30%, 50% and 70%) by considering arterial wall as rigid, using transition SST k-ω model. Blood is treated as non- Newtonian fluid and no slip condition was applied at vessel wall. Patient specific images were selected from intravascular ultrasound. WSS values of laminar and SST k-ω model was compared and observed that, the values of WSS increases with increase in turbulence level in the blood flow. By comparing WSS and Oscillatory shear index (OSI) values of both laminar and transition model, the study observed difference in values and confirmed the presence of turbulent zones. The turbulence intensity was also plotted in each stenosis case and found that the turbulence intensity increases significantly for 70% stenosis compared to 50% or lower stenosis cases. It was found that the onset of transition to turbulent flow seemed to occur from 50% stenosis.

Earlier studies considered blood flow as laminar one. However, to account the turbulence and transition stages, the researchers started considering turbulence flow models. It was found that the DNS and LES model are more accurate to capture turbulence effectively but requires more computational power and time. SST k-ω model gives comparatively good results than other models in transition region with less computational power, thus saving time and will be a good choice to represent transient flow for patient specific models.

Blood is a two-phase mixture comprising of red blood cells, white blood cells, platelets, nutrients, etc. suspended in an aqueous solution called plasma. Due to its multi-component nature, blood exhibits complex rheological properties. The rheological

characteristics of blood are determined by the properties of these components and their interaction with each other.

Newtonian fluid obeys Newton's law of viscosity while non-Newtonian fluid does not obey it. While the plasma essentially is a Newtonian fluid (Schlichting, 1968), the blood as a whole behaves like a non-Newtonian fluid (Ku, 1997; Biswas, 2002; Phillips and Roberts, 2011). In computational fluid-dynamics, the assumption of Newtonian flow (i.e., constant viscosity) is generally accepted for blood flow in large-sized arteries, such as the aorta (Chatzizisis et al., 2007), where the shear rates are high, while the non-Newtonian behaviour of blood has to be taken into account in small arteries (Fournier, 2017). Pedley (1980) mentioned that in a cardiac cycle, there is a point where shear rate goes below 100 s^{-1}. Literature review in the following section focus on understanding the best model (Newtonian or non-Newtonian) to represent hemodynamics in a stenosed artery in best way.

2.3.2. Newtonian and non-Newtonian models

The computational studies which used ideal stenosed coronary artery geometry with Newtonian models are Nosovitsky et al. (1997), Ghalichi et al. (1998), Long et al. (2001), Ryval et al. (2004), Beratlis et al. (2005) and Tan et al. (2011). Gijsen et al. (1999a) conducted experiment and numerical study in carotid artery using finite element method under steady flow conditions for comparison of Newtonian and non-Newtonian model. The study analysed velocity distribution along the flow and observed striking variations between two models. The experimental and numerical results are in good agreement with each other in both the Newtonian and non-Newtonian cases. The study could very well predict the presence of the shear layer, high velocity gradients near the divider wall and flow reversal near the non-divider wall. The study further noted that the flow separation as observed in non-Newtonian case is absent in the Newtonian model.

To study the impact of the non-Newtonian properties of blood on the velocity distribution, Gijsen et al. (1999b) conducted both experimental and numerical study under transient flow. Carreau Yasuda model (non-Newtonian model) was employed for the computation. Experimental and numerical methods gave results which are in good

agreement to each other in both cases. From the results they observed that, at peak flow, the axial velocity profiles are blunt shape. The difference in flow velocity is more visible in the beginning of diastole in case of both fluids. Flow reversal occurs in case of non-Newtonian fluid. In non-Newtonian fluid case, a secondary flow gradually gets developed in the post stenotic region and were visible from velocity profiles.

Johnston et al. (2004) carried out a comparison between Newtonian and five non-Newtonian models and observed the importance of selecting non-Newtonian models during transient flow simulation in small artery. Blood is assumed as an incompressible fluid with a density of 1050kg/m^3, artery is considered as a rigid tube and velocity profile is assumed as paraboloidal shape with no slip condition applied at the wall. They observed Carreau model as the best to mimic blood viscosity. Johnston et al. (2006) carried out transient simulation in right coronary artery as extended work of their previous paper. In this paper they formulated a factor, known as non-Newtonian importance factor and found out from WSS results that at some phase of transient flow, shear rate goes below 100 s^{-1}. The non-Newtonian behaviour of blood is significant during those phases at this shear rate (Pedley, 1980).

Chen et al. (2006) selected non-Newtonian model (Carreau model) for their studies in stenosed coronary artery with bypass. Differences in axial velocity profiles, secondary flow streamlines and WSS between the non-Newtonian and Newtonian fluid flows are reported in the study. It was found that non-Newtonian property alters WSS and flow pattern. Liu and Tang (2011) simulated blood flow in right coronary artery to investigate the effect of non- Newtonian blood property on WSS distribution. Two non-Newtonian blood models (Carreau and Power law model) and the Newtonian blood model were selected for the study. The study observed that at minimum flow rate, the Newtonian model gives an underestimated WSS. It was also noted that Power Law model produced high WSS compared to the other two models at low flow rate. At maximum flow, Carreau model gives good results compared to other models. The studies' overall conclusions were similar to that made by Johnson et al. (2004 and 2006).

Table 2.1 List of Newtonian /non-Newtonian model studies in arteries

Investigators	Geometry	Stenosis	Newtonian vs non-Newtonian model
Nosovitsky et al. (1997)	Ideal	axisymmetric	Newtonian
Ghalichi et al. (1998)	Ideal	axisymmetric	Newtonian
Long et al. (2001)	Ideal	axisymmetric	Newtonian
Ryval et al. (2004)	Ideal	axisymmetric	Newtonian
Johnston et al. (2004, 2006)	Coronary angiogram data	-	Newtonian and non-Newtonian model comparison
Beratlis et al. (2005)	Ideal	axisymmetric	Newtonian
Chen et al. (2006)	Ideal Stenotic coronaries	axisymmetric	non-Newtonian model
Jeong et al. (2009)	Non-stenotic coronaries Ideal	-	non-Newtonian model
Liu and Tang (2011)	Non-stenotic coronaries Real, 3D	-	non-Newtonian model (Power law)
Tan et al. (2011)	Ideal geometry	-	Newtonian
Kabinejadian et al. (2012)	Non-stenotic coronaries Ideal	-	non- Newtonian model (Carreau-Yasuda)
Wu et al. (2015)	Ideal geometry	axisymmetric	Newtonian
Jabir and Lal (2016)	Ideal geometry	eccentric	non- Newtonian model (Carreau)
Mahalingam et al. (2016)	In vivo coronary stenosed artery	eccentric	non- Newtonian model (Carreau)

Kabinejadian et al. (2012) simulated blood flow through graft section, to investigate the effects of wall compliance and non-Newtonian properties on hemodynamic properties. The flow is considered as a laminar one and blood was modelled as non-Newtonian fluid. In this study, vessel wall was modelled as linear elastic material. The study found that, wall compliance and non-Newtonian behaviour of fluid are inter-dependent. Jabir and Lal (2016) applied Carreau model to represent blood viscosity in eccentric stenosed artery and Mahalingam et al. (2016) used it in patient specific geometry. Table 2.1 mention the main computational studies regarding the use of Newtonian and non-Newtonian models in coronary arteries, either in ideal or real (i.e., patient-specific) geometries.

From literature review it is observed that the shear rate goes below 100 s^{-1} in some phases of cardiac cycle, under transient flow. At that shear rate non-Newtonian behaviour is prominent in small arteries like coronary artery (Pedley, 1980; Huang et al., 1987). It is also noted that the WSS difference between Newtonian and non-Newtonian model were high during the deceleration phase of the pulse. Hence, the selection of blood as non-Newtonian fluid is more appropriate to represent the hemodynamics in coronary artery.

The hemodynamic parameters which are directly related to the formation and growth of stenosis are WSS and FFR. The severity of CAD can be identified and measured by using these parameters and are discussed in the subsequent sections.

2.3.3. Hemodynamic parameters

WSS is defined as the tangential stress on the endothelial surface of the arterial wall. The WSS levels for healthy arteries (coronary artery) were reported to vary between 2 to 16 Pa (Cheng et al., 2007). The behaviour of WSS is an important factor in the genesis and progression of wall deformations in vessels and subsequent wall rupture. Even a small variation of velocity gradient can lead to large effects on the WSS. Higher values of WSS lead to maximum damage of endothelial cell in arteries. When the WSS value goes below the physiological levels of (2 Pa), plaque accumulation is triggered aiding to the progression of stenosis. Thus, high, and low values of the WSS for an artery are critical for the initiation and progression of the atherosclerosis.

FFR is an index used by medical practitioners in defining the severity of stenosis in a patient. Basically, it measures the difference in blood flow when there is a block/ stenosis. There are devices and equipment to measure FFR directly, but the techniques involve invasive procedures and are costly. However, this method cannot be used for patients in critical stages like admitted on behalf of a heart attack, severe chest pain etc. The critical parameters like WSS and FFR, which influence the hemodynamic in stenosed coronary artery are reviewed in subsequent sections.

2.3.3.1. Wall Shear Stress

During the last two decades, many research studies like in-vitro experiments, including clinical observations and numerical simulations have been conducted to study the WSS distribution pattern and to investigate the correlation between the WSS and the localization of lesions and the intima-media thickness. Fry (1968, 1969) conducted experiments in descending thoracic aorta of dogs and observed turbulence and increased high wall shear stresses in stenotic region. It causes degeneration of endothelium cell, further they observed that the endothelium cells appear to remain normal till WSS reaches a critical value of ~ 37.9 Pa. In contrast to Fry's study, Caro et al. (1971) claimed that atherosclerosis occurs in regions of low WSS. Several researchers tried to investigate the conflict within these two hypotheses by Fry and Caro. Zarins et al. (1983) conducted experimental study in carotid artery and measured velocity, using LDA method. The study confirmed the low WSS theory. The study noticed that the intima layer is thicker than normal layer at low WSS region. They also observed that atherosclerosis is developed in low WSS region (1.5 Pa).

Ku et al. (1985) conducted study in carotid artery with pulsatile inflow and velocity was measured using LDA. The fluid selected for the study was a mixture of water and glycerine with kinematic viscosity of 0.12 cm^2 s^{-1}. The study observed that low WSS regions (less than 1 Pa) are more prone to development of plaques. They concluded that temporal variations of WSS on the artery wall have a strong influence on atherogenesis. Friedman et al. (1986) have performed experiment in aortic bifurcation and measured fluid velocities using LDA. The study tried to detect any relationship between thickness of artery layers and shear rate. The results revealed that regions of thinner intima thickness exhibit

higher shear rate. Flow transitions were observed at various locations. De Paola et al. (1992) conducted experiments to study about the variation of WSS in blood vessels. The study noticed that low WSS area is more prone to plaque collection. This is the first study to concentrate on analysis of WSS gradients in plaque region. The study observed higher WSS gradients in plaque collection region and it imparts morphological and functional changes in the endothelium cells.

Ku (1997) carried out a detailed review of stenosis flow studies and the importance of fluid mechanics in clinical medicine. The study observed that,

a) Turbulence and vortex regions are developed in post stenotic region of the stenosed artery,

b) The disturbance is very high in post stenotic region,

c) Three-dimensional study gives more idea about turbulence.

High shear stresses are observed at throat of the stenosis, and it can activate platelets collection and thrombus formation. The one of the best indicators for surgical treatment of arteriosclerosis is the degree of stenosis. The study compared different diagnosis methods. Standard angiography uses radio opaque contrast agent, and a catheter is inserted inside body where study is required. Ultrasound studies have problem with sample volume, transit time, and scattering. Plethysmography study is not able to select exact location of lesions. Intravascular pressure catheterization is invasive and difficult. Magnetic Resonance Imaging (MRI) has no interference with the flow and study can be done easily. The risk associated with MRI is less and give good results compared with the other techniques explained above.

Malek et al. (1999) studied the low and high WSS in stenosed artery (50% and 75% stenosis). The variation of WSS values changes with geometry of artery. In post stenotic region low WSS region is developed and trigger plaque collection. Berger et al. (2000) noticed similar observations that previous researchers got. Low WSS regions are mainly observed in curved surface, bifurcations, sudden change in geometry etc. In post stenotic region flow separation and secondary flows were observed. Long et al. (2001) studied the

WSS variations in axisymmetric and asymmetric stenosis cases in detail. They observed a varying and fluctuating WSS distribution in the post stenotic region. In both cases of axisymmetric and asymmetric stenosis, the secondary peak fluctuation (at post stenotic region) of WSS is observed at 2D distance from throat of the stenosis, in case of 50% case and at 6D distance in 75% case. Further WSS value drop rapidly after the stenosis, and it has prolonged fluctuations extending up to 15D distance in case of 75% stenosis for asymmetric case. The effect of stenosis on WSS fluctuations extends from 4D (at 25% stenosis) to 20D distance (75% stenosis) for axisymmetric cases.

Varghese et al. (2003) applied pulsatile inflow condition in their four-model turbulence comparison study conducted in 75% axisymmetric stenosis. WSS maximum is observed at stenosis region during peak flow and minimum WSS occurs at minimum flow condition. Varghese et al. (2007a, 2007b) selected Re = 500 and 1000 in their axisymmetric (75% stenosis) and eccentric stenosis case. In axisymmetric case, Re and WSS at throat of the stenosis increase by more than thirty times with respect to their upstream values. In eccentric case, transition from laminar to turbulence is observed in post stenotic region. WSS undergoes large variations at transition region. The magnitudes of WSS drop rapidly within the diverging section of the stenosis along with occurrence of flow separation. Flow reattachments gives rise to small jump, and subsequent dip in WSS profile, and it travels further downstream with the reattachment location as the cycle progresses. Shear stress magnitudes increase drastically under peak inlet flow conditions.

Tan et al. (2008) compared Laminar flow, standard k-ε and transitional SST k-ω and its variant model of scale adaptive simulation (SAS) in 70% stenosis. WSS values from SAS and transitional SST produced same results as experimental data of Ahmed and Giddens (1984). WSS values begin to rise in stenosis region and maximum is observed at the throat of stenosis. WSS values in flow reattachment locations are better captured by transitional SST k-ω model than other models. Pulsatile flow in triangular wedge-shaped stenosis is simulated by Guleren (2013) and plotted WSS profiles of lower and upper walls of stenosis. Flow separation is observed in post stenotic region, and it is identified from bell-shaped curves in WSS plots of lower walls. The bell shape of curve is extended up to half of diameter. The variation of WSS in case of upper wall is different from the lower wall. The bell-shaped curves on the upper walls are higher and wider than lower walls. The

results show that, the flow near the upper wall is more turbulent in this stenosis case than that near the lower wall.

LES model is applied for an eccentric stenosis in carotid artery by Jabir and Lal (2016). WSS along top and bottom boundary curves of the pipe surface are plotted and intense fluctuations were observed in post-stenotic region, between 4D and 6D distance from the throat. The secondary peak reaches ~ 50 Pa between 4D and 6D, where flow becomes turbulent. At the end of systole, peak value of WSS drops and fluctuations were observed beyond 6D. Stone et al. (2018) conducted a statistical study to investigate relationship between low WSS and cardiac events. The study was conducted in 697 patients undergoing major adverse cardiac events. The study extended up to 3-4 years. The study found that the some of the lesions did not lead to cardiac events. The value of low WSS found in this group is 1.3 Pa. The WSS value above 1.3 Pa were noted as high WSS in this group. The study also tried to group the lesions, based on the necrotic core dimension presented in images. The study observed that the presence of low WSS added high risk to acute cardiac patients. The non-acute lesions with low WSS were observed to be a reason for major cardiac events in future. The cut-off value of low WSS (1.3 Pa) may vary depending on the sex and body mass index.

2.3.3.2. Fractional Flow Reserve

FFR measured during Invasive coronary angiography (ICA) is the gold standard for lesion-specific coronary revascularization decisions in patients with CAD. The primary aim of the FFR-CT (Computed Tomography) is to identify ischemia noninvasively. FFR is defined as the ratio of pressure after stenosis to pressure before stenosis. pressure upstream of a stenosis to the pressure downstream of the stenosis. The FFR index is an absolute number and can be used to represent the severity of stenosis in coronary artery as this index is customarily used as a mathematical check for the clinical estimation of atherosclerosis.

Muller et al. (2011) selected 6107 patients and carried out the measurement of FFR. The present study is long term study (3 to 5 years) and angiogram for Left Anterior Descending artery (LAD) is taken having stenosis 50% and above. The study reached at

conclusion that, patients with FFR values above 0.80 can be treated with medication. When the FFR value goes below 0.80 the treatment procedure is different. Some patients undergo coronary artery bypass graft surgery and Percutaneous coronary intervention (PCI). The patients with FFR value above 0.80 (no significant stenosis) survived for 5 years and more. Pijls and Sels (2012) explained how FFR is calculated using inserted catheters inside patient's body. For a normal person the FFR value is near to one. The study noticed that the cut off or threshold value is between 0.75 and 0.80. Stenosis with FFR less than 0.75, always develop ischemia. During acute myocardial ischemia the procedure is not acceptable. This is the main limitations of FFR study. De Bruyne et al. (2012) focused their study on FFR in a stable coronary stenosis. The statistical study was conducted in 1220 patients. Percutaneous coronary intervention was applied by inserting guidewire inside body. In 880 patients the FFR value was greater than 0.80. In 330 patients the FFR value is less than 0.80 and critical cases required medical help. The study concluded that, for stable coronary artery disease having at least one stenosis with an FFR of 0.80 or less, FFR-guided PCI is the best method for assessing the severity.

Morris et al. (2013) conducted PCI (invasive study) to find out the FFR. Nineteen patients were selected for the study and underwent rotational coronary angiography and guide wire insertion for FFR measurement. The critical lesions were found out and replaced by stent. The study grouped lesions, based on FFR value such that; FFR $\leq$ 0.80 as physiologically significant and others not. The study has following disadvantage:

(1) The study required rotational Coronary Angiography, which is not universally available, involves more risk to perform the procedures as it is invasive method.

(2) The accuracy of results dependent on resolution of invasive Coronary angiography machine.

Nørgaard et al. (2014) conducted study to determine FFR from coronary computed tomography angiography. The study selected 254 patients to determine FFR and underwent invasive coronary angiography. Thuesen et al. (2018) conducted study in patients with coronary stenosis which replaced graft. The study was conducted in 100

patients in a span of 6 month and FFR was calculated using guide wires. The study took FFR threshold value as 0.80. FFR is calculated before and after graft surgery. The study noticed that the FFR value is reducing and reached safe section (FFR $\geq$ 0.80) in some patients. But the study concluded that FFR based graft surgery also had higher failure.

From numerical, clinical and experimental studies it is well established that the biomechanical forces like WSS and pressure have an important role in deciding the development and progression of stenosis. The low and high values of WSS affects the normality of endothelial cells. The studies in humans and other mammals reveal that, low WSS region undergoes higher plaque growth compared to high WSS regions. From literature it is clear that, high WSS region may lead to bursting or rupturing of artery wall. The low WSS region aids to the collection of fatty or other undesirable substance, which may increase the stenosis size. FFR is an index used for judging or to estimate the severity of blockage by assessing the pressure drop across stenosis. FFR assessment in real, is an invasive technique with lot of associated risk involved in it. Hence, the obtention of FFR using non-invasive technique pose high importance. FFR values in CAD patients varies with elemental composition of the blood and its properties. One of the main factors affecting FFR is blood viscosity. The blood viscosity has a significant relation with disease like diabetes and CAD. Various statistical studies and research works are being conducted across the globe to identify the relation between diabetes and blood viscosity. Following section discuss the studies in patient cases to identify the corelation of diabetes with stenosis.

2.4. Effects of blood viscosity on diabetic patients with atherosclerosis disease

There are various statistical studies analysing the cause and criticality of heart disease across the world viz., Framingham heart study, since 1948. These studies were done over a sample volume and tries to identify the correlation of each medical or biological condition on the heart disorders. All such studies observed significant relation among disease like diabetes and heart disease. The out-turn of the studies suggest higher chances of CAD and its criticalities in patients with diabetes. Further the studies observed

occurrence of CAD in young people having diabetes at their early ages compared to other population.

The criticality of Atherosclerosis diseases (CAD) in diabetic patients are high. Plaque development is mainly due to the collection of fatty materials (Called low-density lipoprotein or LDL) inside blood vessel. LDL is also known as 'bad cholesterol'. The other most common type of fat in the body is Triglycerides. The high level of triglyceride and LDL (bad cholesterol) promotes the collection of fatty deposits within artery wall. This will increase the risk of heart attack and stroke. Increased triglyceride levels in blood effects the normal function of pancreas, which produce insulin to control blood sugar in human body. Finally, pancreas loses its ability to produce insulin leading to diabetic condition. In patients with diabetes, the blood viscosity levels are observed to be varying.

Several studies were conducted on sample populations with diabetes having CAD and patients without diabetes to identify a relation with any rheological parameter. The studies observed noteworthy relation with blood viscosity and diabetes.

Barnes et al. (1977) studied the effect of diabetes on blood viscosity by conducting statistical study in diabetic patients and compared with control population. The study conducted in 64 diabetic patients and whole blood viscosity was measured. The study noticed that in diabetic group the blood viscosity values were two times higher than the normal person's viscosity level. The study also noted that the rigid cells and increased viscosity may lead to the plaque collection in small arteries of diabetic patients.

A detailed study was carried out by Steiner (1981) to know the various phases in the process which leads to atherosclerosis in diabetic patients.

Different phases in the process are as follows

(1) An injury to the endothelium cells (inner layer of artery wall) aggregates the platelets.

(2) Diabetes alters the balance between prostacyclin (prevent platelets aggregation) and Thromboxane (to clot blood) levels.

(3) The diet and polyunsaturated fat also alter the platelets collection.

(4) Lipoproteins, particularly LDL and remnants, can enter these cells and begin the process of lipid deposition.

The above alteration in human body leads to the risk of atherosclerosis. The study also mentioned that atherosclerosis is the most complicated outcome of diabetic patients.

Pyorala et al. (1987) conducted a detailed review of atherosclerosis in diabetic patients and tried to find out the answers for following

(1) The study discusses about the risk factors of atherosclerosis and their impact on diabetic and non- diabetic patients.

(2) Frequency of atherosclerosis in diabetic and non- diabetic patients.

Autopsy study in diabetic patients revealed that size of atherosclerosis in coronary artery is large compared to non- diabetic patients. Study also collected patient data of 2300 cases with coronary atherosclerosis and noted that diabetic patients had excessive complicated lesions (stenosis lesions). Another autopsy study conducted for 1700 cases and revealed that, calcified lesions collection area is large in diabetic cases compared to non-diabetic. The severity of coronary atherosclerosis was high in the diabetic group and glucose intolerance group than in the normoglycemic group. The extent of coronary atherosclerosis at any age of adult life is greater in diabetic patients than in non-diabetic cases. Death due to coronary heart disease in diabetic patients is high compared to non-diabetic patients. The frequency of silent attack is higher in diabetic patients.

Krolewski et al. (1991) conducted statistical study in a group of aged people with diabetes and without diabetes. The study noted that the risk of CAD increases with duration of diabetes. The study could not identify the exact co relation between diabetes and atherosclerotic lesions. Lowe et al. (1997) conducted study in 1592 men and women aged 55-74 years (the Edinburgh Artery Study) in 5 years follow up to know the relation between blood viscosity and CAD. The study prepared a questionnaire and blood test results like; High density lipoprotein (HDL) cholesterol and triglycerides were collected. The study followed American Heart Association protocol. For statistical analysis SPSS-X and SAS software packages were used. In 5-years, 273 patients were dead. The study noted following observations

(1) Whole blood viscosity was higher in subjects undergoing cardiovascular event.

(2) In patients with high blood viscosity, haematocrit and plasma fibrinogen levels are high

(3) Higher levels of blood viscosity, haematocrit, plasma viscosity and fibrinogen were observed in persons who experienced a stroke.

(4) Age and sex along with increased blood viscosity shows good relationship with cardiovascular events.

(5) Decreased red cell deformability was not a major cause of high blood viscosity.

The study concluded that blood viscosity is a strong predictor of cardiovascular events in the older population, along with LDL cholesterol level or diastolic blood pressure. The study also noted that, plasma viscosity and fibrinogen show association with cardiovascular events. The present study suggests that increased blood viscosity may be one mechanism by which hyperfibrinogenaemia (abnormally high level of fibrinogen in blood) may promote cardiovascular events.

Tamariz et al. (2008) checked the hypothesis that blood viscosity increments lose the insulin production which control the sugar in blood and leads to type 2 diabetes. The study selected 15,792 adults aged 45-64 years. The samples were selected from following places: Forsyth County, North Carolina; Jackson, Mississippi; the northwest suburbs of Minneapolis, Minnesota; and Washington County, Maryland. The following data were collected: Information on age, sex, race, educational attainment, cigarette use, physical activity, and parental history of diabetes etc. Analyses were performed by using SAS software. The study noted that blood viscosity is co-related with systolic blood pressure, fasting glucose, insulin, fibrinogen, white blood cells, and triglyceride levels etc. Therefore, the elevated levels of blood viscosity and haematocrit requires special attention which is one of the reasons for type 2 Diabetes mellitus (DM).

Cho et al. (2008) analysed statistical research works conducted in the field of whole blood viscosity variation in patients with diabetic mellitus. The study observed that, DM alters/ stiffens the erythrocyte and significantly increases the blood viscosity. Irace et al.

(2014) conducted a statistical analysis to identify the relation between blood viscosity and blood glucose level. The study observed interconnecting relationship between both parameters in their sample studies. Richards and Nwose (2010) carried out a statistical study in different samples to investigate the variation of blood viscosity at different stages of diabetes. The study selected 266 samples, which includes details of family history of diabetes, prediabetes, prediabetes with Cardiovascular disease (CVD), DM and DM+CVD etc. The study extended for one year. The study noted that the whole blood viscosity increases at different stages of prediabetic and diabetic cases.

Larsson et al. (2018) tried to find out association between type 1 Diabetes mellitus (DM) and specific cardiovascular diseases. The study also identified relation between DM in relation to risk of aortic valve stenosis, atrial fibrillation, abdominal aortic aneurysm, and intracerebral haemorrhage etc. Study was conducted in 71,483 adults. From the study it was found that DM is associated with an increased risk of myocardial infarction, heart failure and ischemic stroke. DM patients were less likely to be diagnosed with abdominal aortic aneurysm and intra-cerebral haemorrhage. The statistical study concluded that in diabetic patients the risks of cardiovascular diseases are high.

From the above statistical studies, it is concluded that blood viscosity is one of the parameters that varies with time in diabetic patients. The study reveals that blood viscosity of a diabetic person can go as high as 10 times the blood viscosity of normal person. The studies also noted that in diabetic patients, the stenosis formation tendency is very high compared to non-diabetic patients. Hence, the present study considered the impact of high blood viscosity on diabetic patients with CAD.

The literature review analysed various experimental and numerical studies conducted in the field of blood flow in a stenosed coronary artery. In the early days, experimental works were carried out by various researchers, but difficulties in conducting experimental studies and limitations in measurement techniques reduced the development and growth of such studies. The experimental works could identify the flow transitions in a stenosed artery. With the development of CFD techniques and numerical methods a new window is opened for the researchers in this field. The CFD studies could overcome many of the issues related with experimental studies. Most of the researchers considered laminar

blood flow in coronary artery for their studies. A few of the recent studies considered the flow transition in their studies, applying NS equation directly to solve the parameters along with fine mesh. DNS and LES methods can arrive at better results, but the methods require high computational power and fine meshing of the geometry. Transition SST k-ω model gives comparatively good results with less computational power.

From the analysis of said research works in the subject field, following observations and research gaps were carved out for the present study.

Research Gaps:

- The geometry selected for initial studies are ideal stenosed geometries but in real case it is eccentric. Selection of patient specific geometry is very important for finding hemodynamic variables accurately.
- The early studies considered blood as Newtonian model, but for small arteries non-Newtonian behaviour of blood is prominent.
- The post stenotic flow characteristics and its flow transitions were not evaluated completely in these studies.
- None of the studies generated a mathematical relation incorporating the important hemodynamic variables aiding the diagnosis of CAD (for patient specific stenosed coronary artery under hyperaemic flow condition).
- The studies exploring the statistical relation between diabetic patients having CAD shows good correlation among diabetes and CAD. From the literature review, it was observed that one of the haemodynamic parameters which is high in diabetic patients is blood viscosity. Numerical studies in this area are yet to be carried out.

Hence the present study focusses on the evaluation of critical hemodynamic parameters in patient specific coronary artery during transient flow under hyperaemic flow condition by considering blood as non-Newtonian fluid and establishing a non-invasive method to find the practical diagnosis index for identifying the risk in CAD patients.

2.5. Summary

The literature review included the works related to hemodynamics for laminar and turbulent flow in ideal geometry with axisymmetric stenosis. The review points out the significance of using patient specific coronary artery geometry for hemodynamic analysis to access the risk level in CAD patients. The review also discusses about different types of flow models to represent the blood flow as laminar and turbulent. By comparing the efficacy of different models, it was found that SST k-ω model is the best to represent the transition in flow by consuming less computational power and time. The importance of considering the fluid as non-Newtonian is also elaborated. Impact of blood viscosity and associated risk of CAD in diabetic patients are also debated.

CHAPTER 3

MATERIALS AND METHODS

3.1. General

The thrombus (blood clot) formation and irregularities in the artery geometry are the major factors influencing the occurrence and the growth of stenosis. Most of the studies related to CAD assumed blood flow as laminar and the geometry of coronary artery as ideal because of the complexity observed in real geometry. Few recent studies have investigated the blood flow in stenosed artery as turbulent under normal flow condition. However, turbulent flow condition in patient specific stenosed coronary artery was not investigated in detail under transient flow in hyperaemic state. Replicating the real artery conditions externally was a big challenge for experimental studies demand the use of numerical models. Literature review reported that the studies related to hemodynamics in arteries became easier with the furtherance in numerical techniques and CFD. However, numerical models like DNS and LES used for analysing turbulent blood flow requires high computational power and time. Hence, the current study developed an efficient numerical model for simulating blood flow in a patient specific stenosed coronary artery with relatively less computational power and time by using CFD. This chapter describes the fundamental equations governing the flow, the assumptions, initial and boundary conditions that are required for the solution of the problem under consideration. In the present work, finite volume method was used to discretize the governing equations of fluid flow. The chapter outlines the process of selecting appropriate numerical model and boundary condition for the patient specific stenosed coronary artery. The significant hemodynamic parameters like Wall Shear Stress (WSS) and Fractional Flow Reserve (FFR) are also discussed in the current study.

3.2. Assumptions

Three-dimensional model of fluid is considered for the current study. The following assumptions were used in the analysis.

- The fluid medium is considered as continuum
- Flowing fluid (blood) is incompressible and homogeneous during steady and transient conditions.
- Blood is assumed as non-Newtonian fluid.
- Artery wall is deemed as rigid.
- The cardiac muscle movements are neglected.

3.2.1. Governing equations for fluid flow

Fluid dynamics is governed by fundamental mathematical statements based on three principles in physics viz., (1) conservation of mass, (2) conservation of momentum and (3) conservation of energy. These are the fundamental principles of Computational Fluid Dynamics.

3.2.1.1 Continuity equation (Conservation of mass)

The law of conservation of mass states that the total mass moving into the system is equal to the sum of total mass moving out of the system and the change in storage within the system. The same is represented by the Eqn. 3.1.

$$\frac{\partial \rho}{\partial t} + \frac{\partial (\rho u)}{\partial x} + \frac{\partial (\rho v)}{\partial y} + \frac{\partial (\rho w)}{\partial z} = 0 \tag{3.1}$$

3.2.1.2 Momentum equation (Conservation of momentum)

The motion of fluid is described by Navier-Stokes equations for unsteady 3-Dimensional flow. (Anderson and Wendt, 1995; Fluent Theory Guide, 2012; ANSYS user's manual, 2012). The law of conservation of momentum states that the total momentum in a system remains constant.

The Eqns 3.2, 3.3 and 3.4 represent the conservation of momentum in three directions.

$$\frac{\partial(\rho u)}{\partial t}+\frac{\partial(\rho u^2)}{\partial x}+\frac{\partial(\rho uv)}{\partial y}+\frac{\partial(\rho uw)}{\partial z} = -\frac{\partial \mathrm{p}}{\partial x}+\frac{\partial}{\partial x}\left(\lambda \nabla . V+2\mu\frac{\partial u}{\partial x}\right)+\frac{\partial}{\partial y}\left[\mu\left(\frac{\partial v}{\partial x}+\frac{\partial u}{\partial y}\right)\right] + \frac{\partial}{\partial z}\left[\mu\left(\frac{\partial u}{\partial z}+\frac{\partial w}{\partial x}\right)\right]+\rho f_x \tag{3.2}$$

$$\frac{\partial(\rho v)}{\partial t}+\frac{\partial(\rho uv)}{\partial x}+\frac{\partial(\rho v^2)}{\partial y}+\frac{\partial(\rho vw)}{\partial z} = -\frac{\partial \mathrm{p}}{\partial y}+\frac{\partial}{\partial x}\left[\mu\left(\frac{\partial v}{\partial x}+\frac{\partial u}{\partial y}\right)\right]+\frac{\partial}{\partial y}\left(\lambda \nabla . V+2\mu\frac{\partial v}{\partial y}\right) + \frac{\partial}{\partial z}\left[\mu\left(\frac{\partial w}{\partial y}+\frac{\partial v}{\partial z}\right)\right]+\rho f_y \tag{3.3}$$

$$\frac{\partial(\rho w)}{\partial t}+\frac{\partial(\rho w^2)}{\partial x}+\frac{\partial(\rho uw)}{\partial y}+\frac{\partial(\rho vw)}{\partial z} = -\frac{\partial \mathrm{p}}{\partial z}+\frac{\partial}{\partial x}[\mu\left(\frac{\partial u}{\partial z}+\frac{\partial w}{\partial x}\right)+\frac{\partial}{\partial y}\left[\mu\left(\frac{\partial w}{\partial y}+\frac{\partial v}{\partial z}\right)\right] + \frac{\partial}{\partial z}\left(\lambda \nabla . V+2\mu\frac{\partial w}{\partial z}\right)+\rho f_z \tag{3.4}$$

where,

ρ - Density of flowing fluid, kg/m^3

u,v,w - Fluid velocity components in *X, Y* and *Z* directions, m/s

t – Time, s

p – Pressure, Pa

f_x, f_y, f_z - Body force per unit mass

μ – Dynamic viscosity, Pa.s

3.3. Boundary conditions

The cardiovascular system maintains the blood flow in the system by the rhythmic pumping action of heart. This cyclic operation of heart creates a periodic pulsatile flow fluctuating from zero to maximum in blood vessels. Even though the flow in the human circulatory system is pulsatile, initially ideal steady boundary conditions were selected to provide an insight into the aspects of blood flow through arteries. The Poiseuille flow profile was used in ideal steady flow simulations whereas, Womersley Profile, was used for unsteady/transient flow simulation, as a periodic pulse. To establish a patient-specific boundary condition which accurately represent the realistic condition (transient flow) in an artery, pulsatile velocity and pressure profiles were used (Berne and Levy, 1967; Wiwatanapataphee et al., 2012). The following subsections describe briefly about the details of boundary conditions.

3.3.1. Ideal boundary conditions

3.3.1.1. Poiseuille velocity profile

The steady flow simulation is carried out by applying laminar, fully developed Poiseuille profiles at the inlet. The profile is represented by,

$$U = 2\,u_m\left(1 - \frac{r^2}{R^2}\right) \tag{3.5}$$

where,

u_m - Mean velocity, m/s

R - radius of artery, m

r- radial distance from the vessel centreline, m

3.3.1.2. Womersley profile

Womersley (1955) proposed a procedure for finding the pulsatile velocity field in an artery. The procedure computes the velocity and flow rates from the known gradient of pulsatile pressure. The pulsatile pressure gradient equation for incompressible flow is written as,

$$\frac{\partial^2 w}{\partial r^2} + \frac{1}{r}\frac{\partial w}{\partial r} + \frac{1}{\nu}\frac{\partial w}{\partial t} = \frac{1}{\mu}\frac{\partial p}{\partial z} \tag{3.6}$$

Periodic pressure fluctuation is expressed by

$$\frac{\partial p}{\partial z} - \frac{p1 - p2}{\mathrm{L}} = \mathrm{a}e^{i\acute{\omega}t} \tag{3.7}$$

where,

ώ-angular frequency, rad/s

a-amplitude of pulsation, m

ν - Kinematic viscosity, m^2/s

μ - Dynamic viscosity, Pa.s

The solution presented by Womersley is,

$$\frac{\mathrm{U}}{\mathrm{u_c}} = \left[1 - \frac{\mathrm{r}^2}{\mathrm{R}^2}\right] + \mathrm{a}\left[1 - \frac{\mathrm{J_0}\left(\mathrm{i}^{3/2}\alpha \times 2\mathrm{r/D}\right)}{\mathrm{J_0}(\mathrm{i}^{3/2}\alpha)}\right]\sin(\acute{\omega}\mathrm{t}) \tag{3.8}$$

where,

$\mathrm{y} = \frac{r}{R}$

R - radius of artery, m

r- radial distance from the vessel centreline, m

u_c - cycle-averaged centreline velocity, m/s

$J_0()$ - Bessel function of order zero

a-amplitude of pulsation, m

α - Womersley number ($R\sqrt{\omega/\upsilon}$), rad/s

Fig. 3.1 represents the inlet velocity profile derived from the solution of equation 3.8.

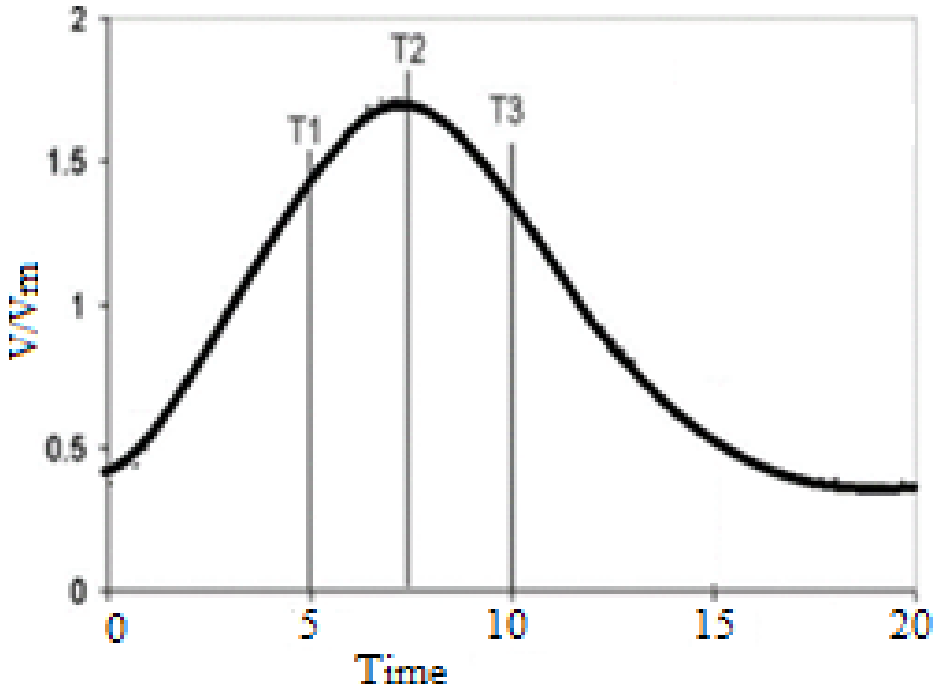

Fig. 3.1 Velocity profile (Ahmed and Giddens, 1984)

3.3.2. Patient-specific boundary conditions

The application of ideal boundary conditions (steady and unsteady flow) could give only an outline view of the hemodynamic variations occurring in stenosed arteries. In order to make accurate predictions of patient specific hemodynamics, real physiological velocity boundary conditions have to be applied. Velocity profile used for FFR study in an ideal coronary geometry are taken for the current study Berne and Levy (1967). Fig. 3.2

shows velocity profile applied at the inlet of an ideal geometry of coronary dimension keeping outlet pressure zero.

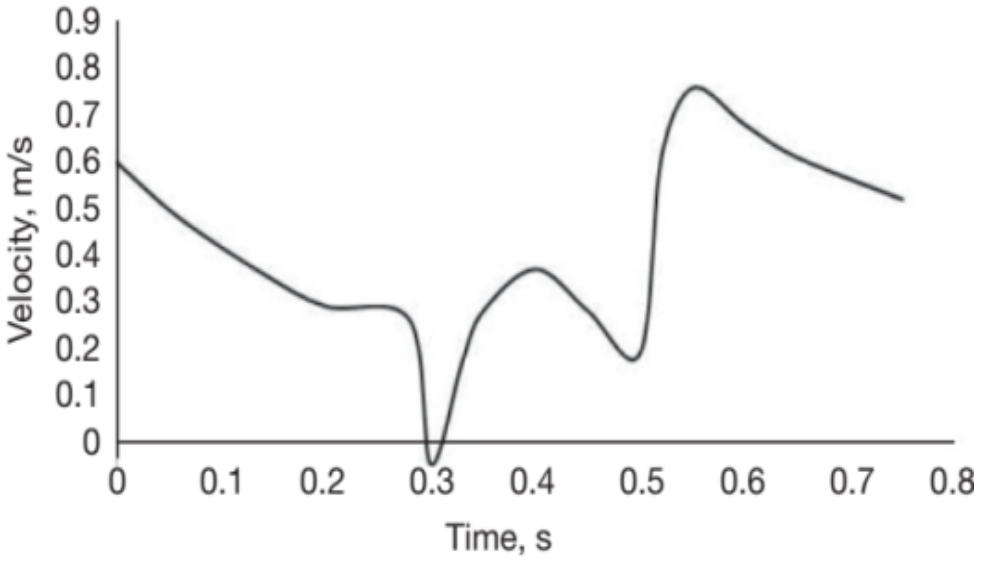

Fig. 3.2 Velocity profile (Berne and Levy, 1967)

To have a better accuracy in the predictions, real boundary conditions (pulsatile velocity and pressure) were applied at the inlet and outlet of patient specific geometries. Eqn.3.9 represents the pulsatile velocity profile applied at the inlet, (Wiwatanapataphee et al., 2012).

$$U(t) = \frac{Q(t)}{A} \tag{3.9}$$

where, Q(t) represents inlet flow rate and A represents cross-sectional area at inlet of the artery. The pressure at the arterial outlet was also represented as pulsatile boundary condition, expressed by Fourier series (Wiwatanapataphee et al., 2012; Attinger et al., 1966). The expressions representing the pulsatile flow rate and pulsatile pressure are given in the equations 3.10 and 3.11 and depicted graphically in Fig. 3.3.

$$Q(t) = \overline{Q} + \sum_{j=1}^{4} \alpha_j^Q \cos(j\acute{\omega}t) + \beta_j^Q \sin(j\acute{\omega}t)$$

(3.10)

$$p(t) = \bar{p} + \sum_{j=1}^{4} \alpha_j^p \cos(j\acute{\omega}t) + \beta_j^p \sin(j\acute{\omega}t)$$

(3.11)

where, Q(t) represents the pulsatile flow rate, $\overline{Q}$, mean volumetric flow rate = 0.1589 l/min, $\bar{p}$, mean pressure, = 84.9722 mmHg, ώ = 2π/t is the angular frequency with a time period t= 0.8 s. A varying mean flow rate $\overline{Q}$ (0.158, 0.237, 0.316, 0.395 and 0.553 l/min) from the normal to hyperaemic flow condition was applied at the inlet (Wiwatanapataphee et al., 2012).

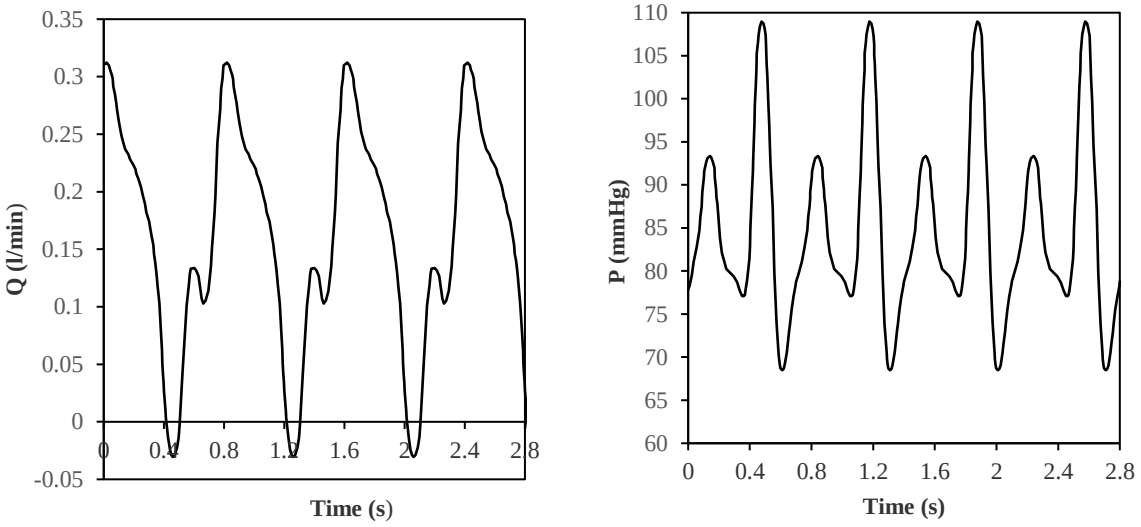

(a) (b)

Fig. 3.3 (a) Pulsatile flow rate; (b) The pulsatile pressure (Wiwatanapataphee et al., 2012)

The constants relate to the normal flow of the Fourier series equations (3.10) and (3.11) are summarized in Table 3.1. For hyperaemic flow conditions at the inlet, the flow profiles of Fig. 3.3(a) are modified with a flow rate corresponding to hyperaemic condition.

Pressure profiles at the outlet were then computed corresponding to the generated flow rate profile at the inlet under hyperaemic condition.

Table 3.1 Values of constants used in Fourier series equations (Eq. 3.10 and 3.11, Wiwatanapataphee et al., 2012)

J	α_j^Q	β_j^Q	α_j^P	β_j^P
1	0.1007	0.0764	-3.3107	-2.2932
2	-0.0034	-0.0092	-9.8639	8.0487
3	0.0294	0.0337	3.0278	3.8009
4	0.0195	-0.0129	2.2476	-3.2564

3.4. Flow models

3.4.1. Laminar flow

Since blood flow in the human body is generally laminar in nature, this study assumes flow as laminar for the initial analysis. Simulation of arterial blood flow with CFD using laminar flow model involves solving of the NS equations directly without any additional terms to include turbulence. Literature review reveals that this model cannot capture the flow transitions and turbulence which is observed in the post stenotic region (Tan et al., 2008 and 2011; Mahalingam et al., 2016). In order to account the effect of turbulence in detail, additional equations are to be solved along with NS equation.

3.4.2. Turbulence flow

Turbulence in fluid flow can be defined as a three-dimensional phenomenon in which variation in flow occurs in all three directions. The flow properties at a point vary randomly with time during turbulent flow. It generates multiple sets of flow vectors (velocity components) randomly forming a chaotic fluid motion. The turbulent flow is characterised by high value of Reynolds number (>4000). The generally used Navier-Stokes equation can solve the effect of turbulence with the help of high computational

power models like DNS model. RANS (Reynolds Averaged Navier-Stokes equation) and LES (Large Eddy Simulation) are other models which employ additional equations to solve flow turbulence.

The first step in RANS approach is the decomposition of flow variables in to its mean and fluctuating parts. Then the time averaging is operated which in turn give rise to an unknown term 'Reynolds-stress tensor. In case of RANS model, two turbulence models are popularly applied in CFD, viz., k-ε model and k-ω model. These models are generally known as two equation models. Following are the different turbulence models used in Computational Fluid Dynamics. (Fluent Theory Guide, 2012; ANSYS user's manual, 2013)

- Spalart-Allmaras
- k-ε models
    - Standard k-ε
    - Re Normalisation Group (RNG) k-ε
    - Realizable k-ε
- k-ω models
    - Standard k-ω model
    - Shear Stress Transport (SST) k-ω model
- Reynolds stress model (RSM) model
- LES

The model of Spalart - Allmaras is a one - equation model which is comparably simple in operating. It was designed explicitly for aeronautics applications. This method is acquiring popularity in turbomachinery applications as well. Industrial applications mainly utilize the standard k-ε model due to the cost effectiveness, robustness and fair accuracy. Some of the k-ε models show zero sensitivity to momentary pressure variations and boundary layer separations, setting a major drawback to this model. They usually envisage

a delayed and narrower separation compared to observation. The k-ε models are generally not recommended for external aerodynamics. Contrarily, k-ω models could normally predict the sudden pressure variations in boundary layer. The SST model could capture flow separations from smooth surface effectively and accurately for its specific calibration. Hence the model predicts the characteristics in wall boundary layer in a better way compared to the Spalart-Allmaras model. It was found that Transition SST k-ω model captures laminar-turbulent transition effectively (Mahalingam et al., 2016). Although LES and DNS give better results, but require highly fine mesh. Hence, the computational power and time required for LES and DNS are also very high.

Shear Stress Transport (SST) k-ω turbulence model was selected for the current study from the available turbulence models as it is suitable for capturing transition flow behaviour correctly (Mahalingam et al., 2016). When blood flows through a stenosed artery, the flow becomes turbulent in the post stenotic region (Re greater than 2000), SST-k-ω model is best suited for representing such turbulent flows (Mahalingam et al., 2016). Unsteady flow simulations can also be carried out using transition SST k-ω model (Tan et al., 2008; Mahalingam et al., 2016). The transitional SST k- ω turbulence model solves additionally two more equations; one representing intermittency (Eqn. 3.12) and other denoting transition onset criteria (Eqn. 3.13). Menter's SST model can be defined as a combination of k-ε and k-ω models. k-ω model is used near the wall and k-ε model, in central flow region. (Tan et al., 2008; Fluent Theory Guide, 2012; ANSYS user's manual, 2013).

The transport equations for k and ω are given as equations 3.12 and 3.13.

$$\frac{\partial(\rho k)}{\partial t} + \frac{\partial(\rho k u_i)}{\partial x_i} = \frac{\partial}{\partial x_i}\left[\Gamma_k \frac{\partial k}{\partial x_j}\right] + G_k + Y_k \tag{3.12}$$

$$\frac{\partial(\rho \omega)}{\partial t} + \frac{\partial(\rho \omega u_j)}{\partial x_i} = \frac{\partial}{\partial x_i}\left[\Gamma_\omega \frac{\partial \omega}{\partial x_j}\right] + G_\omega + Y_\omega + D_\omega \tag{3.13}$$

Where,

k - Turbulent kinetic energy

ω – Specific rate of dissipation

D - cross diffusion term

G_{k-} Generation term of turbulent kinetic energy

G_{ω} - Generation term of specific rate of dissipation

Y_k - Diffusion term of turbulent kinetic energy

Y_{ω} - Diffusion term of specific rate of dissipation

Γ_k - effective diffusivity of k

Γ_{ω} - effective diffusivity of ω

In a highly turbulent flow fluctuation, the particles collide with each other transferring energy and momentum between them is called diffusion mechanism. In general, the momentum is transported from upper layer particles to lower layer particles. It has same direction as velocity gradient. The term cross diffusion is derived in the problem due to the usage of SST k- ω model, which is a combination of k-ε and k-ω model. To blend these two models together, the standard k-ε model has been transformed into equations based on k- and ω, which leads to the introduction of a cross-diffusion term.

3.5. Numerical method

Numerical analysis employs various methods for arriving at the most appropriate solution using numerical approximation. However, the usage of numerical methods was limited mostly to engineering field and physical science problems during early days. With the onset of 21st century this method gained wide popularity in studies related to cardiovascular blood flow and diagnosis of cardiovascular diseases. The method enables the researchers to analyse the blood flow and its physical parameters in a healthy blood

vessel and diseased one. There by aiding the researchers in optimising the design and functionality of vascular medical tools and equipment. Because of the massive evolution in computational technology, the numerical approximation method became most accepted and a contemporary tool for researchers and engineers.

3.5.1. Computational Fluid Dynamics (CFD)

The Computational Fluid Dynamics opened a window for researchers to find near solutions for problems in fluid mechanics which cannot be solved analytically. In an overview, CFD applies the strategy of discretizing a continuous domain problem in to a suitable structured grid. The method defines flow variables in discrete elements instead of defining it continuously. The value of flow variables at other locations are obtained by interpolating the values at elements. The method acquired popularity with the advancements in numerical techniques along with the development of supercomputers.

ANSYS is commercial software having number of tools for continuum mechanics, fluid dynamics and so on. In this study, the flow in artery is analysed using ANSYS Fluent which use FVM for the numerical discretization.

3.5.2. Finite Volume Method (FVM)

In FVM, the flow domain is divided into finite number of small non overlapping control volumes over which the governing equations are discretized. The discretization process yields a set of algebraic equations, which can be solved using iterative methods. Navier-Stokes equations, is discretized by integrating it over the volume of each cell and converted into surface integrals (Eq. 3.14,3.15), (Niyogi et al., 2006; Anderson and Wendt, 1995; Fluent Theory Guide, 2012; ANSYS user's manual, 2013). These surface integrals are then replaced by integrals over the discrete faces of the cell. Values at the faces are then interpolated from cell centre values using suitable interpolation schemes.

Continuity equation:

$$\frac{\partial}{\partial t}\int_{v}^{\cdot}\rho dV + \oint_{s}^{\cdot}\rho(U_i.n)\,dS = 0$$

(3.14)

Momentum equation:

$$\frac{\partial}{\partial t}\int_{V}^{\cdot}\rho U_i dV + \oint_{S}^{\cdot}\rho U_i(U_i.n)dS = \int_{V}^{\cdot}\rho f_e dV + \oint_{S}^{\cdot}[-\mathrm{p}_n + (\bar{\bar{\tau}}.n)]dS$$

(3.15)

Where $\bar{\bar{\tau}}$ = viscous stress tensor

A pressure equation derived from the Navier-Stokes equation is used to connect the pressure-velocity fields as,

$$a_p\bar{u}_p = H - \nabla\mathrm{p}$$

(3.16)

where, a_p is a diagonal matrix containing coefficients obtained from the discretization of convection and diffusion terms, *H* is the residual matrix after extraction of diagonal matrix a_p. The unknowns in the governing equations are pressure and velocity, but there is evidently no equation for pressure. In this case coupling between pressure and velocities were introduced to solve the flow field. Pressure and velocity are coupled using PISO algorithm, explained under section 3.6. Iterations are continued until convergence of the velocity and pressure field is obtained. After obtaining converging solutions, time step is increased. The current values will serve as the initial conditions for the next step.

3.5.3. Solution schemes

To achieve required accuracy, second order discretization techniques must be used. For temporal discretization, a second order accurate, backward differencing scheme is used (Fluent Theory Guide, 2012; ANSYS user's manual, 2013).

The second-order accurate temporal discretization is given by Eqn. 3.17.

$$\frac{3\phi^{n+1} - 4\phi^{n} + \phi^{n-1}}{2\Delta t} = F(\phi) \tag{3.17}$$

ϕ - a scalar quantity

n+1 - value at the next time level t+Δt

n - value at the current time level t

n-1 - value at the previous time level t-Δt

In order to maintain stability *of* the numerical schemes the Courant number (Courant-Friedrichs-Lewy) is utilised for setting Δt. The Courant number is defined as,

$$\mathrm{Co} = \frac{\mathrm{U}\Delta\mathrm{t}}{\Delta x} \leq \mathrm{Co}_{\max} \tag{3.18}$$

where, U is the velocity, Δt is the time step size and Δ*x* is the grid size. The value of maximum Co is kept less than 1 (Co = 0.5) throughout the simulations.

3.6. Pressure - Velocity coupling

To solve pressure-velocity fields, a PISO (Pressure Implicit Splitting of Operators) algorithm-based solver is used (Fluent Theory Guide, 2012; ANSYS user's manual, 2013Jabir and Lal, 2016). The procedure involved are summarised in a flow chart (Fig. 3.4).

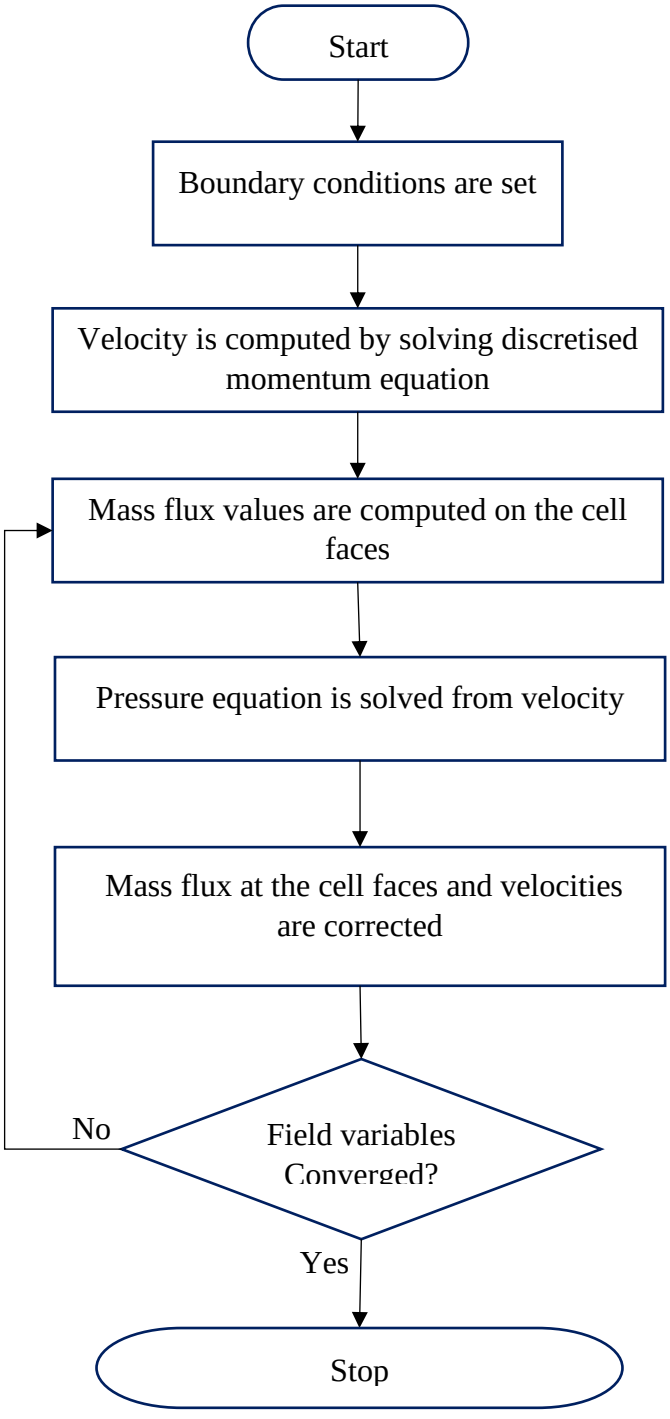

Fig. 3.4 Flow chart of PISO algorithm

3.7. Blood rheology

Blood is assumed as a Newtonian fluid in large arteries like aorta as the shear rate is above 100 s^{-1} in these vessels. However, in case of smaller arteries like coronary artery, the shear rate is found to be less than 100 s^{-1} in some phase of the cardiac cycle (Pedley, 1980). This signifies the application of non-Newtonian behaviour of blood in smaller arteries. This study assumes blood as an isotropic, homogeneous and incompressible viscous fluid, having constant density of 1050 kg/m^3. Carreau model (Carreau, 1972) was used to model the shear thinning behaviour of fluid, which is proven to be appropriate in modelling real blood (Johnston et al., 2004). The dynamic viscosity represented in Carreau model is given by,

$$\mu = \mu_{inf} + \left(\mu_0 - \mu_{inf}\right)\left(1 + (\lambda\dot{\gamma})^2\right)^{\frac{n-1}{2}} \tag{3.19}$$

where,

μ_0 - viscosity at zero shear rate, Pa.s

μ_{inf} - viscosity during infinite shear rate, Pa.s

λ - relaxation time, s

n - power index

$\dot{\gamma}$ - shear rate

Values of the constants and properties of blood are finalised from literature study, Johnston et al. (2004), as μ_0 = 0.056 Pa s, μ_{inf} = 0.00345 Pa.s, λ = 3.313 s, n = 0.3568.

3.8. Geometry acquisition and image segmentation

Patient specific CT scan image (generally known as Digital Subtraction angiography – DSA) is obtained for various stenosis levels. This data contains digital three-dimensional details of the patient anatomy including area of interest - the stenosed blood

vessel. The required geometrical profile (inner lamina of the stenosed vessel) is extracted from the above digital file using appropriate software tool- Vascular Modelling Toolkit (VMTK). Various steps involved in the process are explained below.

The geometry for the study is obtained from the DSA data sheets of patient case. Three dimensional images are built up in the computer system during the scanning process. The scanned image data contains all the anatomical features. The DSA images are stored and handled in a specific standard format called 'Digital Imaging and Communications in Medicine'(DICOM). The required 3D geometry is extracted from the CT image by a process of partitioning DICOM image to multiple segments known as segmentation. In order to segment blood vessel surface from 3D DSA image, a software package VMTK is used. The DSA image was fed in to VMTK (Antiga et al., 2008) software to obtain the patient specific geometry for the study. The superfluous areas (unused area) in the geometry were clipped and necessary smoothing filters were applied. The vessel ends were extended to suitable length for applying standard boundary conditions. The surface thus obtained was exported to Stereolithography (STL) format to carryout mesh/grid generation. The procedure involved are summarised in a flow chart as shown in Fig. 3.5.

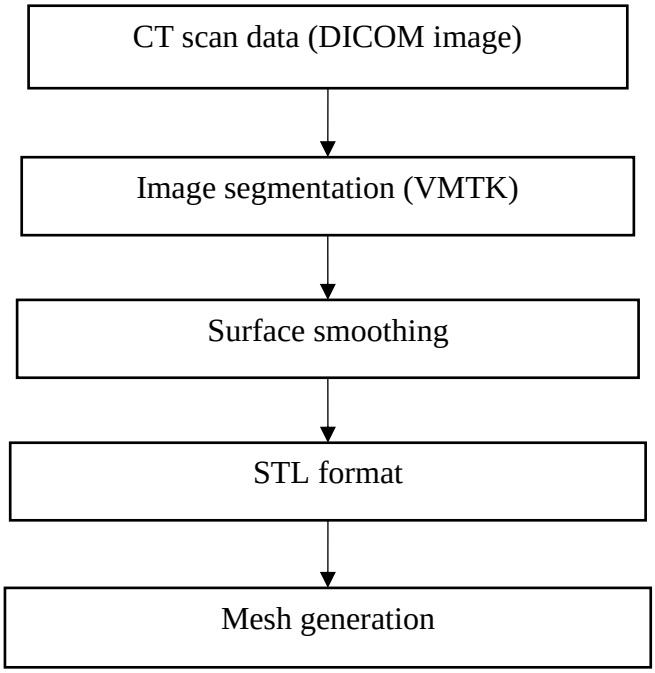

Fig. 3.5 Geometry acquisition procedure – Flow chart

3.9. Grid generation

Hexahedral grid structure was generated using a commercial grid generation package ANSYS ICEM-CFD applying multi-block structured approach. The software includes an interactive interface with tools to ensure good quality and control over hexahedral grid generation. To capture boundary layer features of flow, prism layers were applied near the vessel wall. The mesh generated was converted in to a compatible format for the fluent solver. For patient specific geometries unstructured tetrahedral elements were used for grid generation (ANSYS user's manual, 2013).

3.10. Grid independence study

Richardson extrapolation method (Richardson, 1911; Richardson and Gaunt, 1927) was used for grid independence study to check whether the flow parameters under consideration is grid independent or not. Three significantly different set of grids have to be selected for this study. The representative cell sizes h_1, h_2 and h_3 are obtained using the formula given as in equation 3.20.

$$\text{grid size, } h = \left[\frac{\sum_{i=1}^{N}(\Delta V_i)}{N}\right]^{\frac{1}{3}} \tag{3.20}$$

where,

N = total Number of cells in the domain

ΔV_i is the volume of the i^{th} cell

The grid refinement factor, ï = h_{coarse}/h_{fine}, shall be greater than 1.3 (Celik et al., 2008). Simulations were carried out to find the values of key variables (Φ).

Let $h_1<h_2<h_3$, then the grid refinement ratio, $ï_{21}= h_2/h_1$ and $ï_{32}= h_3/h_2$.

By applying the Eqn.3.21, the value of 'p̈'- apparent order is calculated.

$$\ddot{p} = \frac{1}{\ln(\ddot{r}_{21})}\left|\ln\left|\frac{\varepsilon_{32}}{\varepsilon_{21}}\right| + q(\ddot{p})\right|$$

(3.21)

$$q(\ddot{p}) = \ln\left(\frac{\ddot{r}_{21}^{\ddot{p}} - s}{\ddot{r}_{32}^{\ddot{p}} - s}\right)$$

(3.22)

$$\ddot{S} = 1 \,.\, \mathrm{sgn}\,(\text{Ɛ}32/\text{Ɛ}21)$$

(3.23)

where, ε_{32}= $\ddot{\Phi}_3$-$\ddot{\Phi}_2$, ε_{21}= $\ddot{\Phi}_2$-$\ddot{\Phi}_1$

The extrapolated value of the variable Φ is calculated using the formula 3.24:

$$\Phi_{ext}^{21} = \frac{\left(\ddot{r}_{21}^{\ddot{p}}\ddot{\Phi}_1 - \ddot{\Phi}_2\right)}{\left(\ddot{r}_{21}^{\ddot{p}} - 1\right)}$$

(3.24)

The approximate relative error is found out using the formula 3.25:

$$e_a^{21} = \left|\frac{\ddot{\Phi}_1 - \ddot{\Phi}_2}{\ddot{\Phi}_1}\right|$$

(3.25)

The extrapolated relative error (e_{ext}^{21}) is calculated by:

$$e_{ext}^{21} = \left|\frac{\ddot{\Phi}_{ext}^{12} - \ddot{\Phi}_1}{\ddot{\Phi}_{ext}^{12}}\right|$$

(3.26)

The Grid Convergence Index (GCI) for the fine grid is estimated using the following formula.

$$GCI_{fine}^{21} = \frac{1.25e_a^{21}}{r_{21}^{p} - 1}$$

(3.27)

The convergence conditions of the system are checked before evaluating the extrapolated value. The convergence conditions are;

1. Monotonic convergence; 0<R<1
2. Oscillatory convergence; R<0
3. Divergence; R>1

where R is the convergence ratio and is determined by the equation; $R = \varepsilon_{21}/\varepsilon_{32}$.

The Grid Convergence Index (GCI) can be defined as a measure of grid refinement in the studies. It determines how much the solution approaches the asymptotic value. The GCI value less than 5% is an acceptable measure of grid independent converged solution (Celik et al., 2008).

3.11. Post processing of solution

Post processing involves obtaining and analysing the results by applying the above stated methods. Analysis of direct results like WSS and derived parameter like FFR were the major deciding parameters used in the study. Each parameter is explained as follows.

3.11.1. Wall Shear Stress (WSS)

WSS is defined as the tangential stress on the endothelial surface of the arterial wall. WSS of blood can be calculated using the equation 3.28, by considering blood as incompressible fluid and non-slip condition applied at the arterial wall.

$$WSS = -\mu \frac{\partial u_t}{\partial n}$$

(3.28)

where, μ is the dynamic viscosity, u_t the wall velocity in tangential direction and 'n' is the unit vector perpendicular to the wall.

High shear stress on the vessel wall promotes damage of endothelial cells and cell dormancy, it will further contribute to inflammation in blood vessel leading to vasodilation and coagulation. On the other hand, low shear stress observed during turbulent flow encourage the proliferation of endothelial cells and cell damage. Further it enhances the tendency of monocytes, platelets, etc. to adhere to vessel wall increasing the stenosed area (Paszkowiak and Dardik, 2003).

3.11.2. Fractional Flow Reserve (FFR)

Fractional Flow Reserve (FFR) is defined as the ratio of pressure after stenosis to pressure before stenosis.

$$\text{FFR} = \frac{p_d}{p_a} \tag{3.29}$$

where,

P_d - pressure after stenosis

P_a - pressure before stenosis

Determination of FFR involves invasive technique to send a catheter having pressure transducer inside patient body where block or blood clot is identified. FFR method involves high cost and risk. FFR is a gold standard to determine the criticality of CAD. FFR value of 0.8 is set as the threshold above which one can treat patients with medicine. Any value below 0.8 requires clinical evaluation and monitoring (De Bruyne et al., 2012; Muller et al., 2011; Nørgaard et al., 2014; Pijls and Sels, 2012).

3.12. Flow chart of the methodology

The study initiated with the creation of an ideal geometry in ANSYS software similar to the one used by earlier researchers for validation of earlier research works. Grid

independence study was carried out to select the suitable mesh size. The validation of fluid properties, flow properties in turbulence model were carried out using the above geometry. Form the above study, it is observed that the use of ideal geometry cannot replicate the turbulence and flow variations caused due to irregular shape of blood vessels in coronary artery. To have a realistic modelling of the blood flow parameters in coronary artery, non-Newtonian concepts of blood, pulsatile inlet conditions and patient specific geometries with asymmetric stenosis need to be considered. For this, patient specific geometry has been extracted from CT image data files by employing VMTK software. Subsequently, the geometries were finalised and meshes were generated, grid independence study was carried out for each patient specific stenosed coronary artery. Patient specific geometries of three patient cases having stenosis - 33%, 66% and 85% were created in similar way. Hemodynamic variables were analysed on the above geometries and the risk assessment were carried out for each patient cases by finding the FFR values under different flow and viscosity conditions. FFR is an index used by medical practitioners for evaluating the criticality / risk of CAD patient. In the present study, the risk assessment is carried out by comparing FFR of CAD patient with CAD patient with diabetes. The methodology and details of numerical formulation are summarised in the flowcharts Fig. 3.6(a) and 3.6 (b).

3.13. Summary

The governing equations for fluid flow were discussed in the first part of this chapter. Numerical model adopted for the analysis of ideal geometry and patient specific geometry were discussed further. The procedure for geometry acquisition from Computer tomography (CT) images using VMTK software and the procedure for grid independence study were explained in detail. Selection of Carreau viscosity model and patient-specific flow profile (pulsatile flow) also discussed in the last part of this chapter.

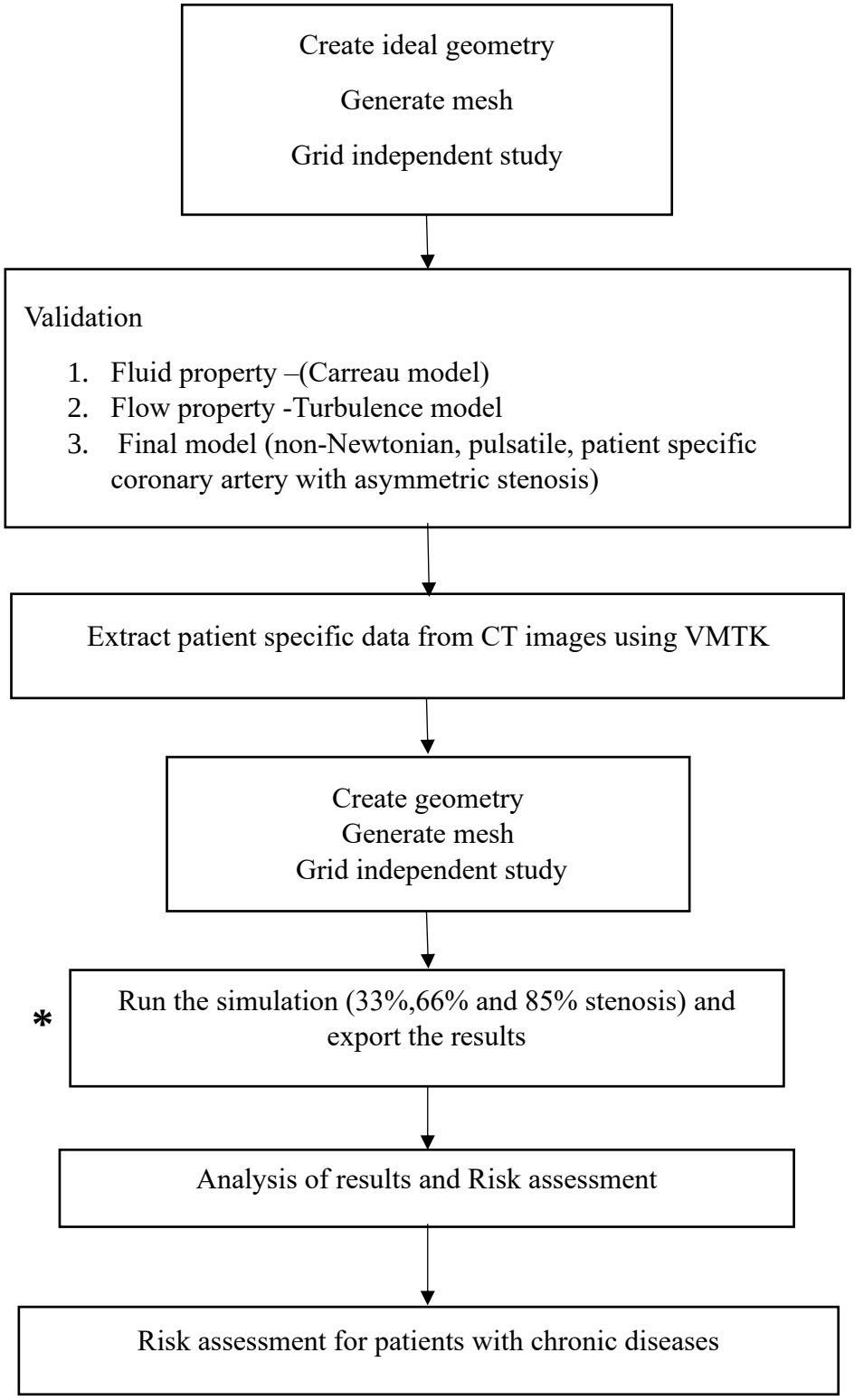

Fig. 3.6 (a) Flow chart of the methodology

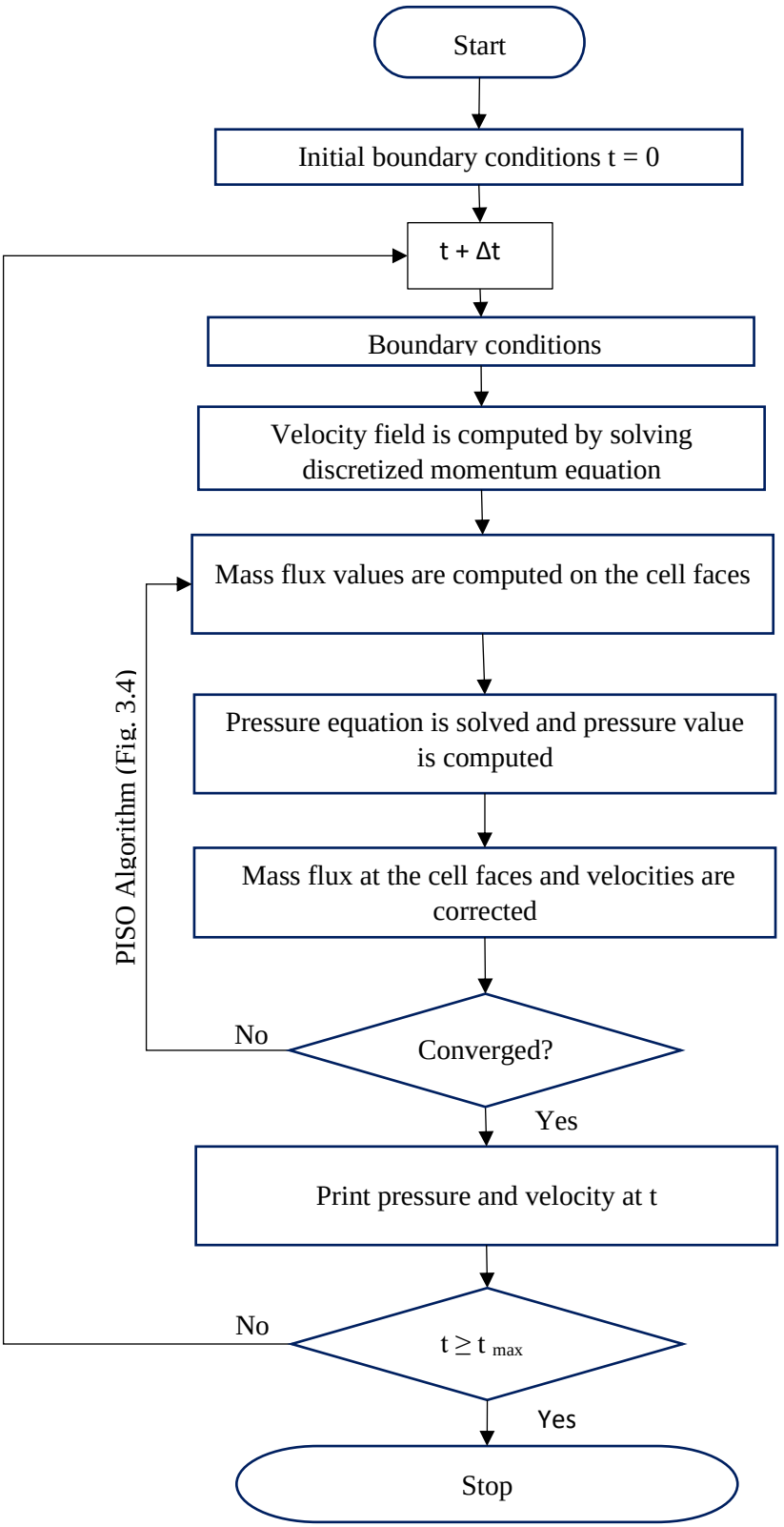

* Fig. 3.6 (b) Details of numerical formulation

CHAPTER 4

VERIFICATION AND VALIDATION OF NUMERICAL MODEL

4.1. General

To verify and validate the methodology adopted (Chapter 3) for the current study, blood flow through a circular pipe with an ideal stenosis is considered for the analysis. Initially, steady laminar flow through a cylindrical tube with a circular axisymmetric stenosis of 75% is taken. The selected laminar model for the analysis is validated with the data published in literature. To accommodate the transient nature of blood flow corresponding to the cardiac cycle, the inlet condition of laminar model is changed from steady to pulsatile flow profile. The model could not capture the flow transitions in the post stenotic region effectively. It is found that the flow disturbance and parameters captured are deviating from the available results which insist the use of turbulent model selection for pulsatile inlet flow condition. In order to relate the computed hemodynamic variables to medical field, FFR value is computed for an ideal geometry (coronary artery with 75% stenosis), as a pilot study. The computed FFR under pulsatile flow condition at the inlet does not justify its significance for 75% stenosis in cylindrical coronary artery which demands the selection of patient specific geometry with stenosis for further study (Pijls and Sels, 2012). The non-Newtonian characteristics of blood flow through coronary artery under low flow rate were also checked by comparing the shear rate for a patient specific geometry with stenosis. Finally, an appropriate model was selected to capture the desired features of transient flow characteristics in a stenosed patient specific coronary artery. Details of all these studies are presented in the subsequent sections.

4.2. Laminar flow through ideal geometry

Steady flow through a cylindrical tube having an axisymmetric circular stenosis with 75% area reduction is investigated in this section by keeping Re, 500 at inlet. ANSYS ICEM-CFD software package was used to generate hexahedral elements.

4.2.1. Geometric details

The study selected a geometry matching to the one used by Ahmed and Giddens (1983a) in their experiment. The geometry is a circular tube with diameter D having pre-stenotic length of 2D, and post stenotic length 16D. The Fig. 4.1(a) depicts the schematic of the geometry. The radius of stenosis (R(x)) is created using a cosine function dependent on axial coordinate, x. The other two co-ordinates, y and z, were calculated using R(x),

$$\mathrm{R}(x) = \frac{D}{2}\left[1 - S_O\left(1 + cos\left(\frac{2\pi(x - x_0)}{L}\right)\right)\right]$$
$$y = \mathrm{R}(x)\, cos\,\theta$$
$$z = \mathrm{R}(x)\, sin\,\theta$$

4.1

where, S_0 is called as the stenosis severity fraction (S_0 = 0.25 for 75% stenosis). L is the length of the stenosis *(L=2D)*, x_o is the location of the centre of the stenosis and r is the radial distance from the central axis.

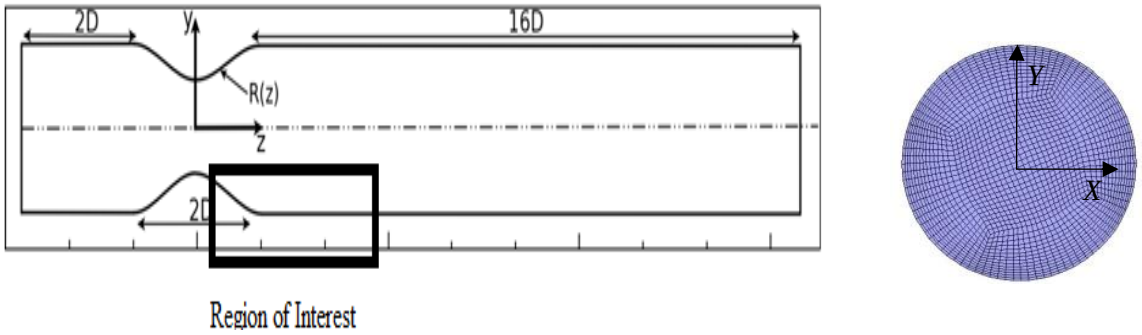

(a) (b)

Fig. 4.1(a) Ideal geometry with an axisymmetric stenosis; (b) Mesh at inlet

Geometric model of 75% stenosis level was generated and exported to ANSYS ICEM-CFD for discretising into hexahedral elements using a block-structured method with high resolution near the wall to capture the boundary layer features as in Fig. 4.1(b).

4.2.2. Grid independence study

The study assumes blood as a Newtonian fluid with constant viscosity (0.00345 Pa s) and density (1050 kg/m^3, Boutsianis et al., 2004). Re in human body varies from 400 (in human common carotid artery) to 1500 (in the human ascending artery) which justifies the selection of laminar assumption (Ghalichi et al.,1998). The governing equations were solved by using PISO algorithm-based solver.

To establish grid independence, steady state simulations were conducted on a 75% stenosis model at Re 500. Table 4.1 shows details of grids used for different trials. Distribution of axial velocity at location 1D, with different grid resolutions is compared as given in Fig. 4.2.

Table 4.1 Details of grids used for grid independence study

No	Mesh	No. of cells
1	Mesh 1	121392
2	Mesh 2	403200
3	Mesh 3	628682
4	Mesh 4	877890

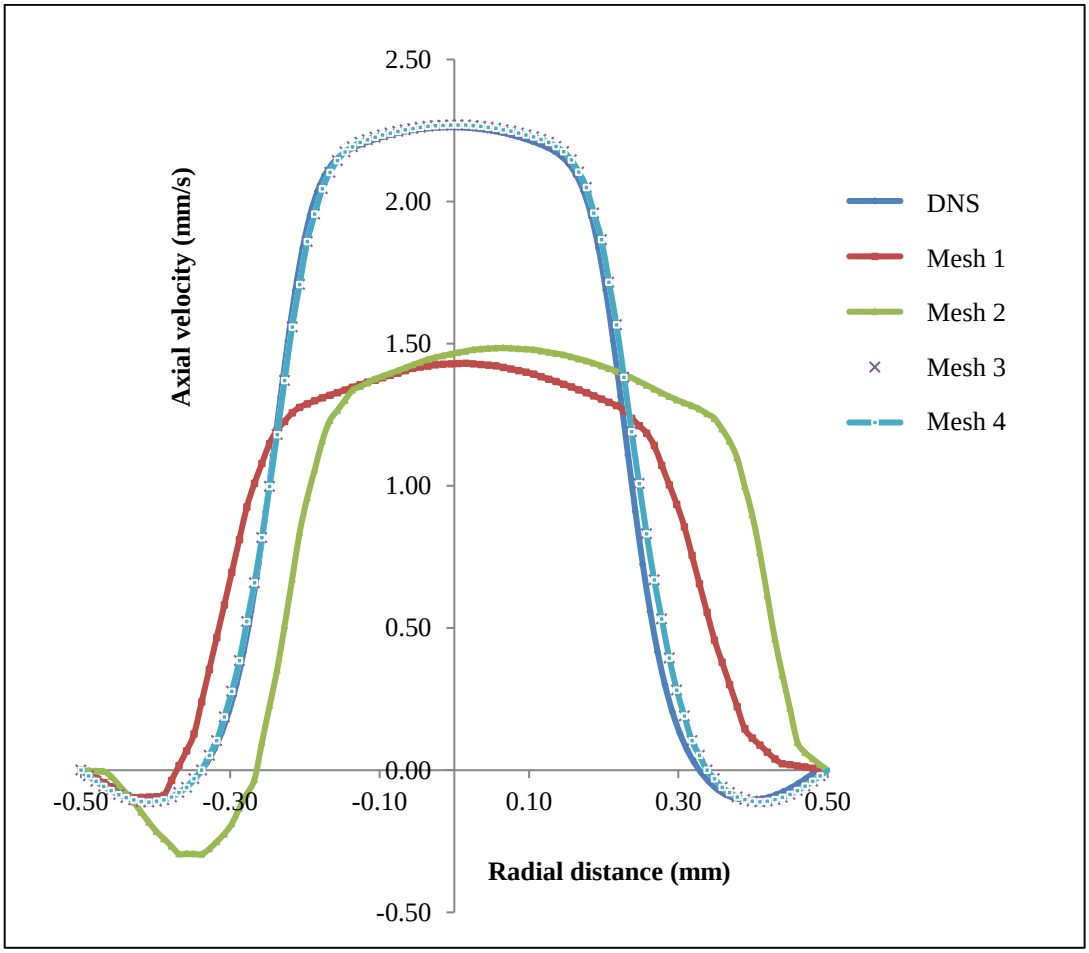

Fig. 4.2 Velocity distribution at 1D

It can be seen that Mesh 3 and 4 produces nearly same results and matching with the results obtained from DNS. Hence, mesh 3 is selected for the simulation.

4.2.3. Validation

For validating the ideal case (laminar assumption), steady Newtonian flow simulations are conducted in a circular axisymmetric stenosis (Fig 4.1(a)) model. A parabolic steady inflow profile with Re 500 is considered for the analysis. Validation of the model is established by comparing velocity profiles at different axial locations with the DNS results of Varghese et al. (2007a). The Fig. 4.3 (a) depicts that, the velocity profile becomes flat plug like form on approaching the stenosis and gets separated from the walls due to the formation of recirculating eddies in post stenotic region (Fig. 4.3(b)). The peak values of velocity vectors are identified immediately after stenosis, which are more than 4 times (2.2 m/s) the mean value of velocity u_m (0.5 m/s).

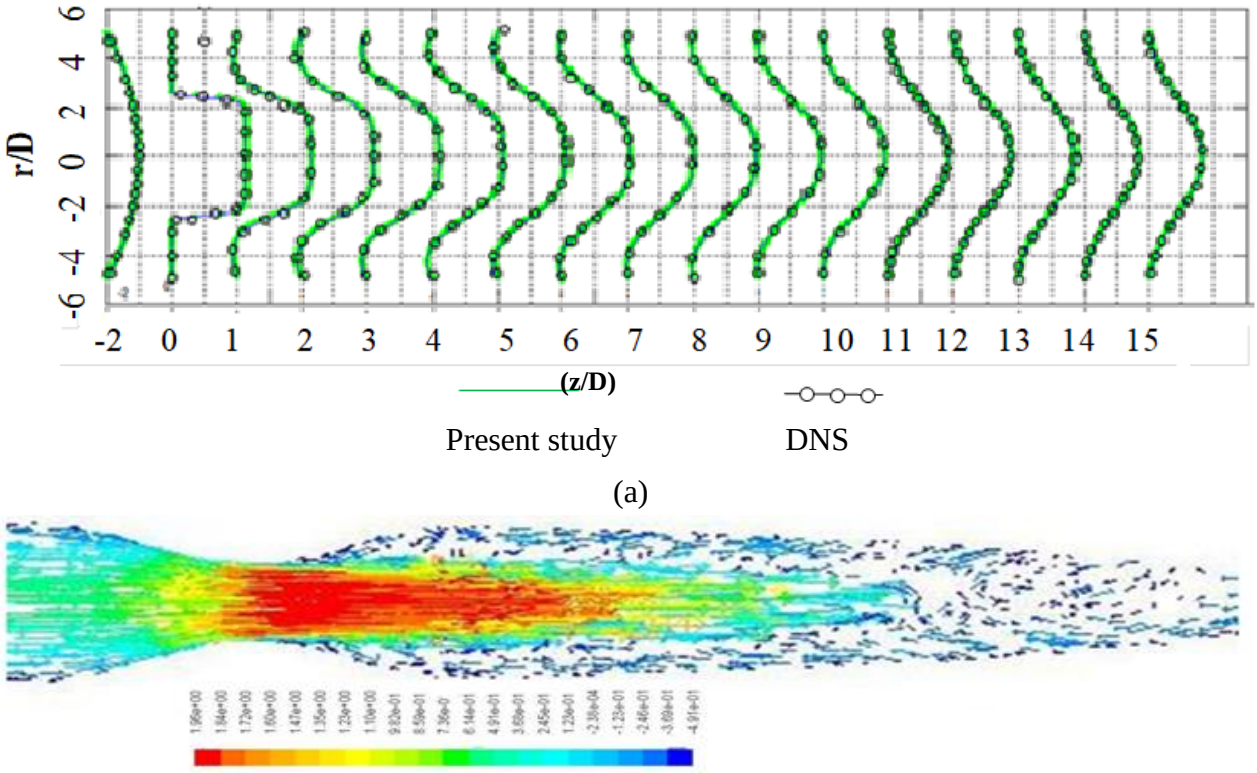

Fig. 4.3 (a) Steady flow velocity profiles at different axial locations, Re = 500;(b) Recirculation zone in post stenotic region close to the wall

The flow field always stays laminar and axisymmetric with no signs of oscillations or jet-breakdown at the downstream. Fig. 4.3(a) shows that predictions of the study, closely match with DNS results at all sections. Hence this model is proposed to use for the further analysis of blood flow.

4.3. Pulsatile flow through ideal geometry

Simulation of flow under laminar assumption is again carried out by changing the inlet flow conditions as pulsatile to connect the periodic nature of cardiac cycle at an average Reynolds number of 600. Womersley flow profile (section 3.3.1.2) was used at the inlet. Values of A and Womersley number (α) selected for the present work are 0.667 and 7.5 respectively (Eqn.3.8) (Ahmed and Giddens (1984). The pulsatile profile (having time period 'T') increases gradually to a maximum at T2 (Fig. 4.4), then varies sinusoidal and finally regains its initial value as time reaches T.

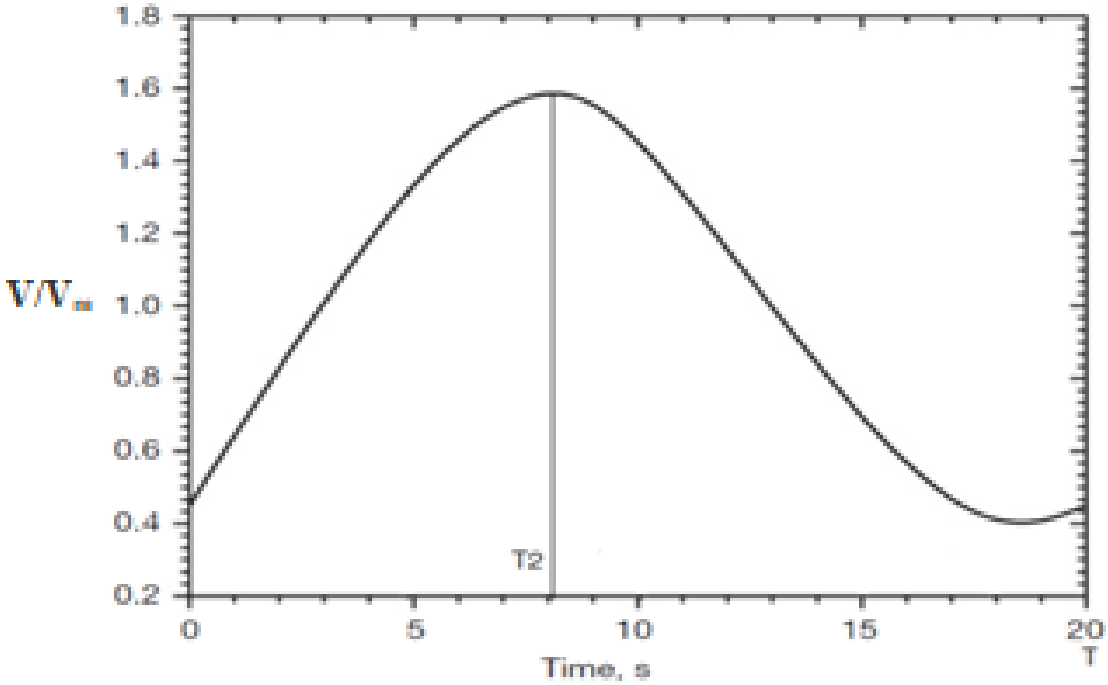

Fig. 4.4 Boundary condition at inlet

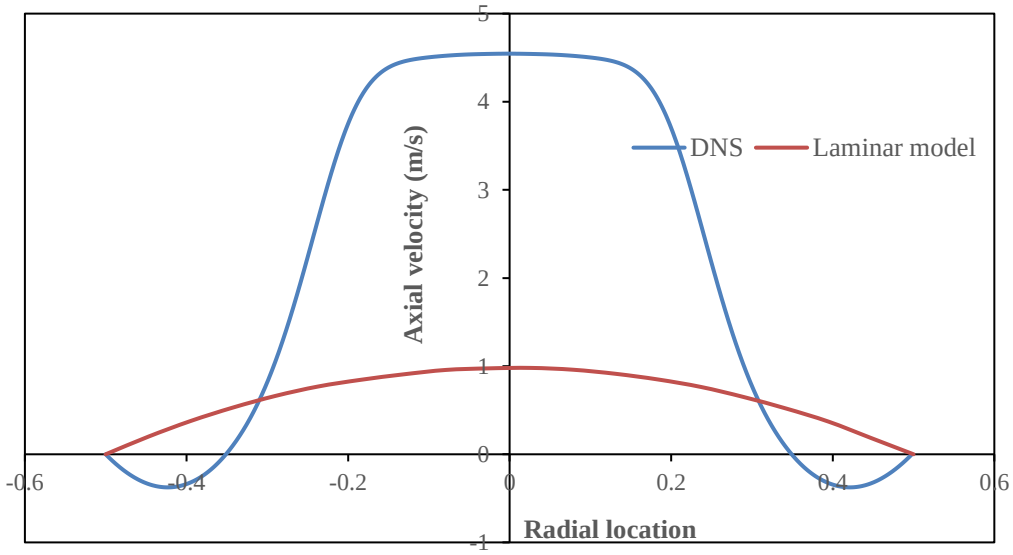

Fig. 4.5 Velocity distribution at Z = 2D

Under pulsatile flow condition, laminar assumption is unable to predict the results matching with DNS (Varghese et al., 2007b) (Fig. 4.5). This indicate the inability of this assumption to represent pulsatile inflow conditions, though the Reynolds number is set as

600. From literature study (Ahmed and Giddens, 1984) it is observed that, local flow transition occurs at post stenotic region. In addition, it is also reported to have recirculation near the wall in laminar assumption under steady inflow conditions (Fig. 4.3(b)). All these observations demand the use of turbulence model for the simulation of transient flow. It is also reported that the prediction of WSS and the turbulence transition are better captured in transition SST k-ω model than k-ε model and k-ω model (Ryval et al., 2004; Tan et al., 2008; Mahalingam et al., 2016). Hence the simulation is repeated by selecting SST k-ω model.

4.3.1. Validation - Transition SST k-ω model

The same geometry was selected for the validation of SST k-ω model. Geometric model of 75% stenosis level was generated and exported to ANSYS ICEM-CFD for discretising into hexahedral elements using a block-structured method with high resolution near the wall to capture the boundary layer features. To establish grid independence, simulations were conducted for this geometry for pulsatile inlet condition at average Re 600. Table 4.2 shows details of grids used for different trials. Distribution of axial velocity at location 2D with different grid resolutions are compared as given in Fig. 4.6. From the fig, it can be seen that axial velocity corresponding to Mesh 3 and 4 produces nearly matching results with DNS results and hence mesh 3 is selected for the analysis.

Table 4.2 Details of grids used for grid independence study in **SST k-ω model**

No	Name	No. of cells
1	Mesh 1	250000
2	Mesh 2	410000
3	Mesh 3	850040
4	Mesh 4	10,45670

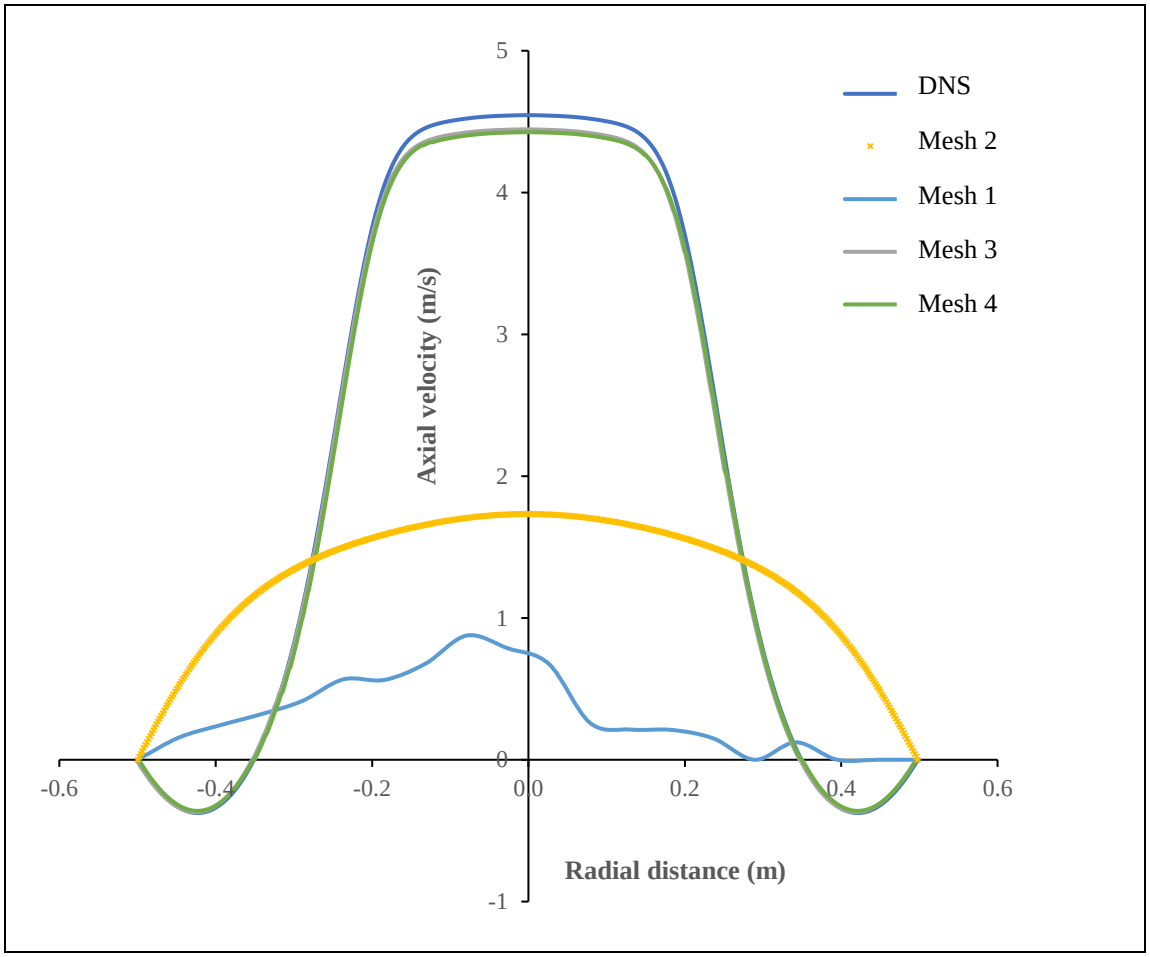

Fig. 4.6 Velocity distribution at Z = 2D (SST k-ω model)

The computed flow profile at stenosis (Z = 0D) are compared with experimental result as shown in Fig. 4.7(a). The axial velocity profiles corresponding to peak flow rate are also plotted and compared with the experimental values of Ahmed and Giddens (1984) at Z = 1D as shown in 4.7(b).

The result shows good agreement with the experimental values (Fig. 4.7(a) and (b)). Fig. 4.7(b) depicts that the present study gives better results than the published results available in the literature for the same problem (Varghese et al., 2007b). Fig. 4.7(c) to (e) shows the axial velocity profiles at Z = 2.5D, Z = 4D and Z = 5D. The results show similar trend and are comparable with the experimental values. Discrepancies were observed in pulsatile flow simulations from Z = 2.5D onwards.

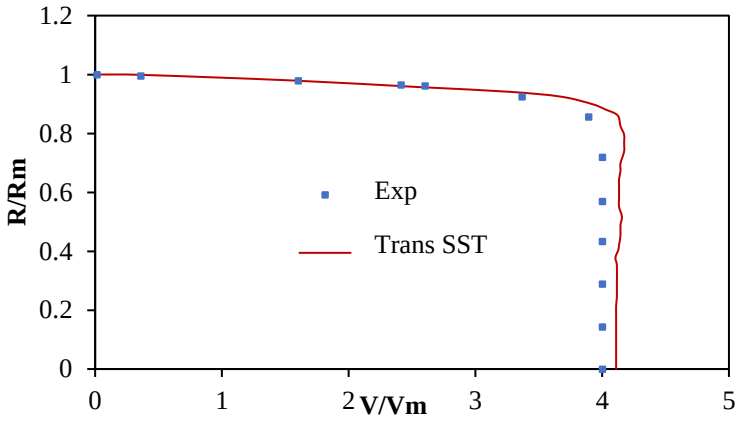

0D
(a)

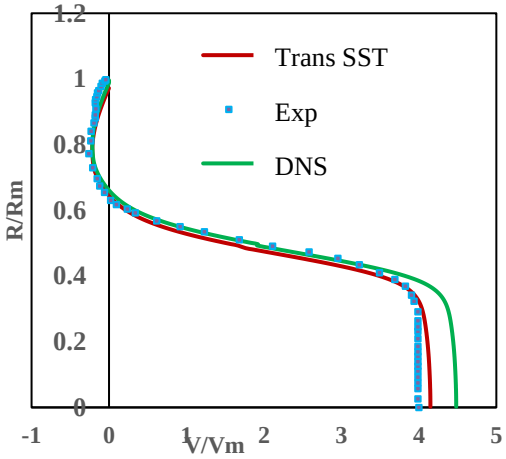

1D
(b)

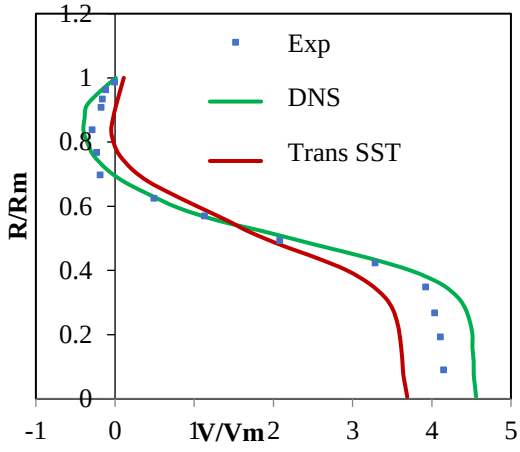

2.5D
(c)

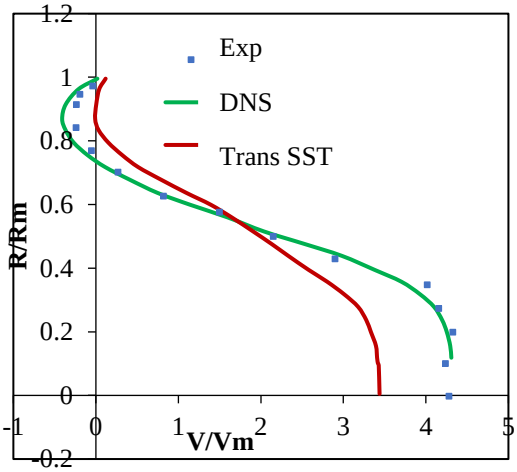

4D
(d)

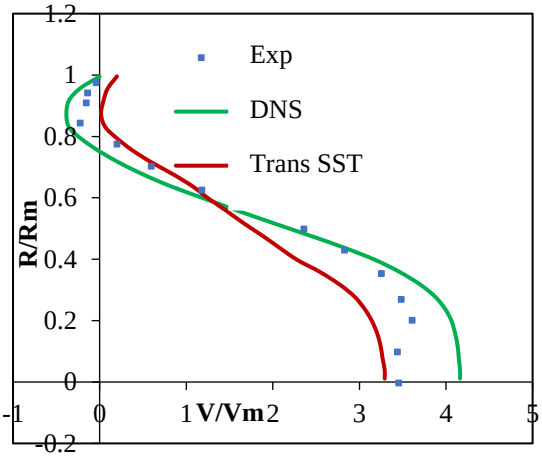

5D
(e)

Fig. 4.7 Velocity profiles corresponding to peak flow rate (a) at Z = 0D; (b) at Z = 1 D; (c) at Z = 2.5D; (d) at Z = 4D; (e) at Z = 5D

The axial variation of WSS corresponding to peak flow were also plotted and compared with the DNS (Varghese et al., 2007b) results. Fig. 4.8 displays the axial variation of WSS at peak flow. The shear stress increases as the flow approaches stenosis and drops drastically immediately after the stenosis in the divergent section of the flow area due to flow separation (Fig. 4.8). The computed WSS shows slight deviation from DNS result at some location of post stenotic region. The deviation from DNS result is also observed when velocity profile plotted at the same location (Fig 4.7 (d)). The SST k-ω model could not capture the flow separation occurring after 1D distance, as the mesh size is inadequate to capture the phenomenon (Tan et al., 2011). Since WSS at other portions of the flow area are closely following the published results and the axial velocity profiles are also agreed at sections Z = 0D and 1D, transition SST k-ω model is taken for the present study.

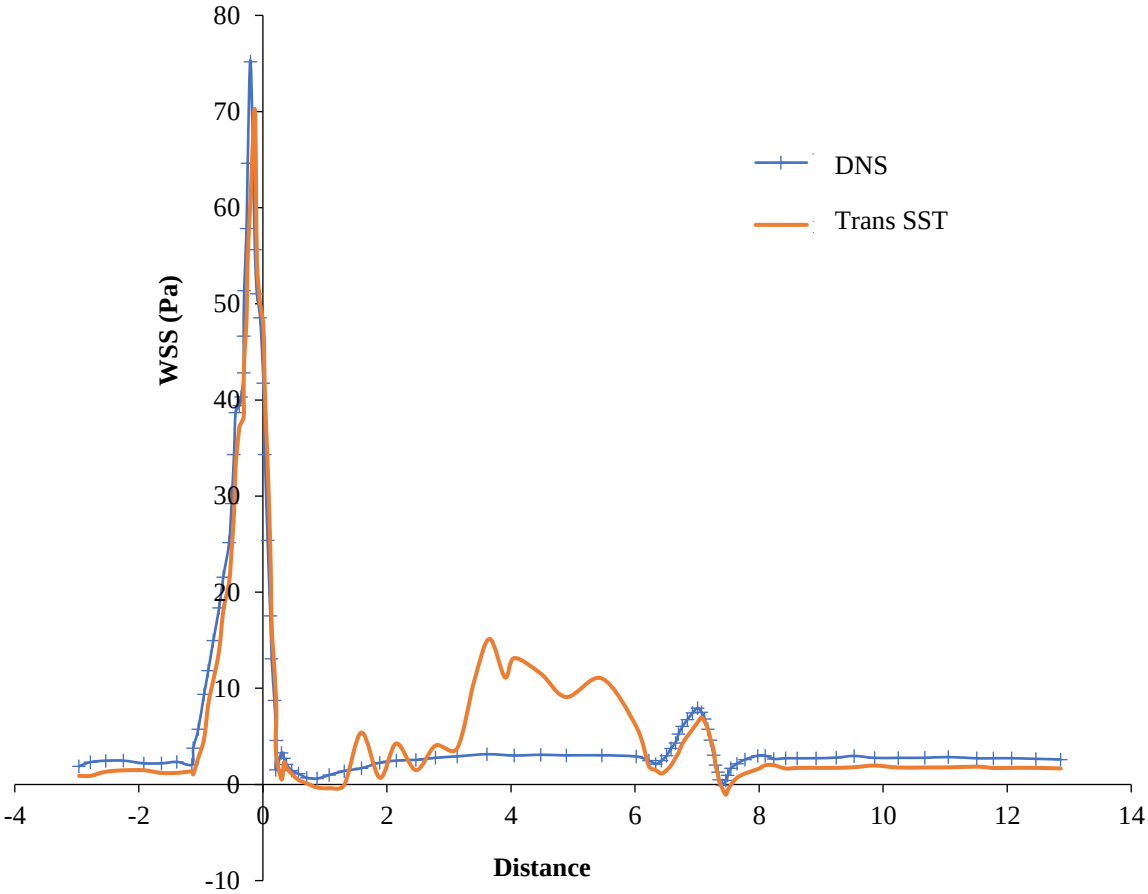

Fig. 4.8 Axial variation of WSS magnitude

4.4. Calculation of FFR - ideal geometry

Since, FFR is the term used to connect the hemodynamic variables into medical field, it is to be computed for the ideal stenosed coronary artery. In order to match with physiological values, Reynolds numbers 300 and 500 were used for normal and hyperaemic flow conditions respectively (Back and Banerjee, 2000). FFR is calculated for two inlet conditions.

(i) Poiseuille parabolic velocity profile is applied at the inlet while keeping the outlet pressure as 85mmHg.
(ii) Pulsatile profile is applied (section 3.3.2, Fig. 3.2) at inlet and FFR is calculated.

Axial velocity and WSS are compared for normal and hyperaemic flows (Fig. 4.9 (a), (b), (c),) with Poiseuille parabolic profile at inlet (Re = 300 and 500). Analysis of velocity contours (Fig. 4.9 (a)) reveal that, after the constriction zone, the value of axial velocity decreases along the radius and have a negative value near the arterial walls when Re = 500 whereas no negative values were observed when Re = 300. It was found that the axial velocity (Fig. 4.9(b)) and WSS (Fig. 4.9 (c)) are maximum at throat of the stenosis in both flow conditions and drops drastically after maximum value.

The pressure distribution along the wall is plotted with inlet boundary conditions of both Poiseuille and pulsatile profiles (Fig. 4.10). Pressure drop across the stenosis is obtained from the plot and FFR is calculated for both cases of Re = 500. The value of FFR under Poiseuille profile is 0.88 at Re = 500, which shows the less criticality (>0.8). Same procedure was followed for pulsatile inlet flow and value of FFR is calculated. The FFR value under hyperaemic flow (Re = 500) obtained as 0.82 (Fig. 4.10 (b)).

However, 75% stenosis is a critical concern for a medical practitioner (Hamilos et al., 2009; Ntalianis et al., 2010). Hence, this finding is not justifiable to an actual medical case where 75% stenosis is considered as highly critical. This demands the necessity for the incorporation of patient specific geometry for hemodynamic analysis.

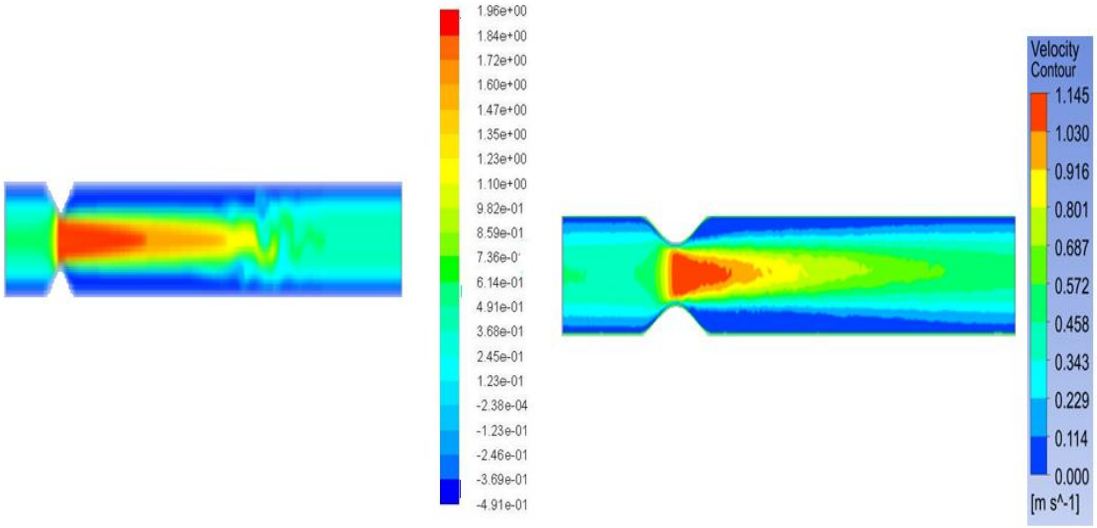

Re = 500 **Re = 300**

(a)

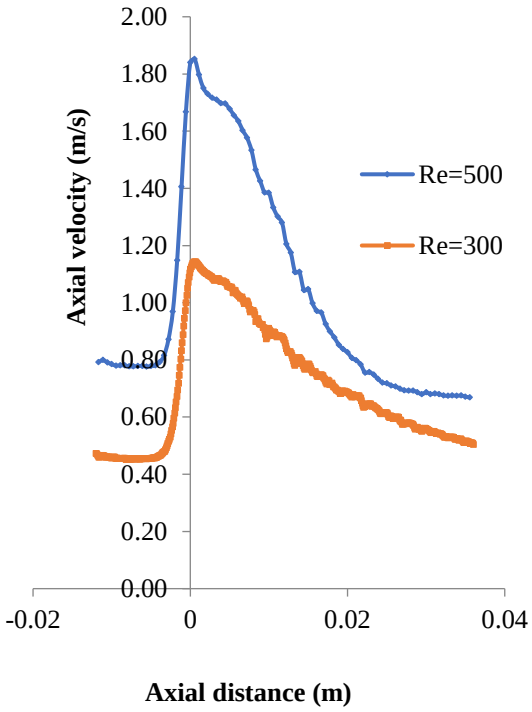

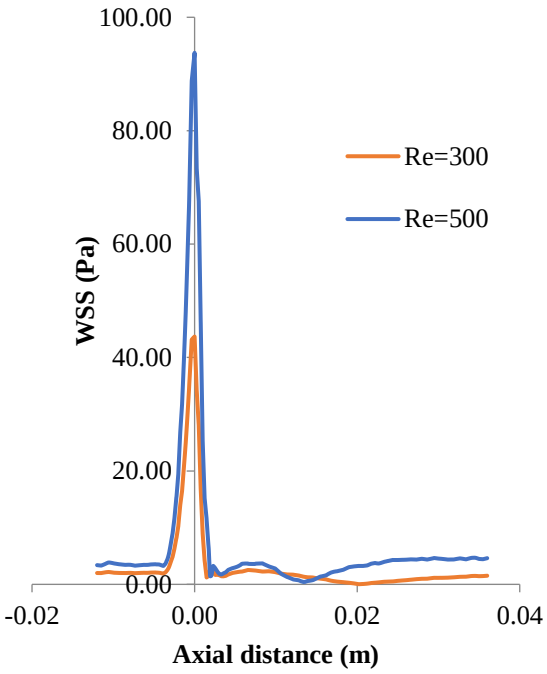

(b) (c)

Fig. 4.9 (a) Velocity contours for Re = 500 and 300; (b) Axial velocity profile; (c) Axial WSS distribution

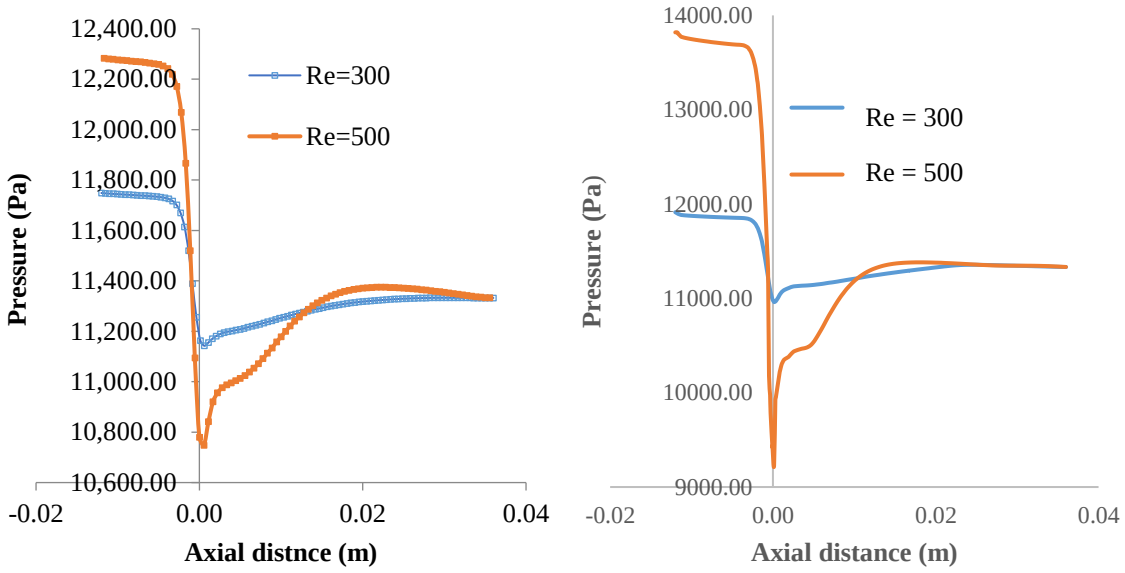

(a) (b)

Fig. 4.10 Axial pressure distribution corresponds to (a) Poiseuille parabolic inlet profile; (b) Pulsatile inlet profile

4.5. Comparison of Newtonian and non-Newtonian blood rheology in patient specific stenosed coronary artery

Most of the investigators considered blood as Newtonian fluid in large arteries like Aorta. However, literature says that since the coronary arteries are small in size and non - Newtonian fluid analysis is more preferable for the study of hemodynamic parameters (Johnston et al., 2006). It is also reported that non-Newtonian behaviour of the fluid becomes prominent in some phases of cardiac cycle under pulsatile flow conditions, where shear rate is below 100 s^{-1} (Pedley, 1980). This section aims at investigating the influence of non-Newtonian blood rheology on the hemodynamic in a stenosed vessel for a patient-specific case. The results are compared with Newtonian blood rheology to ensure what type of fluid behaviour is to be considered for analysing the blood flow through coronary artery under transient condition. In the current study, Carreau model is used to describe the non-Newtonian blood rheology. Comparison of results with Newtonian case was done for shear rate, velocity and WSS by considering patient specific geometry with 66% stenosis

as shown in Fig. 4.11. Pulsatile flow profile is given at the inlet which is shown in Fig 4.12.

Fig. 4.11 3-D Geometric model for 66% stenosis

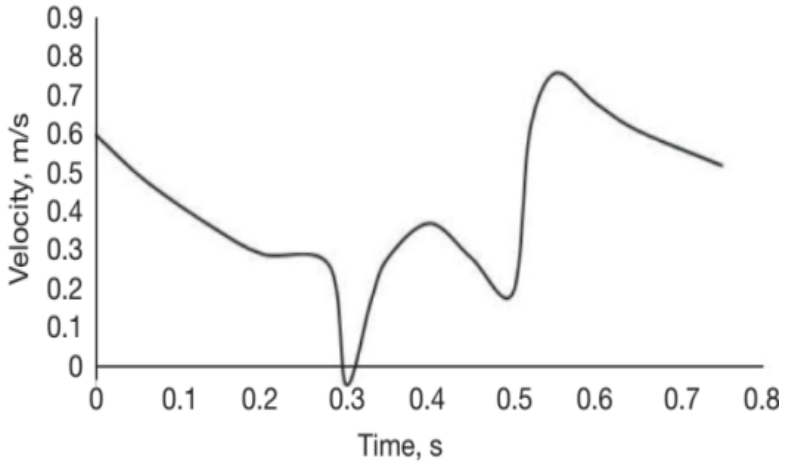

(b)

Fig. 4.12 Boundary condition at inlet (Berne and Levy, 1967)

4.5.1. Comparison of shear rate between Newtonian and non-Newtonian (Carreau) fluid

Patient specific boundary conditions, velocity profile (Fig. 4.12, Berne and Levy, 1967) and average pressure (85 mm Hg, Wiwatanapataphee et al., 2012) are specified at inlet and outlet respectively. Fig. 4.12 shows that minimum velocity occurs at 0.3 s and maximum velocity, at 0.55 s. A comparison of shear rate for Newtonian and non-Newtonian model (Carreau model) is plotted along the axial distance for the flow condition at 0.3 s and 0.55 s (Fig. 4.13 and 4.14) respectively. The shear rate values are found to be within or below $100s^{-1}$ for minimum and maximum velocity condition for both type of fluid.

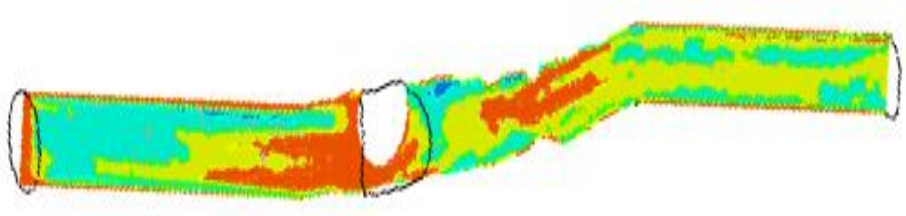

N
(a)

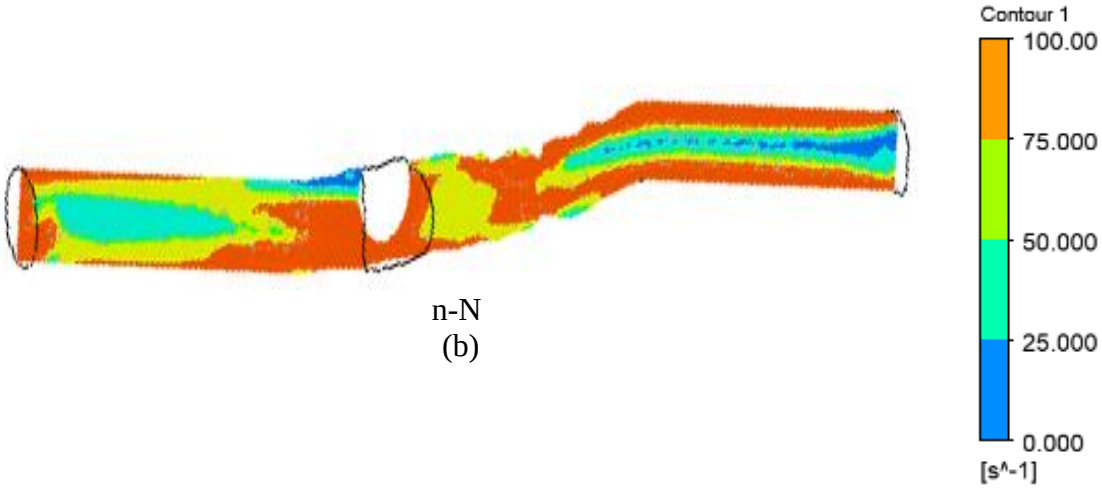

n-N
(b)

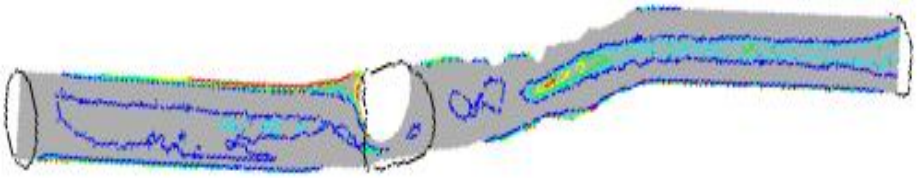

Difference in shear rate
(c)

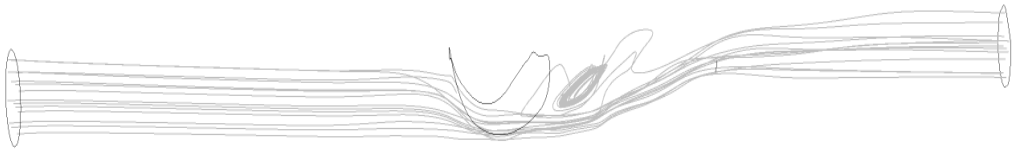

Recirculation zones in non- Newtonian model.
(d)

Fig. 4.13 Shear rate contours, evaluated at 0.3 s (minimum flow) (a) Newtonian model (N); (b) non-Newtonian model (n-N); (c) Difference in shear rate between (a) and (b); (d) streamlines representing recirculation zones in non-Newtonian model

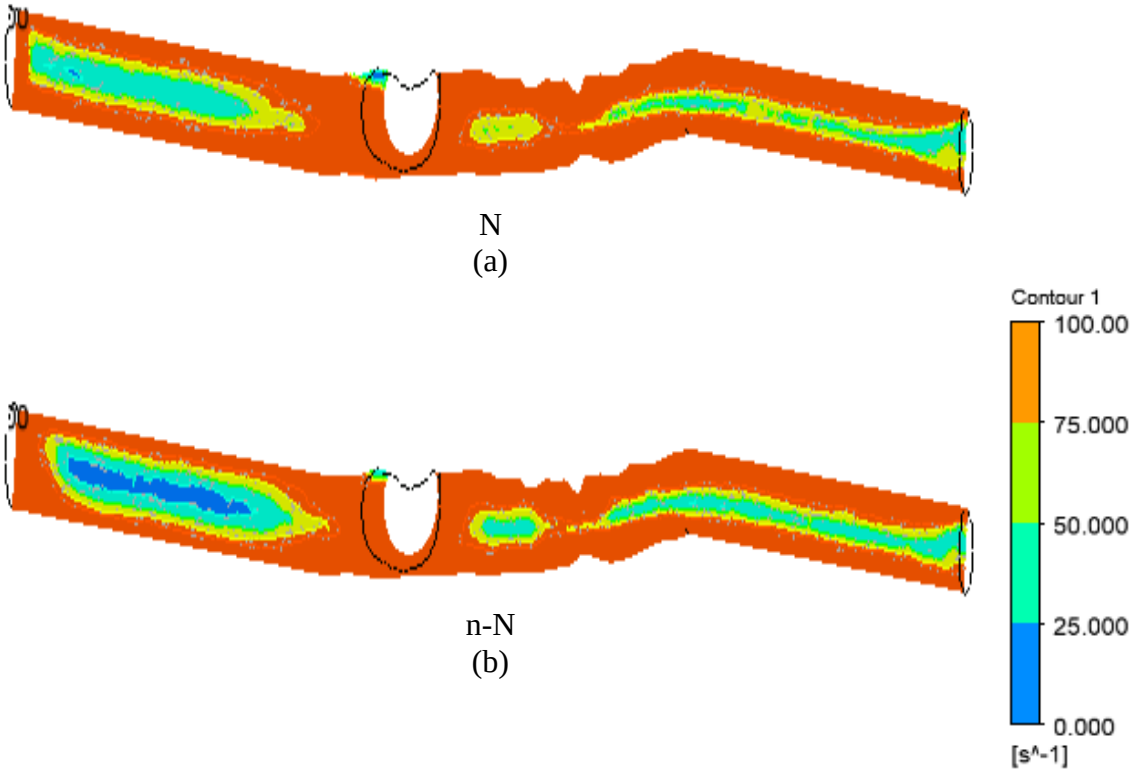

N
(a)

n-N
(b)

Difference
(c)

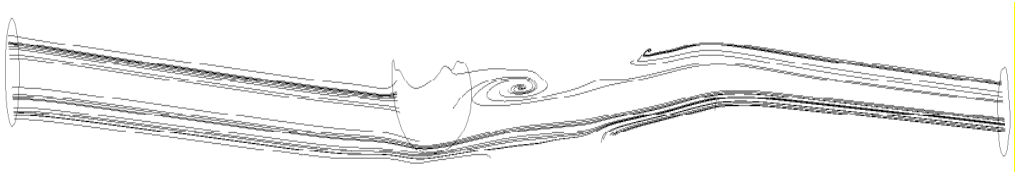

Recirculation zones in non- Newtonian model
(d)

Fig. 4.14 Shear rate contours, evaluated at 0.55 s (maximum flow) (a) Newtonian model (N); (b) non-Newtonian model (n-N); (c) Difference in shear rate between (a) and (b); (d) streamlines representing recirculation zones in non-Newtonian model

4.5.2. Comparison of velocity between Newtonian and non-Newtonian (Carreau) fluid

A comparison study of velocity profiles under Newtonian and Carreau model is shown in Fig. 4.15 (minimum flow, t = 0.3 s) and Fig. 4.16 (maximum flow, t = 0.55 s). Maximum velocity occurs at stenotic region in both cases. The comparison contour depicts that the highest difference in velocity observed is 0.0235 m/s, found at the stenosis for maximum flow and 0.0227 m/s for minimum flow condition. The difference in velocity profile distribution between Newtonian and non-Newtonian models are significant and observed throughout the flow area at maximum flow (0.55 s), though its value is almost same.

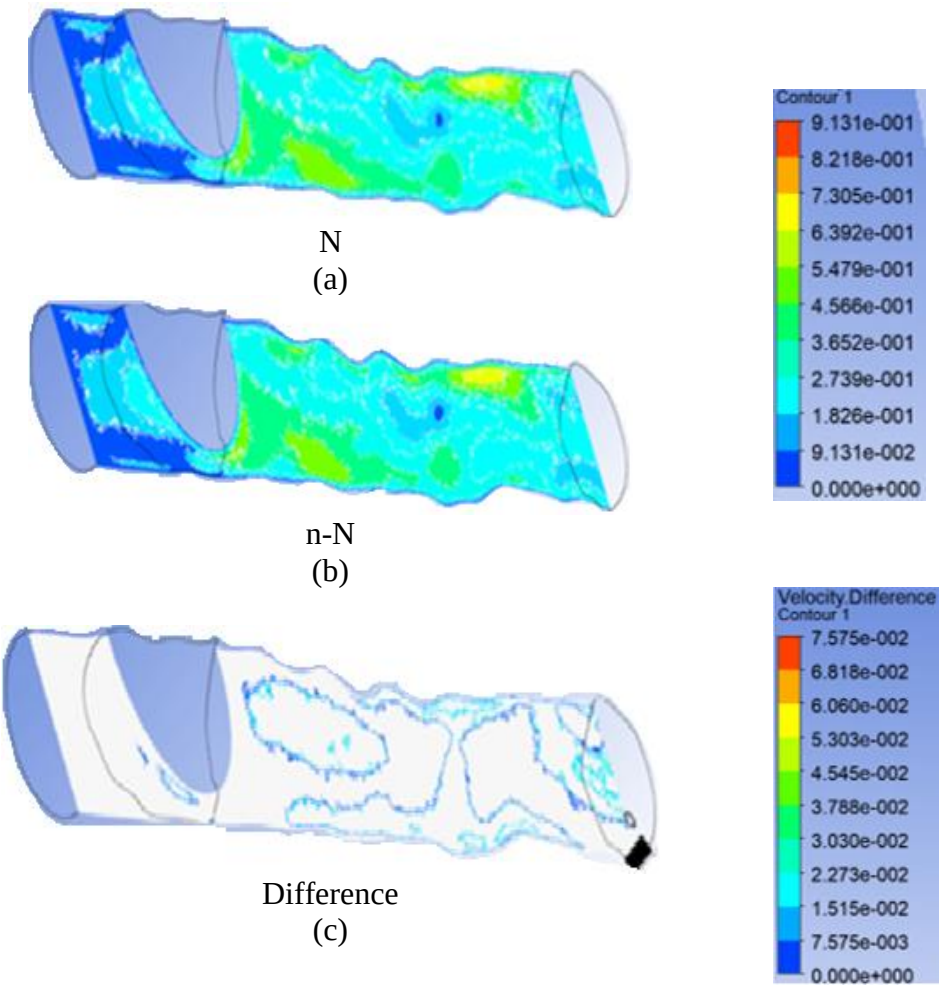

Fig. 4.15 Velocity contours of plane evaluated at 0.3 s (minimum flow) (a) Newtonian model (N); (b) non-Newtonian model (n-N); (c) Difference in velocity contours between (a) and (b)

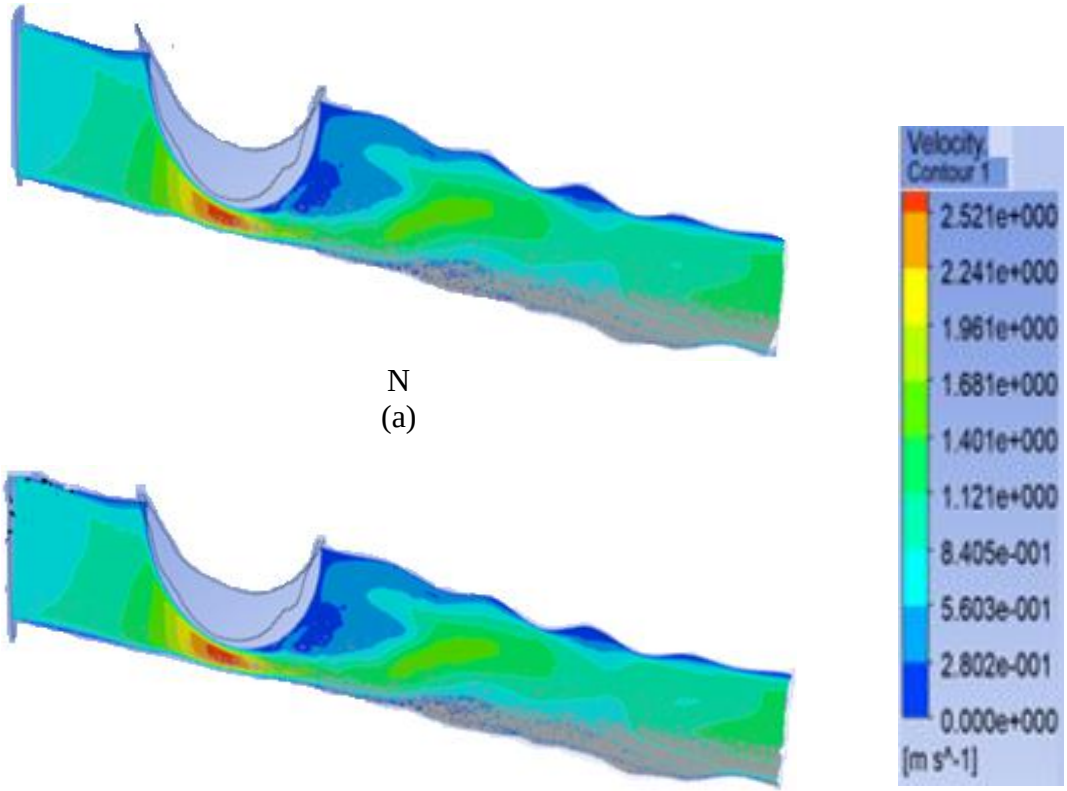

N
(a)

n-N
(b)

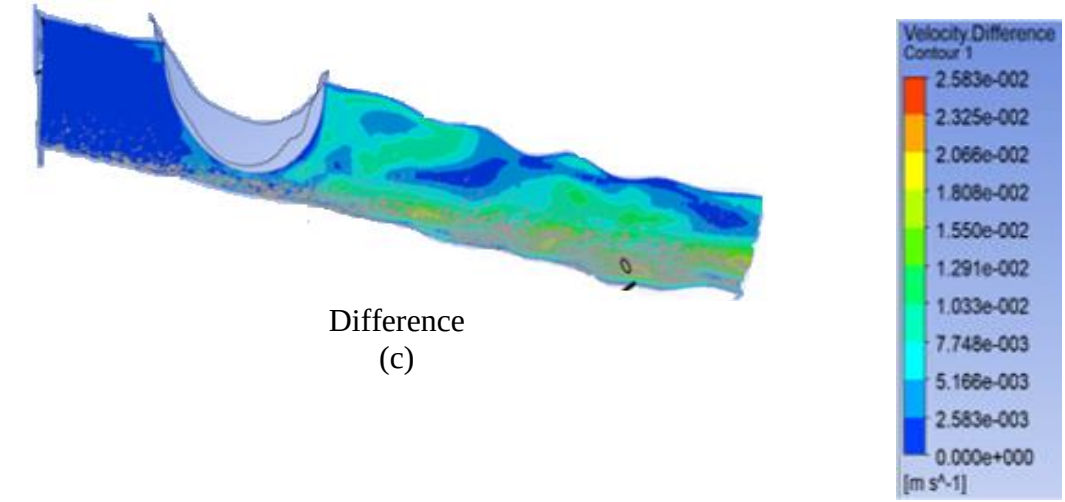

Difference
(c)

Fig. 4.16 Velocity contours of plane, evaluated at 0.55 s (maximum flow) (a) Newtonian model (N); (b) non-Newtonian model (n-N); (c) Difference in velocity contours between (a) and (b)

4.5.3. Comparison of WSS between Newtonian and non-Newtonian (Carreau) fluid

The comparison of WSS profiles for Newtonian and non-Newtonian models clearly shows large difference in values of over ~7 Pa at the stenotic throat for minimum flow condition (Fig. 4.17). The variation in WSS depends upon the flow variations, it increases with decrease in flow rate, where non-Newtonian behaviour is significant (Fig. 4.13 and 4.14). Fig. 4.17(N) and 4.18(N) demonstrates that the predictions of WSS in Newtonian models are consistently lower to those of the non-Newtonian (Carreau) model. The maximum difference in WSS occurs at stenosis in both models, but the predictions by Carreau model is almost double that of the Newtonian model for low flow rates.

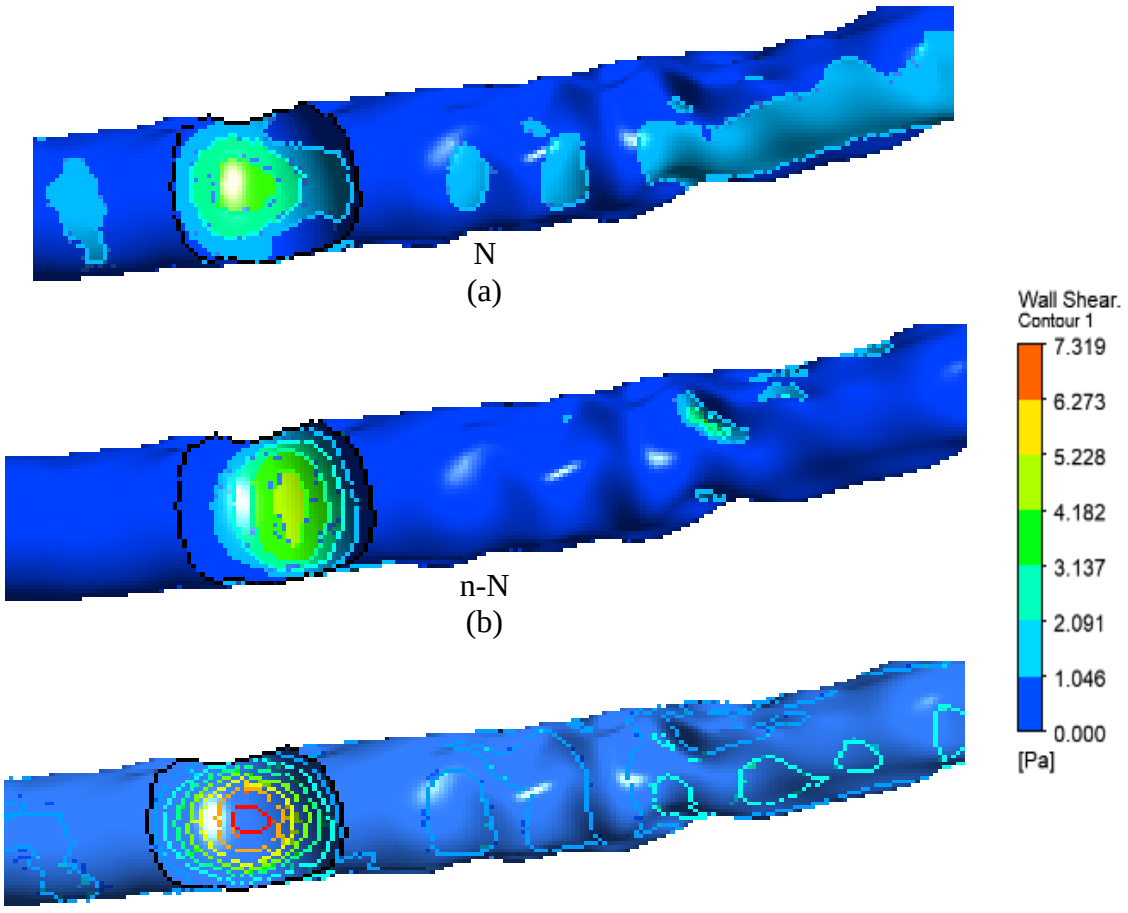

N
(a)

n-N
(b)

Difference
(c)

Fig. 4.17 WSS contours, evaluated at 0.3 s (minimum flow) (a) Newtonian model (N); (b) non-Newtonian model (n-N); (c) Difference in WSS contours between (a) and (b)

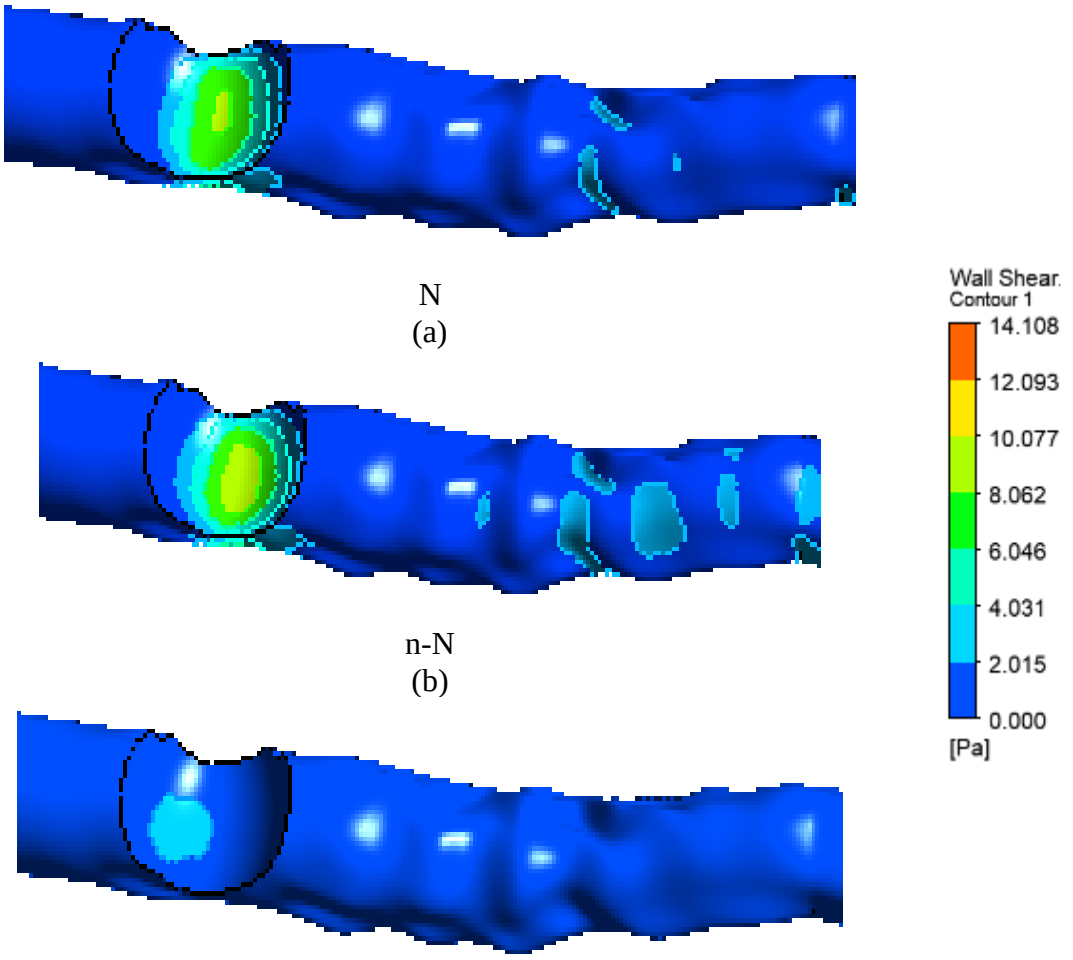

Fig. 4.18 WSS contours, evaluated at 0.55 s (maximum flow) (a) Newtonian model (N); (b) non-Newtonian model (n-N); (c) Difference in WSS contours between (a) and (b)

The above analysis reveals that non-Newtonian behaviour is more significant during minimum flow and produce considerable difference in WSS compared to Newtonian model. In addition, shear rate is less than 100 s^{-1} along the flow area. All the above observations confirm the fact that, the non-Newtonian model represents the hemodynamic parameters better compared to Newtonian model for smaller arteries like coronary artery as reported in literature (Pedley, 1980; Johnston et al., 2006). Hence, the

present study considers blood as a non-Newtonian fluid for hemodynamic analysis of patient specific models.

4.6. Summary

From the verification and validation of the numerical model with published data for an ideal geometry having an axisymmetric stenosis, it was found that patient specific geometries need to be investigated to obtain more accurate results for the use in medical field. Analysis of the flow characteristics shows that the flow transition from laminar to turbulent and vice versa is better captured by transition SST k-ω model. Comparison of shear rate and WSS indicate the necessity of adopting the non-Newtonian model for the analysis. In order to match with the realistic flow corresponding to cardiac cycle, pulsatile flow conditions are to be provided at the inlet. Hence, transition SST k-ω model is finally selected for the study of hemodynamic parameters in patient specific stenosed coronary artery with pulsatile inlet boundary condition by considering blood as non-Newtonian fluid.

CHAPTER 5

RESULTS AND DISCUSSIONS

5.1. General

Selection of SST k-ϙ model for the simulation of hemodynamic parameters in patient specific stenosed coronary artery with pulsatile inlet boundary condition by considering blood as non-Newtonian fluid is finalised in Chapter 4. In patient specific case, the geometry of stenosis would be asymmetric with irregular shape. It is reported in section 4.4 that, a detailed investigation of patient specific cases can give vital information about FFR in a stenosed vessel. In this chapter the relationship between blood flow rate vs pressure drop across three different patient specific cases, having different degree of asymmetric stenosis (33%, 66% and 85% stenosis) were investigated. A realistic physiological pulsatile flow profile is applied at the inlet to mimic the blood flow inside a coronary artery. Patient specific cases (with asymmetric stenosis) were analysed under normal and hyperaemic blood flow conditions with transition SST k-ω model. The variation in WSS, pressure drop and distribution of velocity at different flow conditions were investigated and presented. The study establishes a relation to link the percentage stenosis with FFR and flow rate by using non-invasive method. It can be used as a diagnostic tool for medical practitioners to check the criticality of percentage stenosis and also become an aid in understanding the early signs of cardiovascular diseases during clinical diagnosis. Details of the computational procedure are discussed in the subsequent sections.

5.2. Patient specific coronary artery - modelling and meshing

The study used CT images of three CAD patients having significant levels of stenosis. To develop lumen and vessel wall surface from CT data, a software named VMTK (Vascular Modelling Tool Kit) is used (Antiga et al., 2008). The obtained surfaces from VMTK were fed in to commercially available ICEM CFD 3D modeller to develop and generate the required continuous surface. SOLIDWORKS, a 3D modelling software

is engaged for smoothening of the surface. Computational models of asymmetric geometries were generated for three patient cases as shown in Fig. 5.1.

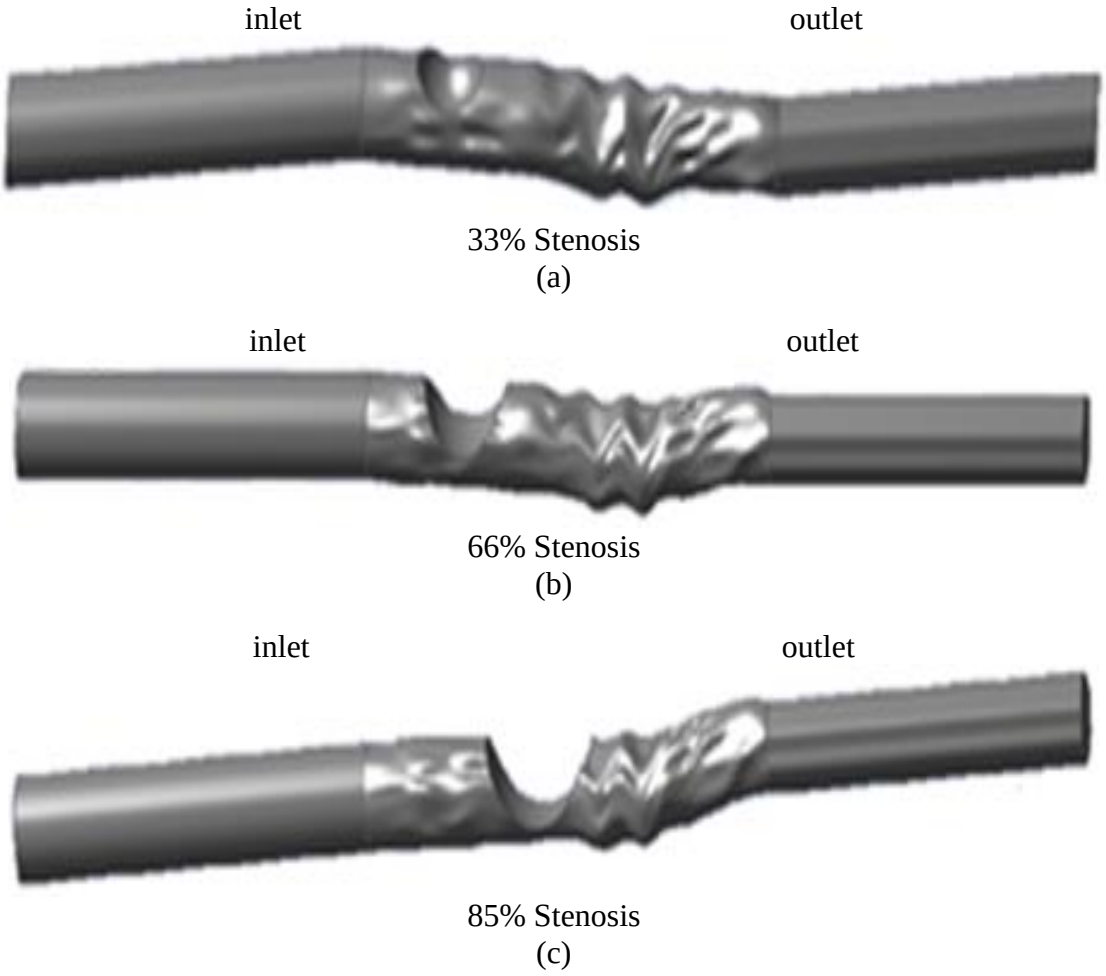

Fig. 5.1 3-D Geometric model for (a) Patient 1- 33% stenosis; (b) Patient 2- 66% stenosis; (c) Patient 3- 85% stenosis.

The geometry is then loaded in to design modeler platform of ANSYS Fluent software to discretize the geometry in to unstructured tetrahedral meshes. Prism layers are used to capture the boundary layer effects (Fig. 5.2(b)). Fine grids with y+ value less than 1 is used near the wall, in all the stenosis cases (ANSYS user's guide, 2012). Inlet and outlet sections of vessel geometry were extended to attain the fully developed flow. Similar procedure was endorsed for the remaining two geometries: 33% and 85% stenosis (Fig. 5.2 (a), (c)). In order to ensure the periodicity, four cardiac cycles were considered for

each transient simulation. The results were interpreted from the third cycle onwards in order to avoid initial fluctuations due to starting surges. An iterative PISO algorithm is adopted to decouple pressure and velocity fields, and to solve the incompressible form of Navier-Stokes equations. Second order accurate central differencing scheme was used for discretization as explained in section 3.5.3.

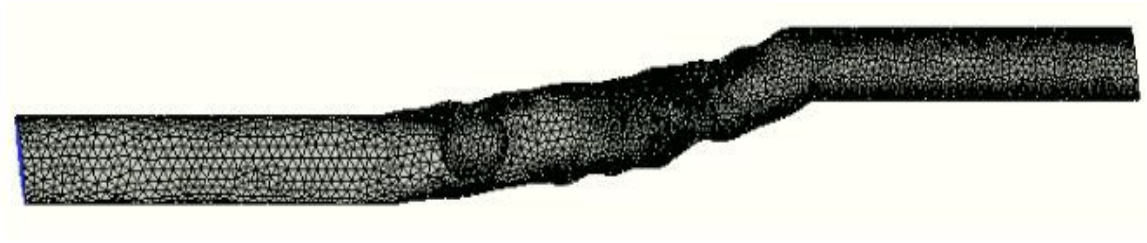

33% Stenosis
(a)

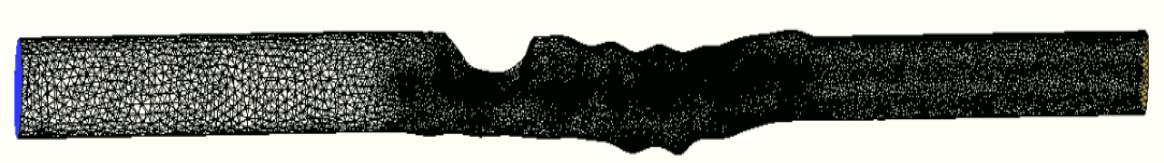

66% Stenosis
(b)

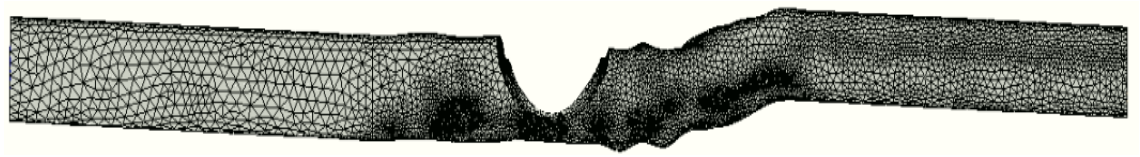

85% Stenosis
(c)

Fig. 5.2 Computational mesh (a) 33% stenosis; (b) 66% stenosis; (c) 85% stenosis

5.2.1. Boundary conditions

The flow and pressure profiles used at the inlet and outlet were obtained from the solution of equation presented in section 3.3.2 as shown in Fig. 5.3. Blood was assumed as a homogeneous, isotropic and incompressible viscous fluid, with a constant density of 1050 kg/m^3 and the non-Newtonian behaviour of blood is modelled using Carreau model as explained in section 3.7.

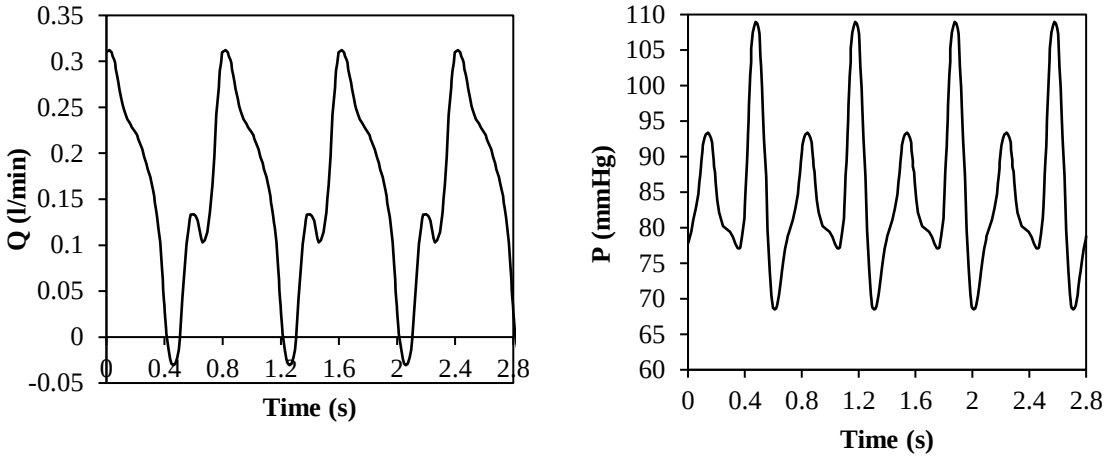

(a) (b)

Fig. 5. 3 Boundary conditions (a) Volumetric flow rate of blood in the arterial inlet; (b) The pulsatile pressure of blood in the arterial outlet

5.2.2. Grid independence study

To establish the grid independence of results for patient specific stenosis cases (33%, 66% and 85%), pulsatile flow was simulated for different grids of increasing mesh density. The procedure followed for grid independence study has been explained in section 3.10. For 66% stenosis, the study considered three tetrahedral meshes (M1, M2 and M3) with mesh elements as shown in Table 5.1.

Table 5.1 Grid independence study for the case, with 66% stenosis

No	Name	Mesh	WSS (Pa)	Change in WSS %
1	M1	101284	11.325	-
2	M2	467009	12.87	13.6
3	M3	687564	13.013	1.1

WSS values during maximum flow condition at different mesh levels, (M1, M2 and M3) were compared to establish grid independence. From the tabulation of results, it is noted that the error is minimum (1.1% only) between the meshes M2 and M3. Hence M2 mesh

containing 467009 elements was selected for 66% stenosis case for further studies and investigations. Grid Convergence Index (GCI) was also calculated as explained in section 3.8 and in this case, the obtained value is 0.048% (Table 5.2). The same procedure was repeated for 33% and 85 % stenosis cases and GCI values of 0.02% and 0.04% are obtained respectively (Table 5.2).

Table 5.2 Calculation of Grid Convergence Index

Particulars	33%	66%	85%
N1	637268	687564	690000
N2	423208	467009	497000
N3	100098	101284	101587
r̈$_{21}$	1.179	1.1285	1.3
r̈$_{32}$	1.696203	1.696203	1.696203
Φ̈1	10.03	13.03	15.13
Φ̈2	9.87	12.87	14.8
Φ̈3	8.325	11.325	13.320
ε$_{32}$	-1.545	-1.545	-1.480
ε$_{21}$	-0.16	-0.16	-0.33
S̈	1	1	1
p̈	2.270131	2.270131	2.270131
q	-1.6322	-1.99302	-1.04657
P’	3.858733	2.270194	1.730913
p̈- p’	-1.5886	-6.2e-5	0.539218
$\Phi^{21}{}_{ext}$	10.21022	13.53635	15.70411
$e^{21}a$	0.015952	0.012279	0.021811
$e^{21}{}_{ext}$	0.017651	0.037407	0.036558
GCI	**0.02%**	**0.048%**	**0.04%**

The GCI value less than 5% is an acceptable measure of grid independent converged solution (Celik et al., 2008). Hence the grid element count considered for different stenosis cases in the investigation is well within the permissible limits.

5.3. Wall Shear Stress

In order to have better idea about the effect of stenosis on WSS in a diseased artery, the study initially analysed the WSS values at various locations in a normal artery (at 0% stenosis). The study was performed with 0% stenosis for all the three patient specific cases under consideration (3mm, 3.2 mm and 4 mm diameter) in normal (mean flow rate - 0.158 l/min) and hyperaemic flow conditions (Table 5.3). WSS values thus obtained were within the range of normal healthy person (2 to 16 Pa, Cheng et al., 2007) in normal flow conditions. The WSS value is observed to boost with increase in flow rate from normal to hyperaemic.

Table 5.3 WSS variation in an artery (without stenosis)

Diameter, correspond to patient specific coronary artery (D) in mm	WSS_{max} (Pa)	
	Normal flow	Hyperaemic flow
3	4.01	33.41
3.21	3.98	25.01
4	2.67	12.67

To know more about the behaviour of WSS profiles in one full cardiac cycle, WSS values were plotted for 33%, 66% and 85% stenosis against time at specific locations. Three different positions were selected in each geometry (x = 0, x = 1D, close to the throat of stenosis and x = 5D, where x = 0 is the start of CT scan image in all cases, and D is the artery inlet diameter) and WSS values were plotted. Instantaneous values of WSS during the 3rd cardiac cycle is shown in Fig. 5.4 (a1), (a2), (a3) and 5.4 (b1), (b2), (b3) for 33%, 66%, and 85% stenosis cases respectively, during normal and hyperaemic flows. For a healthy person the WSS value lies between 2 to 16 Pa under normal flow, anything higher or lower beyond this limit would be critical for the patient. From the results, it is observed

that, at x = 1D (point nearer to stenosis) WSS values vary between 5.21 to 0.063 Pa for 33% case, whereas the values vary between 154.11 to 0.06 Pa in case of 66% stenosis and 140.6 to 0.107 Pa in case of 85% stenosis. At x = 0 and x = 5D WSS values are close to the maximum limit of the allowable range for all the three stenosis cases under normal flow (Fig. 5.4 (a1) (a3)). But under hyperaemic conditions, WSS increases considerably at these locations and reaches value higher than the permissible limit. The maximum WSS with respect to the increase in percentage of stenosis (from 33% to 85%) at x = 0D, x = 5D were quantified and it was found that the WSS increase 1.54 times and ~ 2.36 times in respective cases at hyperaemic flow condition. This higher value of WSS would lead to damage of endothelial cell in arteries (Ku et al., 1985). The WSS values were observed to go below the minimum limiting value of the allowable range with increase in stenosis percentage. From Fig. 5.4 (a1), (a2), (a3) and 5.4 (b1), (b2), (b3)) it was found that at some phase of cardiac cycle, the WSS goes below the physiological levels of (2 Pa). This low WSS leads to the accumulation of plaques, that promotes the progression of stenosis (Malek et al., 1999; Berger et al., 2000; Cheng et al., 2007). Thus high, and low values of the WSS are critical for a stenosed artery. Fig. 5.4 indicates that the shape of WSS curve closely reproduces the shape of the flow curve (Fig. 5.3(a)).

The maximum WSS values at x = 1D, under the hyperaemic condition of 33%, 66% and 85% stenosis cases were 368.02 Pa, 701.42 Pa and 625.56 Pa respectively, which are much higher than the values in normal condition (5.21 Pa, 154.11 Pa, 140.60 Pa). From table 5.4, maximum WSS values (368.02 Pa and 625.56 Pa) with respect to increase in percentage stenosis (from 33% to 85%) is observed to increase by 1.69 times for the same flowrate at hyperaemic flow condition. When flow increase from normal to hyperaemic condition, WSS increases by ~4.5 times for both 66% and 85% case. Table 5.4 shows the comparison of WSS values during both flow conditions at x = throat (maximum area reduction). It is observed that the WSS values increases along with the flow rate. From Table 5.4, the maximum WSS values at throat of 33%, 66% and 85% stenosis under normal flow conditions are 48.08 Pa, 165 Pa and 260 Pa. Under hyperaemic flow, WSS values are 430 Pa, 844 Pa and 1326 Pa respectively. It is observed that when stenosis percentage increased from 33% to 85%, WSS increases by 5.4 times under normal flow and 3 times

in hyperaemic flow conditions. When flow increase from normal to hyperaemic conditions for both 66% and 85% case, WSS increases ~ 5.1 times.

Table 5.4 Maximum and minimum value of WSS under normal and hyperaemic flow

Diameter (D) (mm) /% stenosis	Location x= 0			
	WSS_{max} (Pa)		WSS_{min} (Pa)	
	Normal	Hyperaemic	Normal	Hyperaemic
3(33%)	4.13	18.12	0.026	0.42
3.21(66%)	6.10	23.85	0.10	0.34
4(85%)	7.09	27.98	0.13	0.28
Diameter (D) (mm) /% stenosis	Location x= 1D			
	WSS_{max} (Pa)		WSS_{min} (Pa)	
	Normal	Hyperaemic	Normal	Hyperaemic
3(33%)	5.21	368.02	0.063	0.8
3.21(66%)	154.11	701.42	0.066	0.02
4(85%)	140.60	625.56	0.107	0.43
Diameter (D) (mm) /% stenosis	Location x= 5D			
	WSS_{max} (Pa)		WSS_{min} (Pa)	
	Normal	Hyperaemic	Normal	Hyperaemic
3(33%)	5.21	43.43	0.063	0.95
3.21(66%)	15.93	80.70	0.155	0.24
4(85%)	16.46	102.62	0.14	0.31
Diameter (D) (mm) /% stenosis	Location x= throat			
	WSS_{max} (Pa)		WSS_{min} (Pa)	
	Normal	Hyperaemic	Normal	Hyperaemic
3(33%)	48.08	430	2.71	5.43
3.21(66%)	165	844	0.67	15.94
4(85%)	260	1326	0.74	4.16

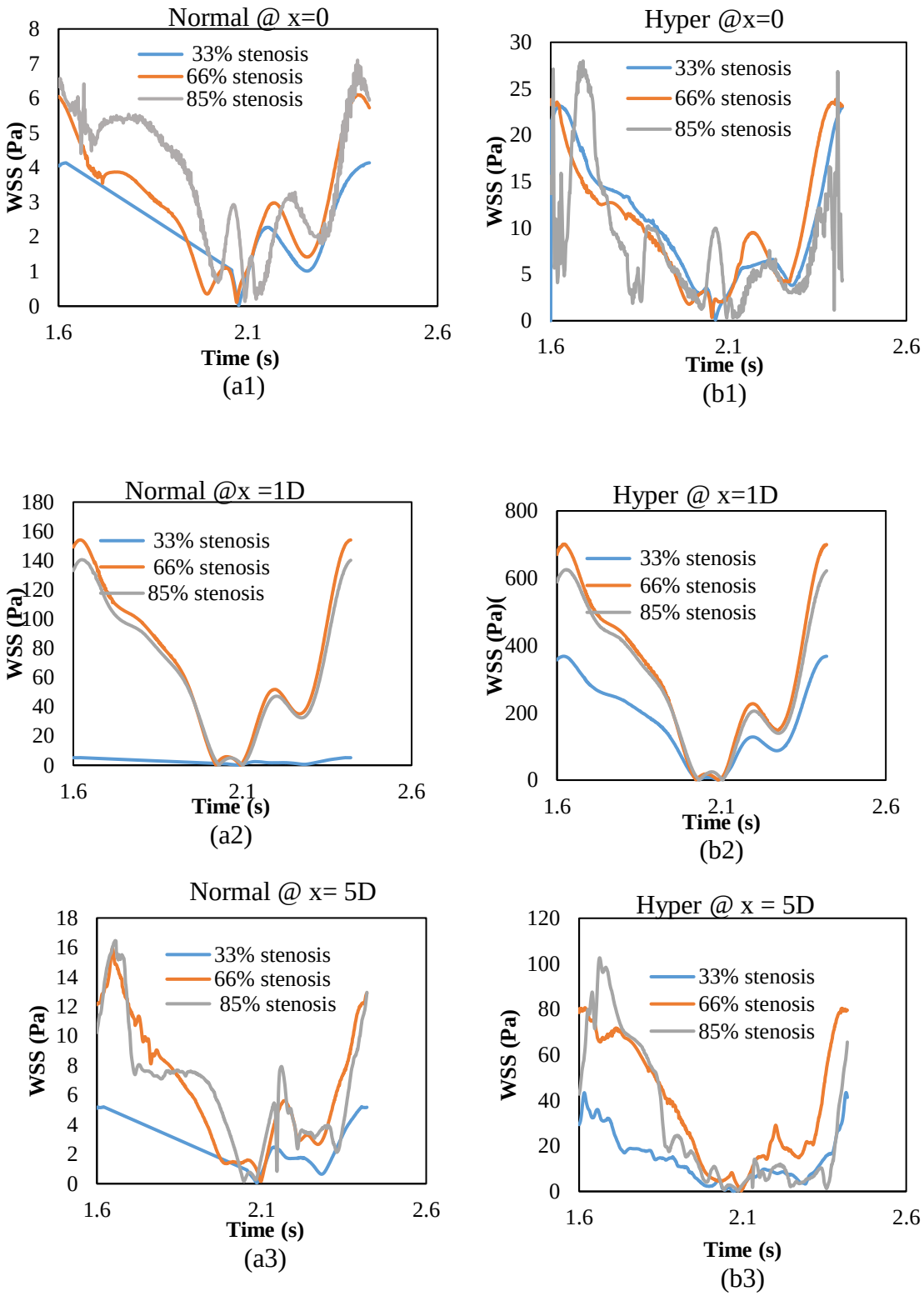

Fig. 5.4 WSS at x=0, x= 1D, x=5D for 33%, 66% and 85% stenosis: (a1), (a2), (a3) - Normal condition; (b1), (b2), (b3) - Hyperaemic condition

From the results (Fig. 5.4) it is established that the percentage stenosis and flow rate play a very important role in deciding the WSS values. The position of stenosis is also a decisive factor of WSS values. Very large increment in WSS value is observed against increase in degree of stenosis. Further, with increase in flow from normal to hyperaemic, WSS values increases manyfold in each stenosis case.

5.3.1. WSS variation along the artery wall

The behaviour of WSS is observed to be an important factor in progression of vessel wall deformations and subsequent wall rupture. The figures 5.5 and 5.6 represents various plots of WSS along the vessel wall. WSS along the wall is plotted at different phases of the flow pulse (of 3rd cycle) for different stenosis cases under normal and hyperaemic flow conditions. The plot gives better understanding about WSS values at different locations at a particular phase of the pulse.

Fig. 5.5 (a) represents the WSS distribution of 33% stenosis case along the artery wall. The WSS plots at different phases of the pulse; 1.62 s, 2.05 s, 2.19 s and 2.26 s are plotted under normal flow. The diameter of 33% stenosis is 3 mm. The length of CT scan image is extended to 5D on both ends for obtaining a fully developed flow. The throat of 33% stenosis is located at 3.29 mm from starting point of CT scan image. Two important phases in cardiac cycle are` 1.62 s (maximum flow) and 2.05 s (minimum flow). The value of WSS begin to increase in the pre stenotic region and attains maximum value at throat of the stenosis. The observed value of WSS at pre-stenotic region was ~12 Pa at 1.62 s phase, while the same is 1.24 Pa for 2.05 s phase of the cardiac cycle. In pre- stenotic region WSS values are found to be in the range of healthy person (2 -16 Pa). The WSS value reaches maximum value of 48.08 Pa and 4 Pa at the throat of the stenosis during maximum flow (1.62 s) and minimum flow (2.05 s) respectively. WSS value starts falling down immediately after the stenosis throat and falls below the safe value of 2 Pa in the post stenotic region. The trend is common is in all four different phases. WSS fluctuations were observed in post stenotic region. These fluctuations damps down in the downstream and becomes stable.

Fig. 5.5(b) and 5.5(c) depicts the WSS variation of 66% and 85% stenosis cases under normal flow. The position of stenosis throat from the starting point is different in each case. The throat position is at 3.89 mm in case of 66% stenosis and it is 8.68 mm in case of 85% stenosis. WSS values are found to be in the range of healthy person in the pre-stenotic region during all phases of the pulse. The value begins to shoot up at stenosis region with reduction in flow area. WSS attains its maximum value at throat of the stenosis. The maximum value of WSS at maximum flow (1.62 s) in 66% and 85% stenosis are 165 Pa and ~260 Pa respectively. The WSS values drops drastically after the highest peak value in both cases. Strong secondary oscillations of WSS were observed in all the phases of cardiac cycle in the post stenotic region. At this region, WSS goes below the safe limit of 2 Pa. As reported, this area of turbulence transitions creates rough WSS profiles with a number of peaks and valleys, caused by surface irregularities, recirculation and reattachment zones (Jabir and Lal, 2016). At downstream the WSS fluctuations attenuates and approaches the WSS value at upstream.

WSS distribution along the vessel wall was plotted at hyperaemic flow for different stenosis levels, represented in Fig 5.6 (a), (b) and (c). The WSS profile follows similar trend of normal flow for the hyperaemic condition as well, but intensity is different. At throat of stenosis, WSS reaches as high as 430 Pa, 844 Pa and 1326 Pa at 1.62 s. These maximum values are ~8.9 times (for 33% case) and ~5.1(for both 66% and 85% cases) times of the corresponding values during normal flow. In post stenotic region the WSS value goes below 2 Pa where secondary fluctuations were observed. These areas were identified as the recirculation regions, by the velocity vector diagrams. Stenosis severity is also one of the most important factor that affects the flow behaviour and hence the WSS. Same can be well perused by comparing WSS plots of each stenosis case. The maximum WSS value at hyperaemic flow conditions of 85% stenosis case (1326 Pa) is much higher (~3 times) than the maximum WSS value of 33% case (430 Pa). Next section clearly explains the details of high WSS areas with the help of WSS contours.

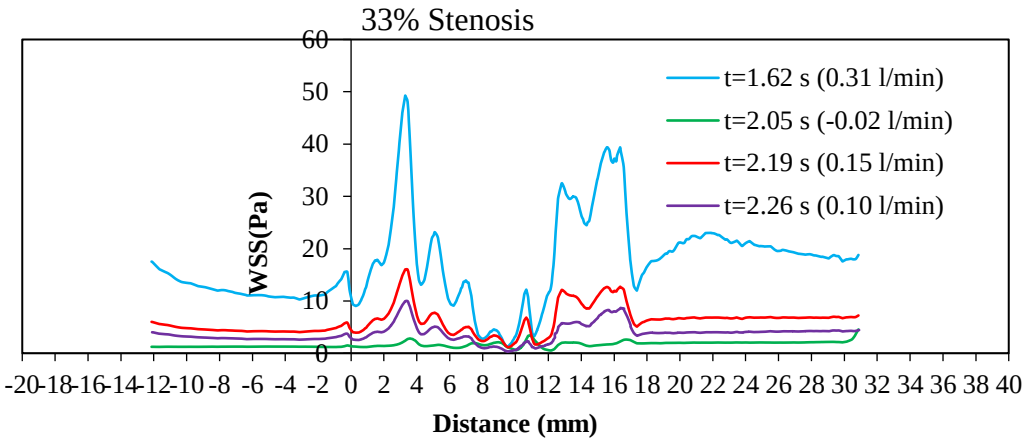

(a)

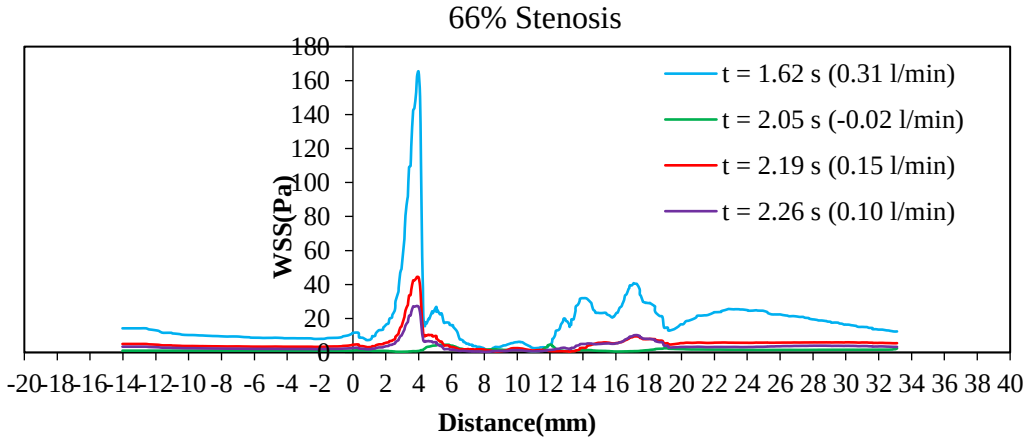

(b)

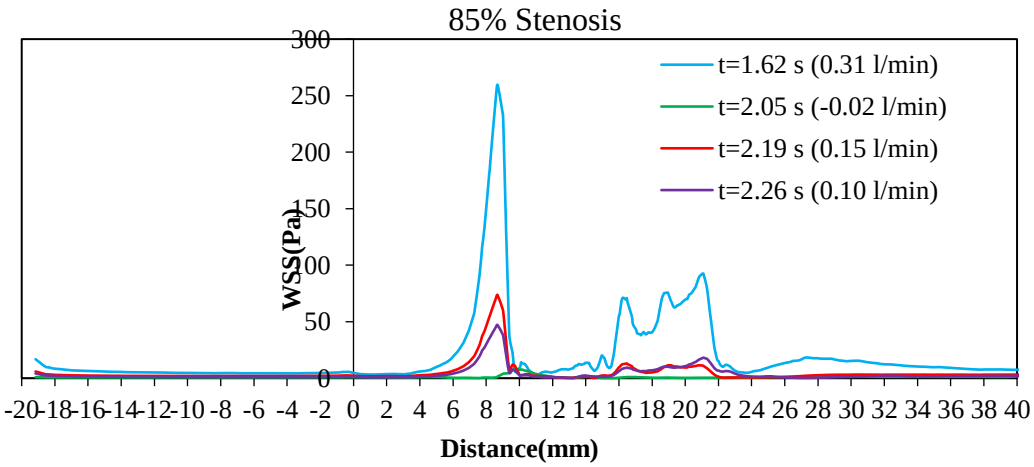

(c)

Fig. 5.5 WSS variation along the artery wall for different phase of cardiac cycle in normal condition (a) 33%; (b) 66%; (c) 85%

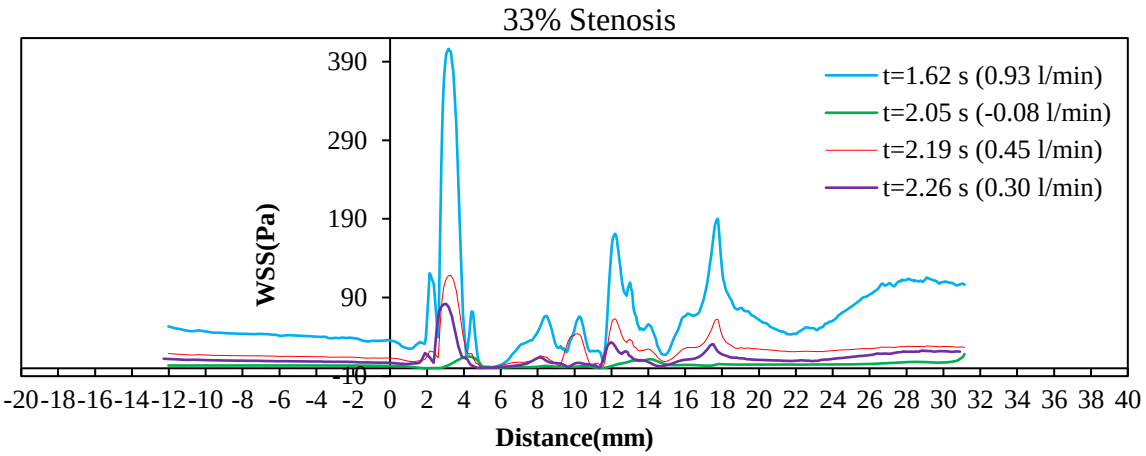

(a)

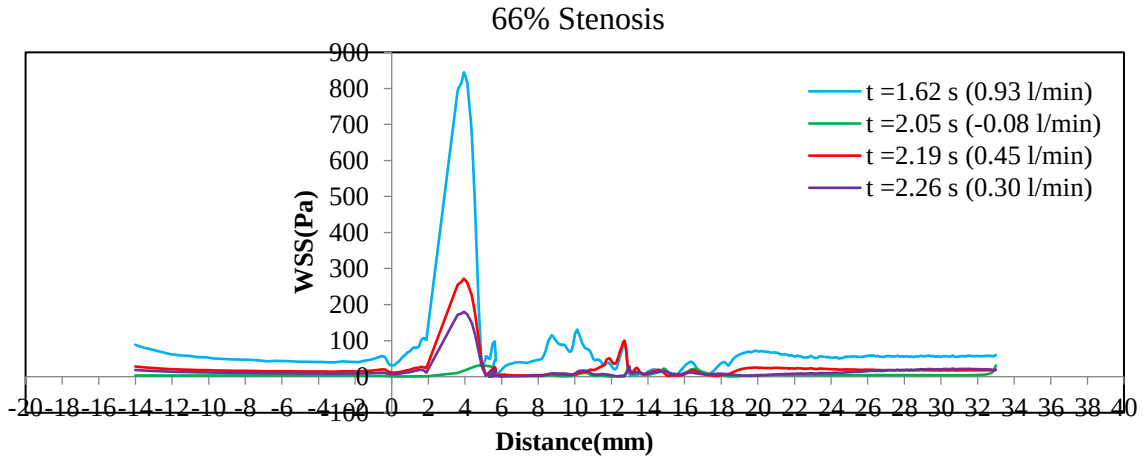

(b)

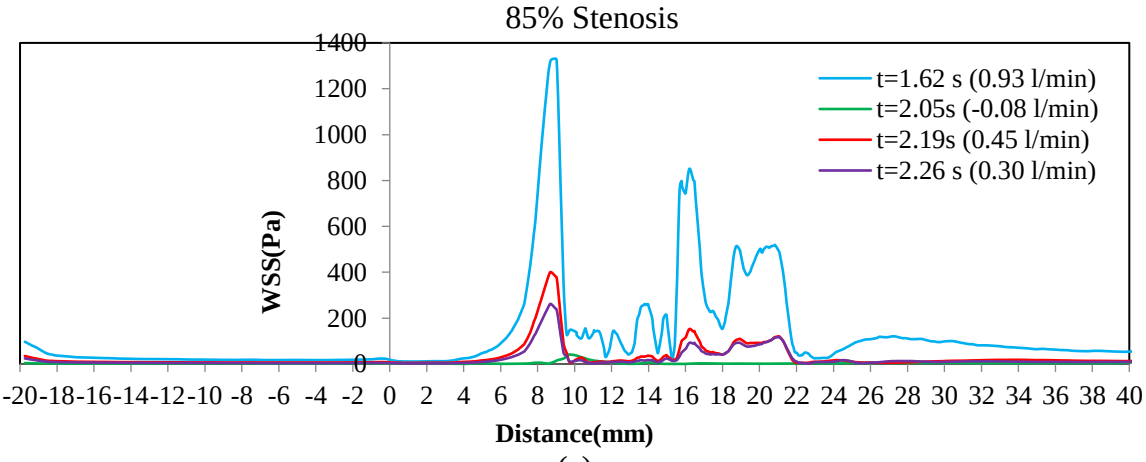

(c)

Fig. 5.6 WSS variation along the artery wall for different phase of cardiac cycle in hyperaemic condition (a) 33%; (b) 66%; (c) 85%

5.3.2. WSS contours

The Fig. 5.7(a), (b) represents contour plots showing WSS distribution of three stenosis cases under normal and hyperaemic conditions at peak flow (1.62 s). The contour plots give a better understanding of the WSS distribution. From the figure it is clear that in all cases the WSS values are between 0 Pa to 241.38 Pa under normal flow, the value goes up to ~260 Pa in case of 85% stenosis case. Under hyperaemic flow condition the value of WSS observed at stenosis were 430 Pa and 844 Pa for 33% and 66% case respectively. However, the corresponding value of WSS observed in case of 85% case is considerably high. The value observed in case of 85% case at hyperaemic flow is 1326 Pa at the centre of the stenosis, which is much higher compared to the values of other two cases. The study reveals that, the peak WSS value is higher by ~26 times or more compared to its maximum permissible value (2-16 Pa). Comparing the WSS contours of each case, it is understood that the size of the stenosis has a significant effect on the WSS. The point at which WSS_{max} occurs on the artery surface depends mainly on the size and geometry of the stenosis (Fig. 5.7).

5.4. Velocity profiles

Velocity profiles give better idea about the nature of blood flow in a stenosed artery. Since size and geometry of the stenosis have a major impact on WSS, velocity profiles are plotted only for 66% and 85% stenosis. At maximum flow (1.62 s), velocity profiles were plotted in each section (Fig. 5.8 (a), (b), (c) and (d)) under normal and hyperaemic conditions for 66% and 85% stenosis. It is observed that velocity profiles are parabolic in nature before the flow reaching the stenosis. The profile shape gets changed to plug profile while passing through the narrow region (stenotic region). Flow velocity is very high at throat of the stenosis. Due to asymmetric stenosis, flow profile becomes skewed towards opposite side of stenosis geometry (towards geometric eccentricity) as reported by Jabir and Lal, 2016. It is observed that, the flow profiles regain its parabolic shape after the stenosis constriction area in artery. From the velocity profile, it is found that the flow becomes turbulent immediately after stenosis throat due to sudden change in flow velocity and flow pattern near the plaques.

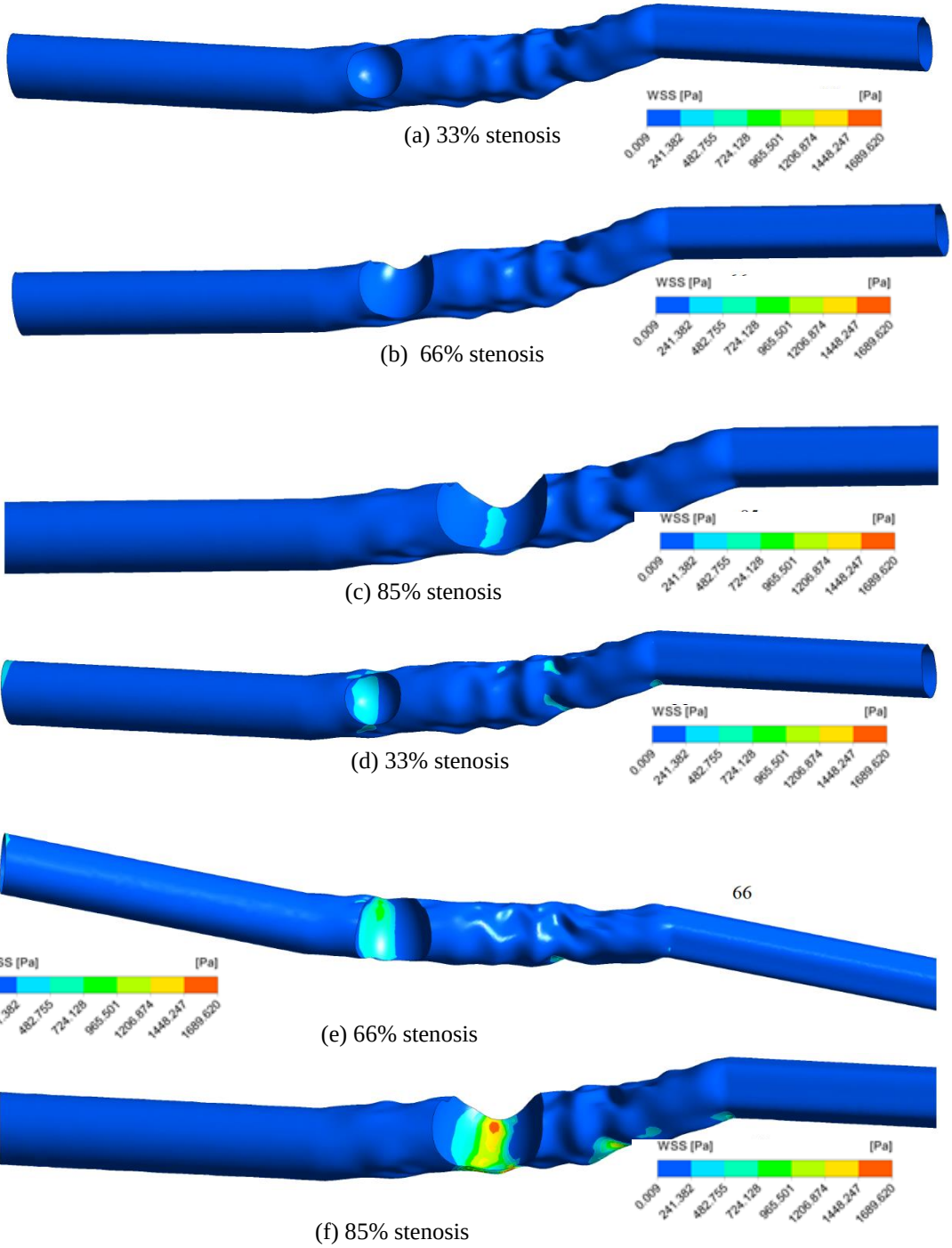

(a) 33% stenosis

(b) 66% stenosis

(c) 85% stenosis

(d) 33% stenosis

(e) 66% stenosis

(f) 85% stenosis

Fig. 5.7 Contour plots of WSS at normal and hyperaemic condition for different % stenosis at maximum flow (i.e., 1.62 s of cardiac cycle) (a-c) Normal condition; (d-f) Hyperaemic condition

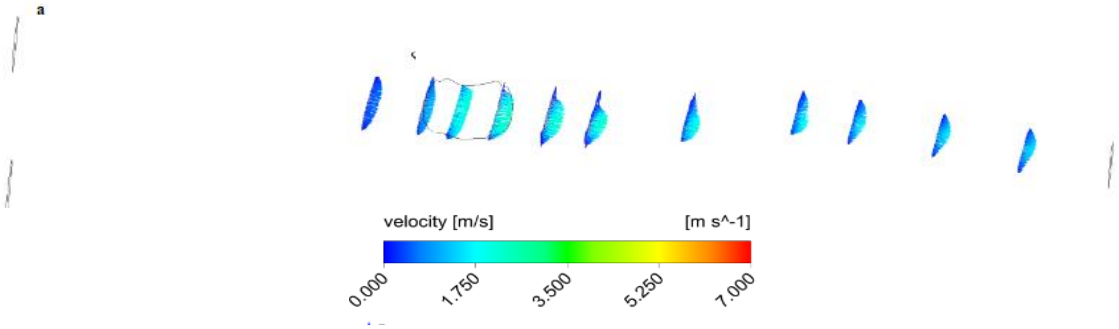

Normal flow-66% stenosis case

(a)

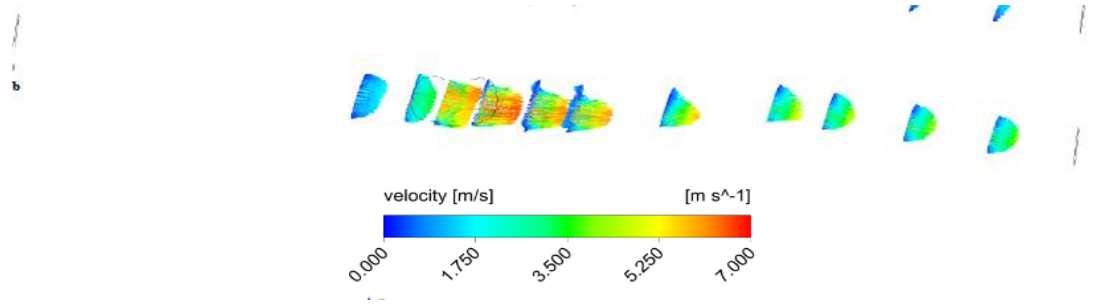

Hyperaemic flow- 66% stenosis case

(b)

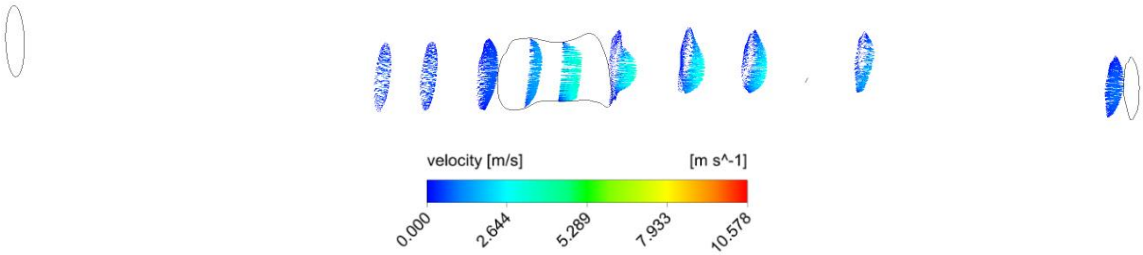

Normal flow-85% stenosis case

(c)

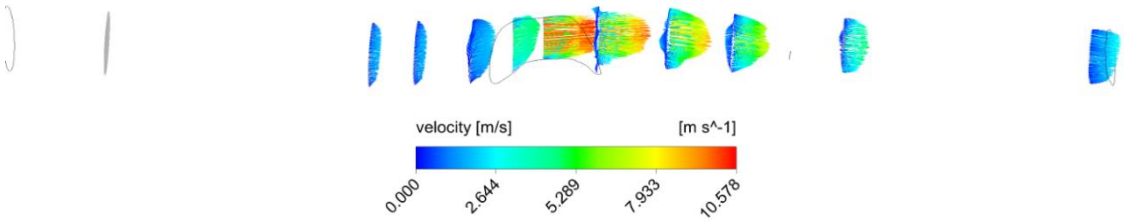

Hyperaemic flow- 85% stenosis case

(d)

Fig. 5.8 Velocity field profile at normal and hyperaemic condition (a-b) 66% stenosis; (c-d) 85% stenosis

5.4.1. Velocity vector diagrams

To have a better understanding and clarity on the flow characteristics in post stenotic region, velocity vector diagrams are also plotted for 66% and 85% stenosis cases under hyperaemic flow condition (Fig.5.9 (a), (b)). The diagram clearly depicts drastic change in velocity immediately after the stenosis as mentioned in earlier sections (Fig. 5.8). This rigorous change in velocity leads to proportionate variations in Reynolds number figures along the vessel length. The Re in post stenotic region is high due to this increase in velocity, which develops turbulence. The maximum Re value noted in the region before stenosis, upstream side, is in the range of 1500 ~ 1680 for 66% and 85% cases. The value spans as high as ~5005 and ~6256 respective cases at the stenosis neck and in the downstream. This wide range of Reynolds number found across the vessel length justify the use of turbulence model in the study.

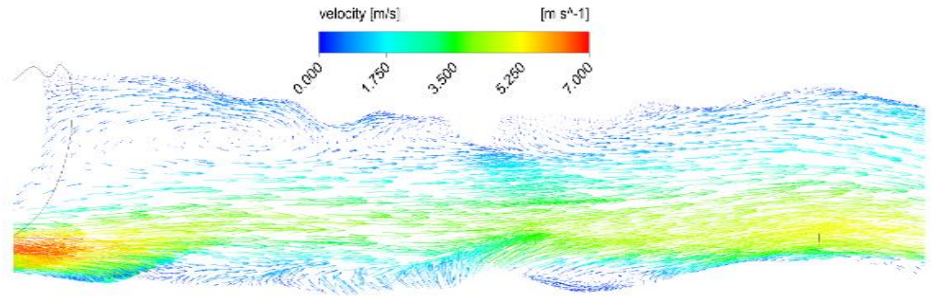

(a)

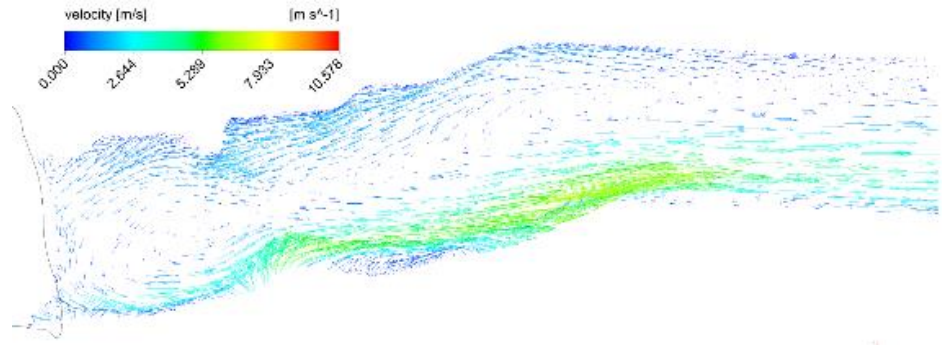

(b)

Fig. 5.9 Vector field along flow direction under hyperaemic condition (a) 66% stenosis; (b) 85% stenosis

Fig. 5.9 depicts that the turbulence formed in post stenotic region depends on flow rate and size of stenosis. Recirculation zones are also noted after the stenosis. Because of

turbulence and associated recirculation, secondary WSS fluctuations were examined in post stenotic region (Fig. 5.5 and 5.6). In both flow conditions the recirculation length is different and depends on shape and size of the stenosis. High WSS and recirculation regions stimulates the platelets formation and thus leads to thrombus (Fry, 1969). From the above analysis it is presumed that the flow fluctuations due to stenosis will lead to formation of recirculation zones in the downstream which may lead to secondary thrombus formation. The risk of such secondary stenosis formation increases with increase in stenosis severity.

5.5. Pressure distribution

This section discusses the pressure variation occurring inside a stenosed artery. The pressure drop is directly proportional to the work load on heart to supply sufficient amount of blood flow to organs, hence an important parameter in the coronary artery system. Pressure drop across the stenosis is plotted against the flow rate (from 0.158 l/min to 0.553 l/min) for different stenosis cases - 33%, 66% and 85% as shown in Fig. 5.10. From the figure it is observed that considerable pressure drop occurs across the occlusion area during higher degrees of stenosis. The study also observed that at same flow rate pressure drop is more for higher percentage stenosed artery. Fig. 5 .10 clearly depicts that pressure drop is very high for 85% stenosis.

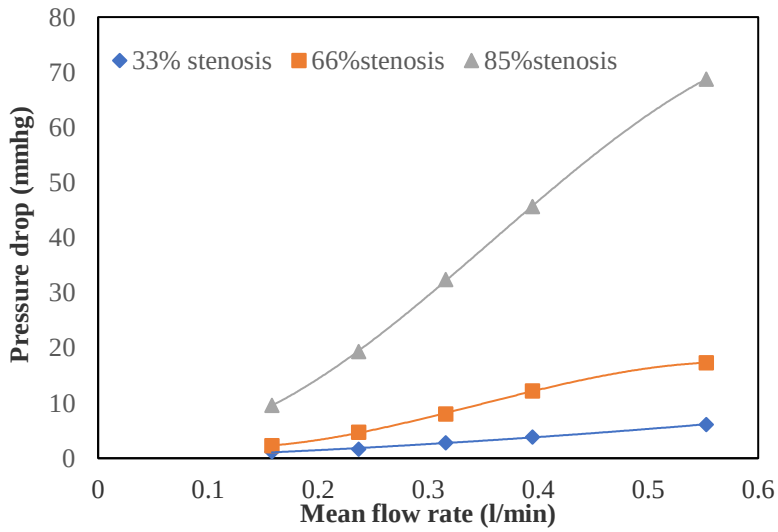

Fig. 5.10 Pressure drop for different degrees of stenosis

5.6. Calculation of FFR - Patient specific coronary artery

FFR is an index, used by medical practitioners for diagnosing the severity of stenosis, the study computed the FFR values for all patient specific cases from the pressure drop (Fig. 5.10). FFR corresponding to each mean flow rate is computed for all patient specific cases (Table 5.5). The Table 5.5 shows that the FFR value for 33% stenosis ranges from 0.98 to 0.89 at varying flow rates from normal to hyperaemic condition (0.158 - 0.553 l/min). The limiting value of FFR is 0.8. If it is found below 0.8, demands detailed investigation (Pijls and Sels, 2012). In the case of 66% stenosis, the FFR value ranges from 0.93 to 0.61. The FFR value crosses the critical value of 0.80 when flow rate is above 0.3 l/min. Further, in case of 85% stenosis, the FFR value ranges from 0.82 to 0.35, which indicates the severity of 85% stenosis for almost all flowrates.

Table 5.5 FFR vs percentage stenosis for the variation in mean discharge

Q l/min	0.158	0.237	0.316	0.395	0.553
% stenosis	FFR				
0.33	0.987	0.967	0.946	0.931	0.896
0.66	0.932	0.867	**0.788**	0.722	0.617
0.85	**0.828**	0.700	0.602	0.510	0.358

5.6.1. Devising method for relating percentage stenosis and FFR

FFR values obtained at each stenosis cases were plotted against stenosis percentage at various flow rates as depicted in Fig. 5.11. Five different curves were generated corresponding to each flow rate. The relationship between FFR and percentage stenosis are established by means of second order polynomials in the form of ax^2+bx+c, for each flow rate. Fig. 5.11 shows five equations corresponding to five flow rates. From the plot, it is noted that these second order polynomial fit with the data points very well. The regression coefficients are obtained near to one. Each polynomial has different coefficients and constant (a, b and c) (Table 5.6). From these coefficients, one can calculate the FFR

for an unknown percentage stenosis corresponding to that flow rate. Table 5.7 represents evaluation of FFR of unknown stenosis cases (0.50, 0.47 and 0.45) by applying this method. With the help of CT scan data, FFR can be calculated for each flow rate by this non-invasive method. Fig. 5.12 shows the FFR vs flow rate plot corresponding to each stenosis case and found that 47% stenosis stay at the borderline of criticality and safe zone (FFR>0.8). Hence, with the help of the above methodology one can determine the criticality of stenosis. This information is vital as far as a medical practitioner is concerned because if otherwise, he has to follow invasive methods like the usage of a pressure catheter for finding FFR, which is very risky for a CAD patient apart from its high cost. However, now by using non-invasive methods, FFR can be computed by analysing CT image with the help of CFD and decision making can be done faster.

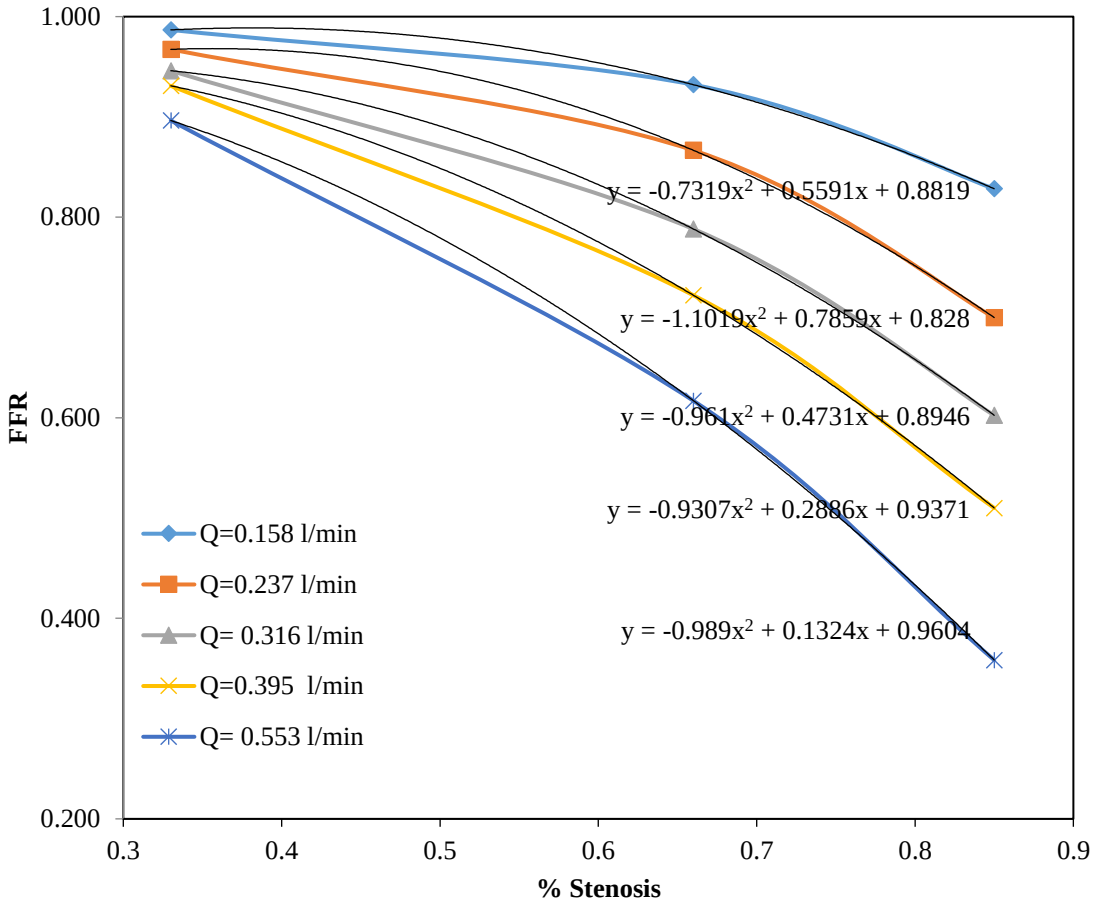

Fig. 5.11 FFR vs percentage stenosis (from normal to hyperaemic flow condition)

Table 5.6 Coefficients of FFR and percentage stenosis relation for each mean flow rate

Q (l/min)	Coefficients (x^2+x+c)			FFR correspond to unknown percentage stenosis *0.47
	x^2	x	c	
0.158	-0.7319	0.559	0.8819	0.983
0.237	-1.1019	0.7859	0.828	0.954
0.316	-0.961	0.4731	0.8946	0.905
0.395	-0.9307	0.2886	0.9371	0.867
0.553	-0.987	0.1324	0.9604	0.805
* Indicates unknown percentage stenosis				

Table 5.7 FFR vs mean flow rate for different percentage stenosis

%stenosis	0.33	0.66	0.85	*0.50	*0.47	*0.45
Q (l/min)	FFR					
0.158	0.987	0.932	0.828	0.978	0.983	0.985
0.237	0.967	0.867	0.700	0.945	0.954	0.958
0.316	0.946	0.788	0.602	0.890	0.905	0.912
0.395	0.931	0.722	0.510	0.848	0.867	0.878
0.553	0.896	0.617	0.358	0.779	0.805	0.820
* Indicates unknown percentage stenosis						

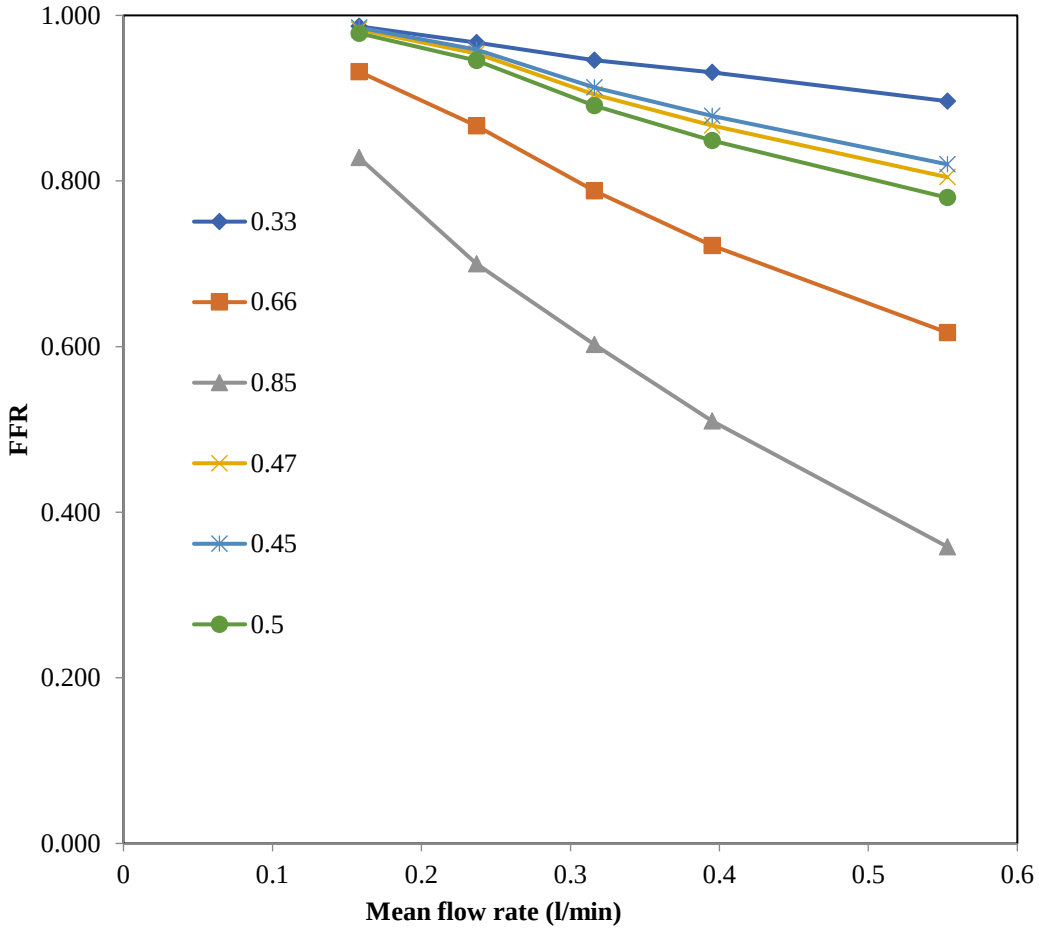

Fig. 5.12 FFR vs mean flow rate relation for different percentage stenosis

5.7. Effect of blood viscosity on hemodynamic properties

According to Sloop et al., (2015) pathogenesis of chronic cardiovascular diseases like atherosclerosis is not completely understood by the mainstream due to the failure in understanding the role of blood viscosity in it. The increase in osmolarity causes increased capillary permeability and consequently, increased haematocrit and viscosity. Stenosis and CAD cases have been increasing in younger age groups in the recent past. The studies reveal that, these cases are diagnosed in people with early Diabetes mellitus. The statistical data analysis of such CAD cases identifies strong bond between the CAD cases in young people having early diabetes. Further studies in this area reveal that, one of the major factors for early occurrence of CAD in diabetic patients is high blood viscosity (Cho et al.,

2008). Blood viscosity is a measure of resistance to flow and higher viscosity level increases the criticality of CAD. The studies observed that blood viscosity of people with diabetes go as high as 36.4 cP (Cho et al., 2008) which is more than ten times of a normal person (3.45 cP, Johnston et al., 2004). Hence the study of variation in blood viscosity on CAD patients is also significant in evaluating the risk while analysing hemodynamic parameters by conducting CFD studies (Cho et al., 2008; Irace et al., 2014).

The analysis considered geometries similar to the ones used in section 5.2 to determine the impact of viscosity variations on hemodynamic parameters. In order to understand the effect of variation in blood viscosity, a higher viscosity of 0.0364 Pa s (viscosity higher than 10 times of a normal person) was applied in non-Newtonian model to mimic the flow in coronary artery. Non-Newtonian studies were conducted by applying higher blood viscosity values matching with blood viscosity in diabetic patients (0.0140 Pa s, Le Devehat et al., 2001; and 0.0364 Pa s, Barnes et al., 1977). The study analysed WSS, pressure drop and FFR values in each case.

5.8. Non- Newtonian model

From the literature study, it is observed that the blood viscosity in diabetic patients go as high as 0.0364 Pa s. The study analysed the effect of hyper viscosity on hemodynamic parameters of the patient specific cases. Accordingly, two values of viscosity commonly found in diabetic patients are taken (0.0140 Pa s and 0.0364 Pa s) for the current study. The results of each case are discussed in the following sections.

5.8.1. WSS along the wall

Since size and geometry of the stenosis have a major impact on WSS, 66% and 85% stenosis cases are considered. To know more about the effect of viscosity on WSS, WSS at 1.62 s (maximum flow) and 2.05 s (minimum flow) were plotted along the wall for 66% and 85% stenosis cases (Fig. 5.13 and 5.14). Fig. 5.13 and Fig. 5.14 shows the WSS distribution of 66% and 85% stenosis case at 0.00345 Pa s (normal patient viscosity), 0.0140 Pa s (~4 times the normal viscosity) and 0.0364 Pa s viscosity levels.

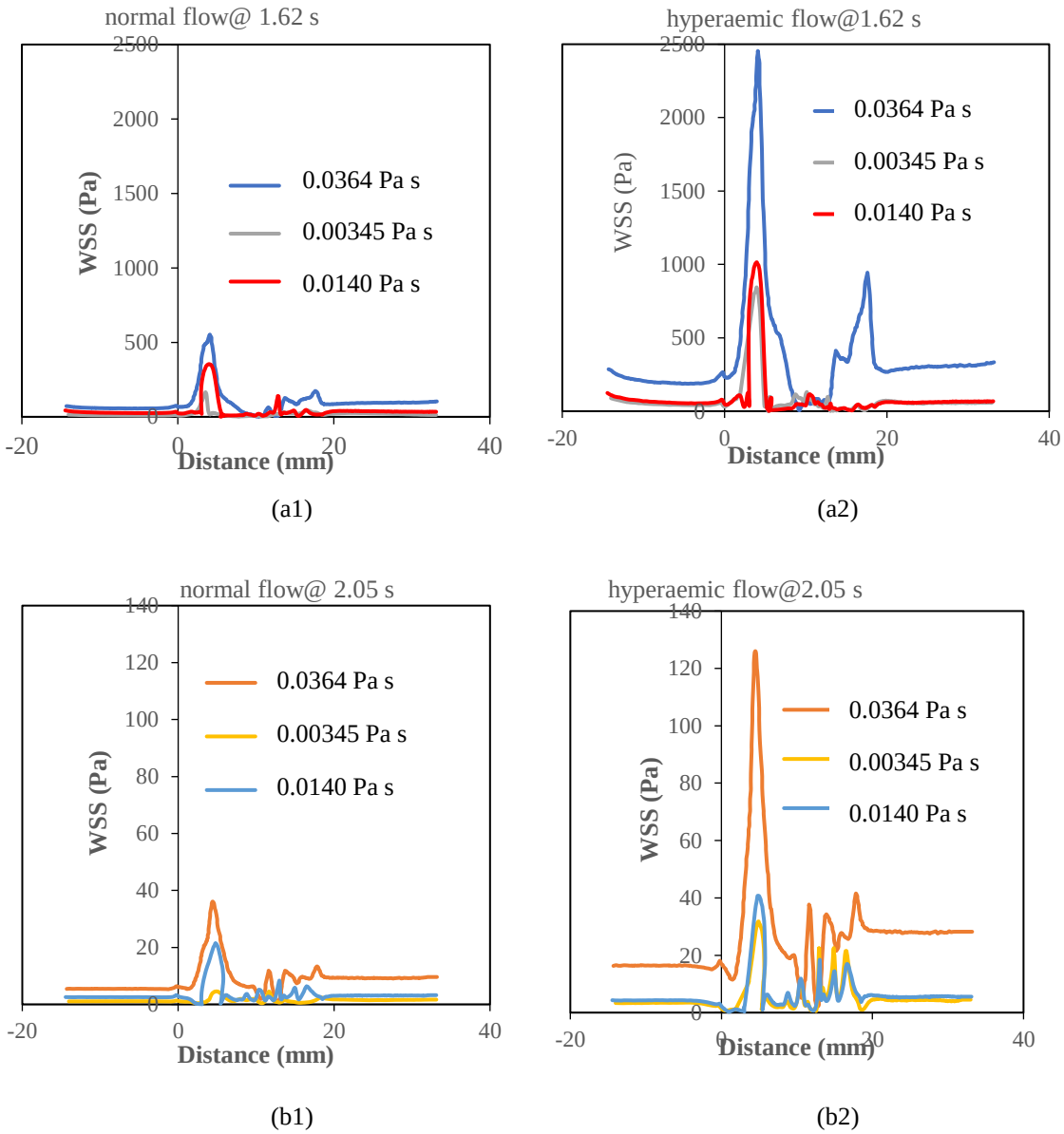

Fig. 5.13 WSS plot along the wall at under normal and hyperaemic flow for 66% stenosis case (a) maximum flow; (b) minimum flow

The study initially analysed WSS of 66% case under normal and hyperaemic flow conditions at higher viscosities (0.0140 Pa s and 0.0364 Pa s). WSS was analysed at maximum flow (1.62 s) and minimum flow (2.05 s) under normal and hyperaemic conditions. At 1.62 s, WSS_{max} observed at hyper viscosity conditions of 0.0140 Pa s and 0.0364 Pa s under normal flow in 66% stenosis case were 304 Pa and 525 Pa respectively. The values are ~1.8 and ~3 times greater than the WSS_{max} value at normal blood viscosity case (165 Pa). Similarly, under hyperaemic condition, the maximum WSS values obtained

were 977 Pa and 2404 Pa respectively, which were ~1.5 and 2.84 times higher than WSS_{max} value for corresponding normal viscosity case (844 Pa). The plots in Fig 5.13 clearly depict the occurrence of secondary oscillations in the post stenotic region due to turbulence. The intensity of turbulence in both hyper viscosity cases at post stenotic region is comparatively higher than the normal viscosity case of 66% stenosis. A similar trend was observed in 2.05 s (minimum flow) phase under normal and hyperaemic conditions.

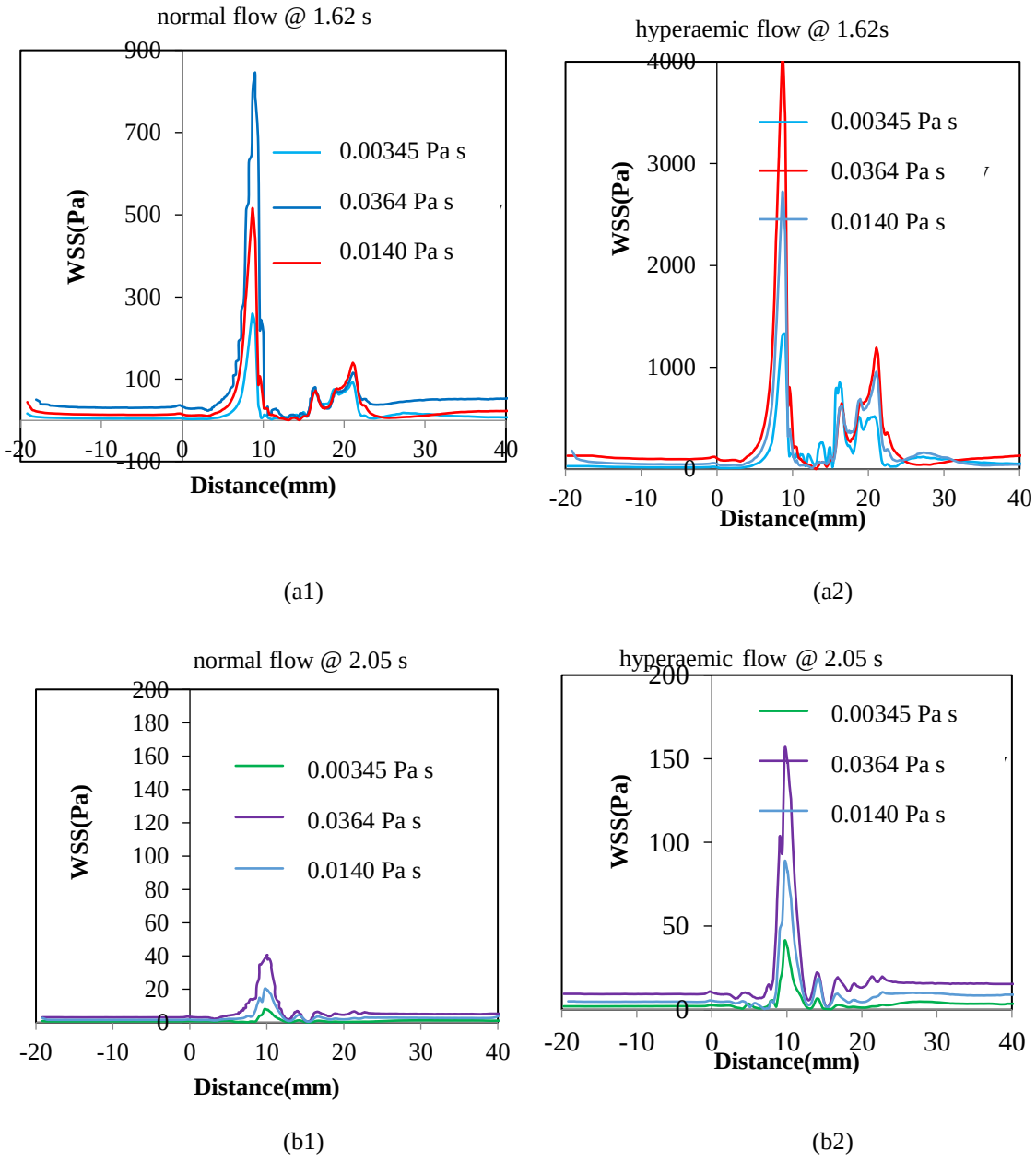

Fig. 5.14 WSS plot along the wall at under normal and hyperaemic flow for 85% stenosis case (a) maximum flow; (b) minimum flow

WSS at hyper viscosity conditions were plotted along the wall for 85% stenosis case. At both hyper viscosity cases of 85% stenosis, WSS_{max} observed under normal flow were 448 Pa and 788 Pa. From this it is noted that WSS_{max} is ~ 1.7 and ~ 3 times higher than WSS_{max} value of normal viscosity (260Pa) case. Under hyperaemic condition WSS values go as high as ~ 2 times (2723 Pa) and ~ 3 times (3903 Pa) of WSS_{max} under normal viscosity (1326 Pa). The plots clearly depict the occurrence of secondary oscillations in the post stenotic region due to turbulence. The intensity of turbulence is comparatively higher than the 66% cases. The secondary peak in post stenotic region is high in hyper viscosity cases. A similar trend was observed in 2.05 s (minimum flow) phase under normal and hyperaemic conditions.

Stenosis restricts free flow of blood by narrowing the flow area which generates high blood velocity followed. To enable transport of the same quantity of blood and to maintain the same volume flow rate, a larger pressure is to be generated at the inlet of the artery. More severe the occlusion, the more restrictive is the quantity of blood transported. The increase in blood viscosity adds up to the flow resistance and will enhance the work load on heart. This again promotes development of plaque and increases the risk of plaque rupture. It is reported that turbulent blood flow occurring immediately after stenosis can also accelerate the deposition of platelets to the plaque leading to its growth in the direction of blood flow (Wootton and Ku, 1999).

5.8.2. Calculation of FFR for diabetic patients

FFR was computed to access the impact of hyper viscosity (viscosity of diabetic patient) on patients with CAD. Following tables (Table 5.8 to 5.10) represent the FFR values of three stenosis cases (33%, 66% and 85%) under different flow conditions ranging from normal to hyperaemic (from 0.158 l/min to 0.553 l/min). For normal viscosity (0.00345 Pa s) and hyper viscosity (0.0140 Pa s) the FFR values were in safe limit for 33% case. The FFR value reached near to critical range when viscosity was 0.0364 Pa s at hyper viscosity condition (Table 5.8).

Table 5.8 FFR at different viscosity levels for 33% stenosis case

Q(l/min)	FFR		
	μ =0.00345 (Pa s)	μ =0.0140 (Pa s)	μ =0.0364 (Pa s)
0.158	0.99	0.976	0.97
0.237	0.97	0.958	0.94
0.316	0.95	0.92	0.90
0.395	0.93	0.90	0.86
0.553	0.90	0.87	0.84

Table 5.9 FFR at different viscosity levels for 66% stenosis case

Q(l/min)	FFR		
	μ =0.00345 (Pa s)	μ =0.0140 (Pa s)	μ =0.0364 (Pa s)
0.158	0.93	0.900	0.88
0.237	0.87	0.846	**0.80**
0.316	**0.79**	**0.723**	0.68
0.395	0.72	0.645	0.59
0.553	0.62	0.580	0.55

Table 5.10 FFR at different viscosity levels for 85% stenosis case

Q(l/min)	FFR		
	μ =0.00345 (Pa s)	μ =0.0140 (Pa s)	μ =0.0364 (Pa s)
0.158	0.83	**0.72**	**0.70**
0.237	**0.70**	**0.68**	**0.64**
0.316	**0.60**	**0.45**	**0.39**
0.395	**0.51**	**0.36**	**0.30**
0.553	**0.36**	**0.28**	**0.24**

In case of 66% stenosis, FFR value, reached near critical values at mean flow rate, 0.316 l/min at 0.00345 Pa s (normal viscosity) and 0.0140 Pa s (hyper viscosity). Further with a slight decrease in flow (mean flow = 0.237 l/min, Table 5.9), the FFR value reached critical value at hyper viscosity (μ = 0.0364 Pa s) condition in 66% case. Observations of 85% stenosis case shows that, FFR becomes critical at the normal flow condition itself for both normal and hyper viscosity conditions (Table 5.10). From the above study, it is observed that, effect of blood viscosity on hemodynamic parameters is very high during hyperaemia. The risk associated with increase in percentage stenosis increases with increase in viscosity. It can be concluded that, the whole blood viscosity plays a major role in genesis and progression of atherosclerosis in diabetic patients, posing an increased risk of heart attack in them.

5.8.3. Devising method for relating percentage stenosis and FFR

FFR was computed at different % stenosis corresponding to different flow rates under hyper viscosity condition (viscosity = 0.0140 Pa s and 0.0364 Pa s). By applying the procedure adopted in section 5.6 following tabulations and plots were prepared for μ = 0.0140 Pa s [(Tables 5.11, 5.12 and 5.13) and (Figs. 5.15 and 5.16)]. From the tables, it is observed that the stenosis percentage at which CAD become critical is found to be 45% for μ as 0.0140 Pa s compared to that at normal viscosity (47% stenosis).

Table 5.11 FFR vs percentage stenosis for the variation in mean discharge at viscosity 0.0140 Pa s

Q l/min	0.158	0.237	0.316	0.395	0.553
% stenosis	FFR				
0.33	0.976	0.958	0.920	0.900	0.870
0.66	0.900	0.846	**0.723**	0.645	0.580
0.85	**0.720**	0.680	0.450	0.360	0.280

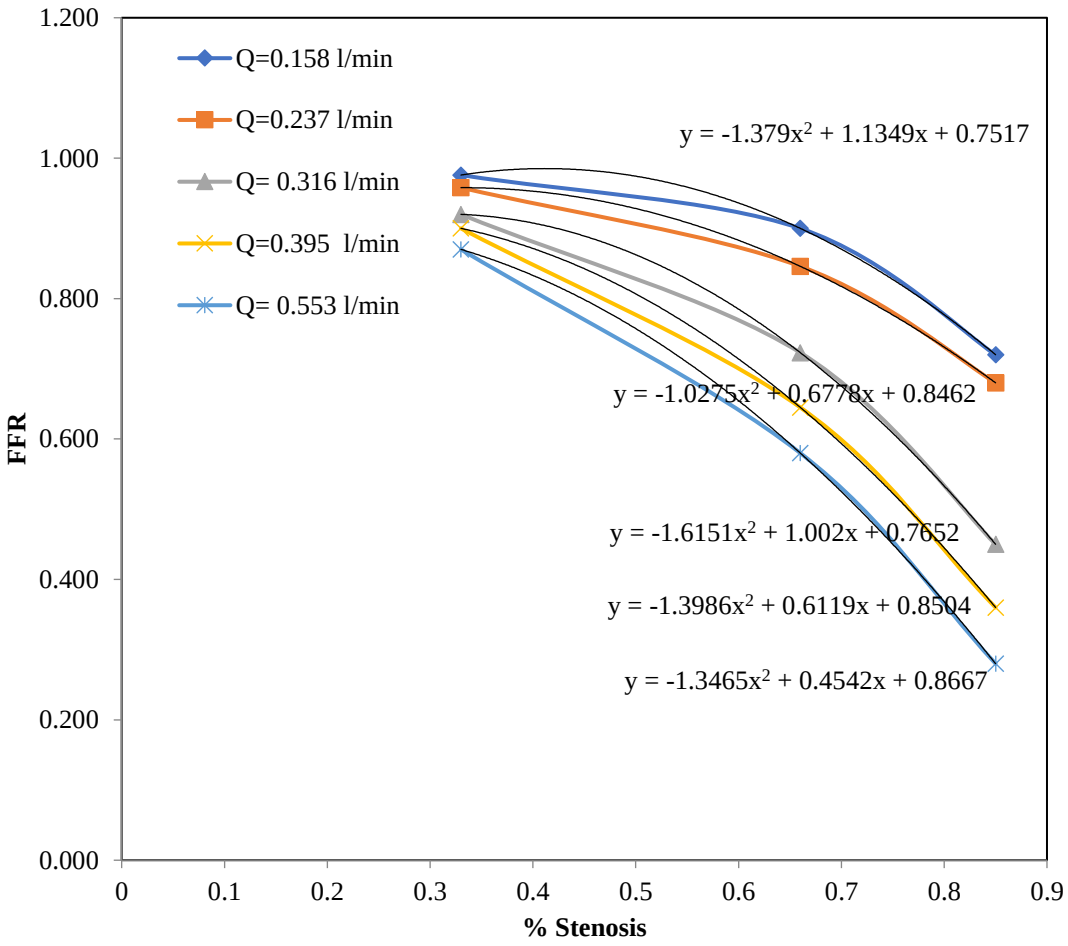

Fig. 5.15 FFR vs percentage stenosis at 0.0140 Pa s (from normal to hyperaemic flow condition)

From Fig. 5.15, five different second order polynomials were obtained. Coefficients and constants (a, b and c) of polynomials are tabulated in Table 5.11. FFR for an unknown percentage stenosis can be computed using the above five equations. From Tables 5.11, 5.12 and Fig. 5.16 it is observed that, at higher viscosity (0.0140 Pa s), 45% stenosis become critical during hyperaemic flow condition.

Table 5.12 Coefficients of FFR and percentage stenosis relation for each mean flow rate at viscosity 0.0140 Pa s

Q (l/min)	Coefficients (x^2+x+c)			FFR correspond to % stenosis *0.45
	x^2	x	C	
0.158	-1.379	1.1349	0.7517	0.983
0.237	-1.0275	0.6778	0.8462	0.943
0.316	-1.6151	1.002	0.7652	0.889
0.395	-1.398	0.6119	0.8504	0.843
0.553	-1.3465	0.4542	0.8667	0.798

Table 5.13 FFR vs mean flow rate for different percentage stenosis at viscosity 0.0140 Pa s

% stenosis	0.33	0.66	0.85	*0.5	*0.45	*0.4
Q (l/min)	FFR					
0.158	0.976	0.900	**0.720**	0.974	0.983	0.985
0.237	0.958	0.846	0.680	0.928	0.943	0.953
0.316	0.920	0.723	0.450	0.862	0.889	0.908
0.395	0.900	0.645	0.360	0.806	0.843	0.871
0.553	0.870	0.580	0.280	0.757	0.798	0.833
* Indicates unknown percentage stenosis						

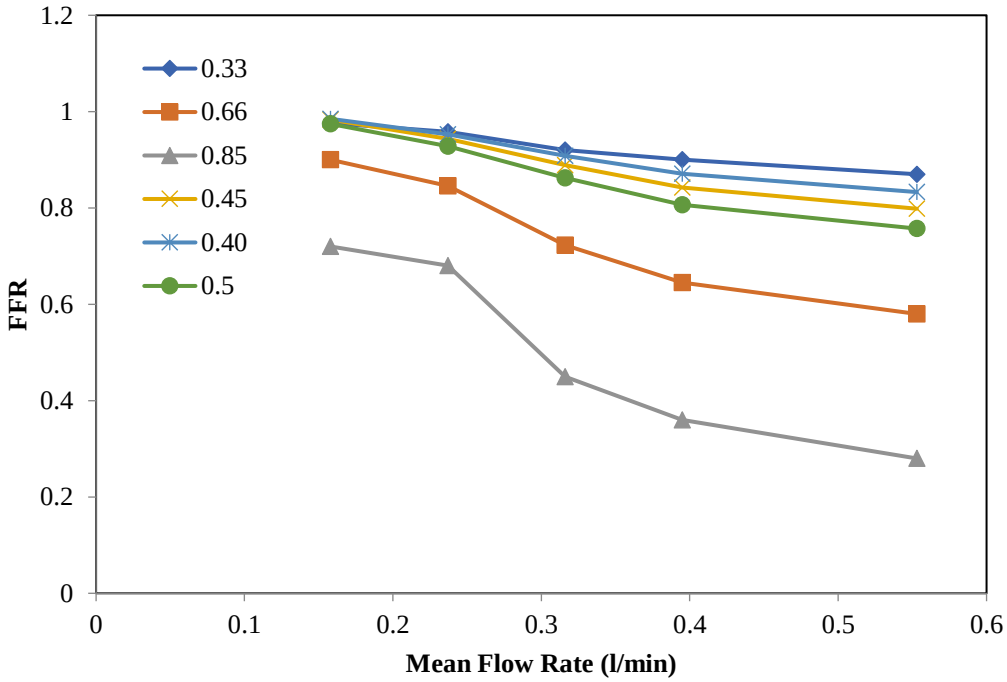

Fig. 5.16 FFR vs mean flow rate relation for different percentage stenosis at 0.0140 Pa s

Simulations were again carried out for hyper viscosity case (0.0364 Pa s). The step-by-step procedure is explained with help of Tables (5.14,5.15 and 5.16) and Figs (5.17 and 5.18).

Table 5.14 FFR vs percentage stenosis for the variation in mean flowrate at viscosity 0.0364 Pa s

Q (l/min)	0.158	0.237	0.316	0.395	0.553
% stenosis	FFR				
0.33	0.970	0.940	0.900	0.860	0.840
0.66	0.880	**0.800**	0.680	0.590	0.550
0.85	**0.700**	0.640	0.390	0.300	0.240

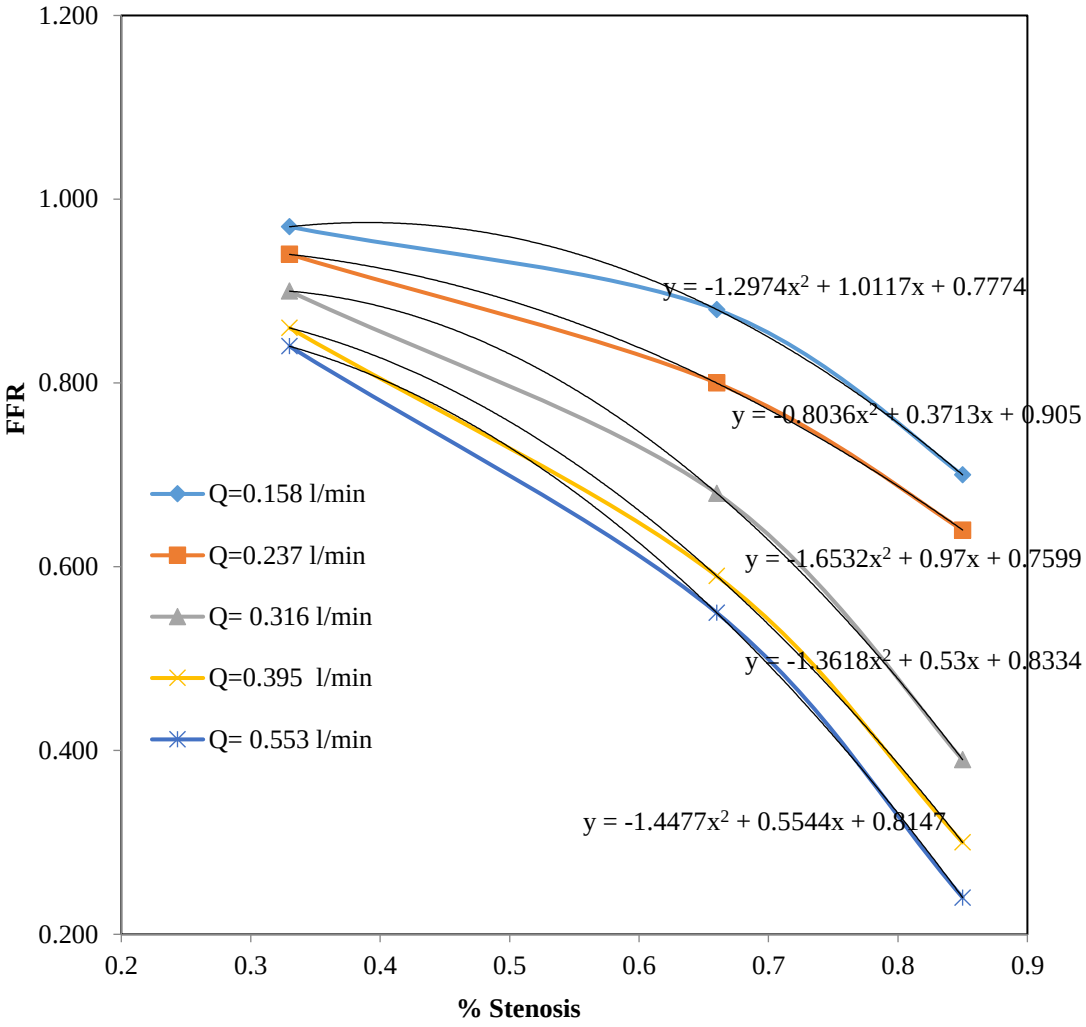

Fig. 5.17 FFR vs percentage stenosis at viscosity 0.0364 Pa s (from normal to hyperaemic flow condition)

Fig. 5.17 and Table 5.15 represents the coefficients and constants (a, b and c) of five polynomials. These equations were used for computing the FFR of an unknown percentage stenosis. It is observed that FFR value reaches critical at 40% stenosis during hyperaemic condition at higher blood viscosity of 0.0364 Pa s.

Table 5.15 Coefficients of FFR and percentage stenosis relation for each mean flow rate at viscosity 0.0364 Pa s

Q (l/min)	Coefficients (x^2+x+c)			FFR correspond to unknown percentage stenosis *0.40
	x^2	x	c	
0.158	-1.297	1.0117	0.7774	0.97
0.237	-0.803	0.3731	0.905	0.92
0.316	-1.6532	0.97	0.7599	0.88
0.395	-1.361	0.53	0.8334	0.83
0.553	-1.4477	0.5544	0.8174	0.80
* Indicates unknown percentage stenosis				

Table 5.16 FFR vs mean flow rate for different percentage stenosis at viscosity 0.0364 Pa s

% stenosis	0.33	0.66	0.85	*0.5	*0.45	*0.4
Q (l/min)	FFR					
0.158	0.970	0.880	**0.700**	0.96	0.96	0.97
0.237	0.940	**0.800**	0.640	0.89	0.91	0.92
0.316	0.900	0.680	0.390	0.83	0.86	0.88
0.395	0.860	0.590	0.300	0.76	0.80	0.83
0.553	0.840	0.550	0.240	0.73	0.77	0.80
* Indicates unknown percentage stenosis						

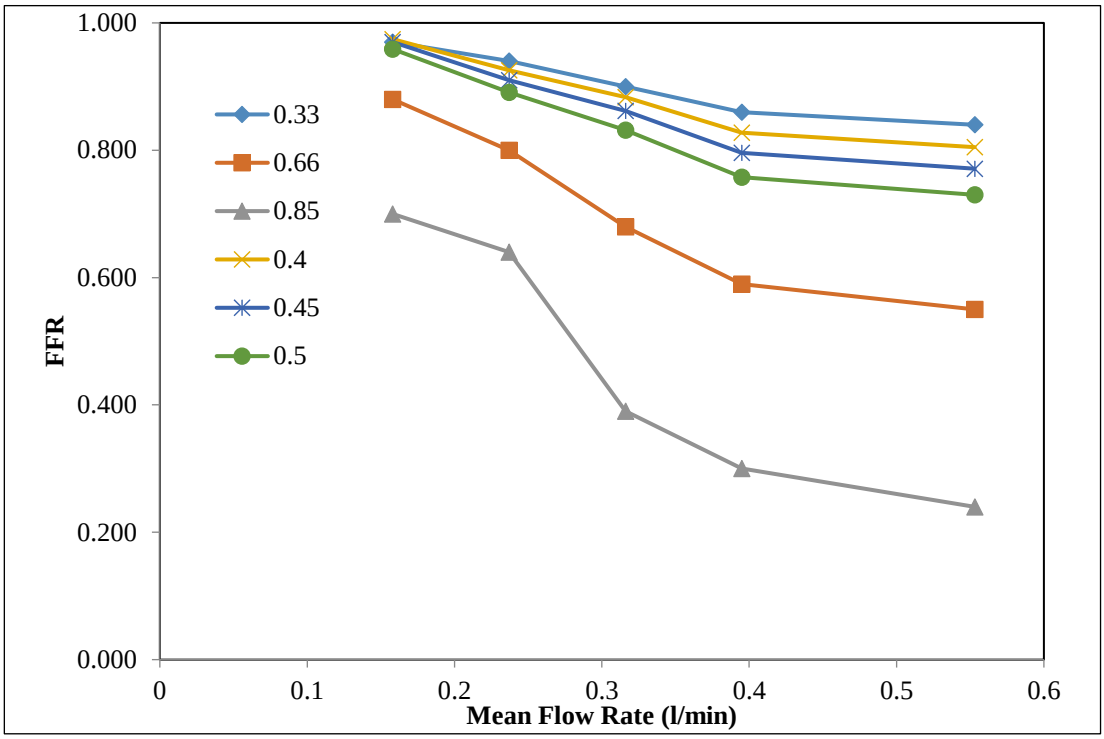

Fig. 5.18 FFR vs mean flow rate relation for different percentage stenosis at 0.0364 Pa s

The methodology developed can be summarized as follows;

The study collected CT scan image of coronary artery of CAD patients with different stenosis levels (33%, 66% and 85%) for creating patient specific geometries. CFD studies were conducted at different stenosis levels by applying transition SST k-ω model for the simulation of hemodynamic variables. Pulsating flow profiles were applied at the inlet of the geometry. Five different mean flow rates (0.158 l/min. 0.270 l/min, 0.336 l/min, 0.395 l/ min 0.553 l/min) were applied to mimic the arterial blood flow from normal to hyperaemic. FFR is calculated from the simulated results of pressure corresponding to the flow based on the above mean flow rates. These FFR values at each stenosis case was plotted against stenosis percentage for the above flow rates. Five graphs are generated by plotting FFR vs % stenosis for the above-mentioned flow rates. Each graph is mapped to a second order polynomial. Each polynomial has two different coefficients and a constant. In a nutshell, five different second order polynomial equations are established

corresponding to each graph (representing different flow rates). Using these coefficients and constant of a particular flowrate, one can calculate the FFR for an unknown percentage stenosis corresponding to that flow rate. Similarly, one can generate the FFR value of any percentage stenosis for all the above-mentioned flowrates. By comparing this generated FFR value with the limiting value of FFR, one can determine the criticality of % size of stenosis. Similar procedure is adopted for the hyper viscosity case as well.

5.9. Summary

The study observed flow transition from laminar to turbulent and re-laminarization in the post stenotic region at higher stenosis cases (66% and 85 % cases). The study observed that the flow rate and pressure drop are directly proportional to the stenosis size and hence the FFR. FFR value becomes critical even at normal flow in 85% case and at slightly higher flows in 66% stenosis case. A methodology is developed to compute the FFR value of an unknown percentage stenosis case from the simulated results of 33%, 66% and 85% stenosis cases. Using the above procedure critical value of stenosis is identified as 47%, above which the FFR value will become unsafe. The procedure can be used as a primary (non-invasive) evaluation tool for accessing the risk levels associated with each stenosis case. Further the study investigates the effects of diabetic mellitus and blood viscosity on stenosis, another important parameter influencing pressure drop and FFR. It was found that the critical value of stenosis size at high viscosity is identified as 45% in case of μ, 0.0140 Pa s and 40% at μ ,0.0364 Pa s. The study observed that increase in blood viscosity leads to high WSS and thus cause heavy damage to endothelial cells, leading to secondary stenosis. The effect gets aggravated during hyperaemic conditions, disturbing the hemodynamic parameters significantly. Thus, increase in blood viscosity directly influence/increase the risk associated with stenosis. It is concluded that the whole blood viscosity plays a major role in diabetic patients with atherosclerosis in genesis and progression of stenosis.

CHAPTER 6

SUMMARY AND CONCLUSIONS

6.1. Summary of the work

The main cause of fatalities due to cardiovascular diseases is associated with stenosis in coronary arteries. A number of experiments and research studies were conducted to understand the process of initiation and propagation of CAD in such arteries. The progress of experimental studies was limited due to difficulties in obtaining measurements from live specimens and because of the limitations in recreating real case experimental setups. The above reasons limited the progress of research studies in this area until the rise of numerical and computational studies. With the development of numerical methods and computer aided studies, the research works in this area gained momentum by the late half of 20th century. The experimental studies revealed few basic ideas like formation of turbulence in blood flow in stenosed arteries. With the advancements in numerical studies the researchers are able to do detailed analysis of flow patterns and hemodynamics. So far, these studies have not attempted to analyse FFR and WSS in patient specific cases to craft a tool for medical practitioners. Further the study intends to analyse the effect of other chronic diseases on hemodynamics and its effect on CAD.

The current study initially analyses the variations in results, when blood is considered under Newtonian and non-Newtonian behaviour in a stenosed vessel. The effect of various boundary conditions and numerical models were studied to select an optimal model for accounting the turbulence and flow separation in post stenotic region. Further numerical studies were conducted on different patient specific vessel geometries with different percentage stenosis and the results are compared. These results were compiled to generate a tool to obtain FFR for an unknown percentage stenosis. The study then analyses the effect of diabetes induced hemodynamic variations on stenosis criticality.

6.2. Conclusions

As a whole, the study concludes that, a stenosis with blockage as low as 47% can become critical under the excised or hyperactive condition. Chronic diseases like diabetic mellitus also increase the risk of stenosis in CAD patients. Following are the specific conclusions tailored from the study.

1. The study observed that the laminar model could not capture the flow transitions accurately due to the presence of turbulence caused by plaques. Hence the turbulence model for blood flow studies in coronary stenosed artery is established and validated.

2. The transition SST k-ω turbulent model, a less computationally intensive model, can give reasonable accuracy compared to DNS model. The model validates the cross-sectional velocity and WSS at different locations of the geometry.

3. Modelling of blood flow through a 75% axisymmetric ideal stenosis case reveals that the FFR value obtained from the study is in the safer range (>0.8), which is against the already known facts in medical science. Hence, the modelling of patient specific case (geometry and boundary conditions) is required to be carried out for the evaluation of FFR value.

4. The Newtonian and non-Newtonian model comparison results clearly shows that the shear values are less than 100 s-1 all along the flow profile in both cases. The results of WSS comparison show variation of 7 Pa between the models. The above results confirm that the study should consider non-Newtonian model in patient specific case of coronary artery (where the vessel size is small).

5. The study proposes a non-invasive technique for evaluating the FFR value of a stenosed artery by using CFD analysis along with the CT scan image of the patient specific coronary artery.

6. A methodology is devised to evaluate the criticality of the stenosis and hence avoid the need for angiography or other invasive methods, for evaluation purpose.

7. The methodology reveals that, stenosis at the order of 47% can be critical under hyperaemic condition.

8. The study of WSS in stenosed coronary artery reveals that the WSS values exceed the lower and upper ranges (2-16 Pa) by a large margin at post stenotic region during various phases of the cardiac cycle and hence can lead to the damage of endothelial cells leading to development of secondary stenosis.

9. The current study reveals that, FFR value of a diabetic patient can reach critical even when the percentage of stenosis is in the range of 40% (while stenosis below 50% is assumed as non-critical by medical practitioners).

6.3. Research contributions

1. Developed a methodology for the determination of FFR (index used to mention the criticality of CAD) with reasonable accuracy from CT scan image of a CAD patient at various flow conditions.

2. The method enables medics to determine the FFR values without any invasive techniques, which may pose higher risk for a critical CAD patient.

3. The tool can be applied to obtain FFR effectively at varying blood viscosities of CAD patients with diabetes.

4. The study can predict the probability of occurrence of secondary stenosis and its tentative location in the downstream of existing stenosis, can aid the design of stents and medication.

6.4. Limitations of the study

- The current study considered only three patient specific cases due to the difficulty in obtaining clinical data and requirement of expertise in extracting the geometry from it. A large sample size can aid in fine tuning the FFR curves and thus the methodology.

- This work assumed the vessel walls as rigid whereas in real case it is compliant and deform according to pressure variations.

- The study extended both ends of CT scan image of left coronary artery to obtain fully developed flow, wherein real case it is short in length and branches in to Left anterior descending (LAD) artery and Left circumflex artery (LCX).

- Extensive requirement of computational power and complexity in solution methodology limited the scope of present study with Fluid structure interaction (FSI).

6.5. Scope for further study

- The mathematical tool developed in this study can be fine- tuned by extending the study to a larger sample group.

- The artery wall is compliant and undergo deformations with pressure variations. This same can be included in the numerical studies to obtain more realistic and accurate results by applying FSI techniques.

- The study can be extended to multiple stenosis in an artery.

- The present study can also be extended to multiphase modelling by considering blood as a combination of blood cells and plasma.

REFERENCES

1. Ahmed, S. A. and Giddens, D. P. (1983a). Flow disturbance measurements through a constricted tube at moderate Reynolds numbers. *Journal of biomechanics, 16*(12), 955-963.

2. Ahmed, S. A. and Giddens, D. P. (1983b). Velocity measurements in steady flow through axisymmetric stenoses at moderate Reynolds numbers. *Journal of biomechanics, 16*(7), 505-516.

3. Ahmed, S. A. and Giddens, D. P. (1984). Pulsatile poststenotic flow studies with laser Doppler anemometry. *Journal of biomechanics, 17*(9), 695-705.

4. Anderson, J. D. and Wendt, J. (1995). *Computational fluid dynamics*. New York.

5. ANSYS user's manual (2013). ANSYS Inc. Canonsburg, PA, USA.

6. Antiga, L., Piccinelli, M., Botti, L., Ene-Iordache, B., Remuzzi, A. and Steinman, D. A. (2008). *An image-based modeling framework for patient-specific computational hemodynamics. Medical & biological engineering & computing, 46(11), 1097-1112.*

7. Asakura, T. and Karino, T. (1990). Flow patterns and spatial distribution of atherosclerotic lesions in human coronary arteries. *Circulation research, 66*(4), 1045-1066.

8. Attinger, E. O., Anne, A. and McDonald, D. A. (1966). Use of Fourier series for the analysis of biological systems. *Biophysical journal*, *6*(3), 291-304.

9. Back, L. H. and Banerjee, R. K. (2000). Estimated flow resistance increase in a spiral human coronary artery segment. *Journal of Biomechanical. Engineering.*, *122*(6), 675-677.

10. Barnes, A. J., Locke, P., Scudder, P. R., Dormandy, T. L., Dormandy, J. A. and Slack, J. (1977). Is hyperviscosity a treatable component of diabetic microcirculatory disease? *The Lancet*, *310*(8042), 789-791.

11. Beratlis, N., Balaras, E., Parvinian, B. and Kiger, K. (2005). A numerical and experimental investigation of transitional pulsatile flow in a stenosed channel. *Journal of Biomechanical. Engineering.*, *127*(7), 1147-1157.

12. Berger, S. A. and Jou, L. D. (2000). Flows in stenotic vessels. *Annual review of fluid mechanics*, *32*(1), 347-382.

13. Berne, R. M. and Levy, M. N. (1967). *Cardiovascular Physiology*. 3rd Edition. Mosby, St. Louis, 1967.

14. Biswas, D. (2002). *Blood flow models: a comparative study*. Mittal Publications.

15. Bliss, M. R. (1998). Hyperaemia. *Journal of Tissue Viability*, *8*(4), 4-13.

16. Bluestein, D., C. Gutierrez, M. Londono and R. T. Schoephoerster (1999). Vortex shedding in steady flow through a model of an arterial stenosis and its relevance to mural platelet deposition. *Annals of Biomedical Engineering*, 27(6), 763-773.

17. Boutsianis, E., Dave, H., Frauenfelder, T., Poulikakos, D., Wildermuth, S., Turina, M., Ventikos, Y. and Zund, G. (2004). Computational simulation of intracoronary flow based on real coronary geometry. *European journal of Cardio-thoracic Surgery*, *26*(2), 248-256.

18. Caro, C. G., Fitz-Gerald, J. M. and Schroter, R. C. (1971). Atheroma and arterial wall shear-Observation, correlation and proposal of a shear dependent mass transfer mechanism for atherogenesis. *Proceedings of the Royal Society of London. Series B. Biological Sciences*, *177*(1046), 109-133.

19. Carreau, P. J. (1972). Rheological equations from molecular network theories. *Transactions of the Society of Rheology*, *16*(1), 99-127.

20. Carreras, E. T. and Mega, J. L. (2014). Dual antiplatelet therapy for heart disease. *Circulation*, *129*(21), e506-e508.

21. Cassanova, R. A. and Giddens, D. P. (1978). Disorder distal to modeled stenoses in steady and pulsatile flow. *Journal of biomechanics*, *11*(10-12), 441-453.

22. Celik, I. B., Ghia, U., Roache, P. J. and Freitas, C. J. (2008). Procedure for estimation and reporting of uncertainty due to discretization in CFD applications. *Journal of fluids Engineering-Transactions of the ASME*, *130*(7).

23. Chatzizisis, Y. S., Coskun, A. U., Jonas, M., Edelman, E. R., Feldman, C. L. and Stone, P. H. (2007). Role of endothelial shear stress in the natural history of coronary atherosclerosis and vascular remodeling: molecular, cellular, and vascular behavior. *Journal of the American College of Cardiology*, *49*(25), 2379-2393.

24. Chen, J., Lu, X. Y. and Wang, W. (2006). Non-Newtonian effects of blood flow on hemodynamics in distal vascular graft anastomoses. *Journal of Biomechanics*, *39*(11), 1983-1995.

25. Cheng, C., Helderman, F., Tempel, D., Segers, D., Hierck, B., Poelmann, R. and Krams, R. (2007). Large variations in absolute wall shear stress levels within one species and between species. *Atherosclerosis*, *195*(2), 225-235.

26. Cho, Y. I., Mooney, M. P. and Cho, D. J. (2008). Hemorheological disorders in diabetes mellitus. *Journal of diabetes science and technology*, *2*(6), 1130-1138.

27. Cowan, A. Q., Cho, D. J. and Rosenson, R. S. (2012). Importance of blood rheology in the pathophysiology of atherothrombosis. *Cardiovascular drugs and therapy*, *26*(4), 339-348.

28. De Bruyne, B., Pijls, N. H., Kalesan, B., Barbato, E., Tonino, P. A., Piroth, Z. and Fearon, W. F. (2012). Fractional flow reserve–guided PCI versus medical therapy in stable coronary disease. *New England Journal of Medicine*, *367*(11), 991-1001.DePaola, N., Gimbrone Jr, M. A., Davies, P. F., & Dewey Jr, C. F. (1992). Vascular endothelium responds to fluid shear stress gradients. *Arteriosclerosis and thrombosis: a journal of vascular biology*, *12*(11), 1254-1257.

29. Deplano, V. and Siouffi, M. (1999). Experimental and numerical study of pulsatile flows through stenosis Wall shear stress analysis. *Journal of Biomechanics, 32(10), 1081-1090.*

30. Deshpande, M. D. and Giddens, D. P. (1980). Turbulence measurements in a constricted tube. *Journal of Fluid Mechanics*, *97*(1), 65-89.

31. Fluent, (2012). ANSYS Fluent Theory Guide, ANSYS Inc., Canonsburg, PA, USA.

32. Fournier, R. L. (2017). *Basic transport phenomena in biomedical engineering*. CRC press.

33. Friedman, M. H., Deters, O. J., Bargeron, C. B., Hutchins, G. M. and Mark, F. F. (1986). Shear-dependent thickening of the human arterial intima. *Atherosclerosis, 60*(2), 161-171.

34. Fry, D. L. (1968). Acute vascular endothelial changes associated with increased blood velocity gradients. *Circulation research, 22*(2), 165-197.

35. Fry, D. L. (1969). Certain histological and chemical responses of the vascular interface to acutely induced mechanical stress in the aorta of the dog. *Circulation research,* 24(1), 93-108.

36. Ghalichi, F., Deng, X., De Champlain, A., Douville, Y., King, M. and Guidoin, R. (1998). Low Reynolds number turbulence modeling of blood flow in arterial stenoses. *Biorheology*, *35*(4-5), 281-294.

37. Giddens, D. P., Mabon, R. F. and Cassanova, R. A. (1976). Measurements of disordered flows distal to subtotal vascular stenoses in the thoracic aortas of dogs. *Circulation Research, 39*(1), 112-119.

38. Gijsen, F. J. H., Allanic, E., Van de Vosse, F. N. and Janssen, J. D. (1999b). The influence of the non-Newtonian properties of blood on the flow in large arteries: unsteady flow in a 90 curved tube. *Journal of Biomechanics, 32*(7), 705-713.

39. Gijsen, F. J., van de Vosse, F. N. and Janssen, J. D. (1999a). The influence of the non-Newtonian properties of blood on the flow in large arteries: steady flow in a carotid bifurcation model. *Journal of Biomechanics, 32*(6), 601-608.

40. Guleren, K. M. (2013). Numerical flow analysis of coronary arteries through concentric and eccentric stenosed geometries. *Journal of Biomechanics, 46*(6), 1043-1052.

41. Hamilos, M., Muller, O., Cuisset, T., Ntalianis, A., Chlouverakis, G., Sarno, G. and De Bruyne, B. (2009). Long-term clinical outcome after fractional flow reserve–guided treatment in patients with angiographically equivocal left main coronary artery stenosis. *Circulation*, *120*(15), 1505-1512.

42. He, X. and Ku, D. N. (1996). Pulsatile flow in the human left coronary artery bifurcation: average conditions. *Journal of Biomechanical Engineering*, *118*(1), 74-82.

43. Huang, C. R., Pan, W. D., Chen, H. Q. and Copley, A. L. (1987). Thixotropic properties of whole blood from healthy human subjects. *Biorheology*, *24*(6), 795-801.

44. Irace, C., Carallo, C., Scavelli, F., De Franceschi, M. S., Esposito, T. and Gnasso, A. (2014). Blood viscosity in subjects with normoglycemia and prediabetes *Diabetes care*, *37*(2), 488-492.

45. Jabir, E. and Lal, S. A. (2016). Numerical analysis of blood flow through an elliptic stenosis using large eddy simulation. *Proceedings of the Institution of Mechanical Engineers, Part H: Journal of Engineering in Medicine*, *230*(8), 709-726.

46. Jeong, S. K., Cho, Y. I., Duey, M. and Rosenson, R. S. (2010). Cardiovascular risks of anemia correction with erythrocyte stimulating agents: should blood viscosity be monitored for risk assessment? *Cardiovascular drugs and therapy*, *24*(2), 151-160.

47. Jeong, W. W. and Rhee, K. (2009). Effects of surface geometry and non-newtonian viscosity on the flow field in arterial stenoses. *Journal of mechanical science and technology*, *23*(9), 2424-2433.

48. Johnston, B. M., Johnston, P. R., Corney, S. and Kilpatrick, D. (2004). Non-Newtonian blood flow in human right coronary arteries: steady state simulations. *Journal of Biomechanics*, *37*(5), 709-720.

49. Johnston, B. M., Johnston, P. R., Corney, S. and Kilpatrick, D. (2006). Non-Newtonian blood flow in human right coronary arteries: transient simulations. *Journal of Biomechanics*, *39*(6), 1116-1128.

50. Kabinejadian, F. and Ghista, D. N. (2012). Compliant model of a coupled sequential coronary arterial bypass graft: effects of vessel wall elasticity and non-Newtonian rheology on blood flow regime and hemodynamic parameters distribution. *Medical Engineering & Physics*, *34*(7), 860-872.

51. Kern, M. J., Lerman, A., Bech, J. W., De Bruyne, B., Eeckhout, E., Fearon, W. F., Higano, S.T. and Spaan, J. A. (2006). Physiological assessment of coronary artery disease in the cardiac catheterization laboratory: a scientific statement from the American Heart Association Committee on Diagnostic and Interventional Cardiac Catheterization, Council on Clinical Cardiology. *Circulation*, *114*(12), 1321-1341.

52. Khalifa, A. M. A. and Giddens, D. P. (1978). Analysis of disorder in pulsatile flows with application to poststenotic blood velocity measurement in dogs. *Journal of Biomechanics*, *11*(3), 129-141.

53. Khalifa, A. M. A. and Giddens, D. P. (1981). Characterization and evolution of poststenotic flow disturbances. *Journal of Biomechanics*, *14*(5), 279-296.

54. Krolewski, A. S., Warram, J. H., Valsania, P., Martin, B. C., Laffel, L. M. and Christlieb, A. R. (1991). Evolving natural history of coronary artery disease in diabetes mellitus. *The American journal of medicine*, *90*(2), S56-S61.

55. Ku, D. N. (1997). Blood flow in arteries. *Annual review of fluid mechanics*, *29*(1), 399-434.

56. Ku, D. N., Giddens, D. P., Zarins, C. K. and Glagov, S. (1985). Pulsatile flow and atherosclerosis in the human carotid bifurcation. Positive correlation between plaque location and low oscillating shear stress. *Arteriosclerosis: An Official Journal of the American Heart Association, Inc.*, *5*(3), 293-302.

57. Larsson, S. C., Wallin, A., Håkansson, N., Stackelberg, O., Bäck, M. and Wolk, A. (2018). Type 1 and type 2 diabetes mellitus and incidence of seven cardiovascular diseases. *International journal of cardiology*, *262*, 66-70.

58. Le Devehat, C., Khodabandehlou, T. and Vimeux, M. (2001). Impaired hemorheological properties in diabetic patients with lower limb arterial ischaemia. *Clinical hemorheology and microcirculation*, *25*(2), 43-48.

59. Lieber, B. B. and Giddens, D. P. (1990). Post-stenotic core flow behavior in pulsatile flow and its effects on wall shear stress. *Journal of biomechanics*, *23*(6), 597-605.

60. Liu, B. and Tang, D. (2011). Influence of non-Newtonian properties of blood on the wall shear stress in human atherosclerotic right coronary arteries. *Molecular & cellular biomechanics: MCB*, *8*(1), 73.

61. Long, Q., Xu, X. Y., Ramnarine, K. V. and Hoskins, P. (2001). Numerical investigation of physiologically realistic pulsatile flow through arterial stenosis. Journal of Biomechanics, *34*(10), 1229-1242.

62. Lowe, G. D. O., Lee, A. J., Rumley, A., Price, J. F. and Fowkes, F. G. R. (1997). Blood viscosity and risk of cardiovascular events: the Edinburgh Artery Study. *British journal of haematology*, *96*(1), 168-173.

63. Lowe, G. D., Drummond, M. M., Lorimer, A. R., Hutton, I., Forbes, C. D., Prentice, C. R. and Barbenel, J. C. (1980). Relation between extent of coronary artery disease and blood viscosity. *Br Med J*, *280*(6215), 673-674.

64. Mahalingam, A., Gawandalkar, U. U., Kini, G., Buradi, A., Araki, T., Ikeda, N., Nicolaides, A., Laird, J.R., Saba, L. and Suri, J. S. (2016). Numerical analysis of the effect of turbulence transition on the hemodynamic parameters in human coronary arteries. *Cardiovascular Diagnosis And Therapy*, *6*(3), 208.

65. Malek, A. M., Alper, S. L. and Izumo, S. (1999). Hemodynamic shear stress and its role in atherosclerosis. *Jama*, *282*(21), 2035-2042.

66. Manuck, S. B., Kaplan, J. R. and Matthews, K. A. (1986). Behavioral antecedents of coronary heart disease and atherosclerosis. *Arteriosclerosis: An Official Journal of the American Heart Association, Inc.*, *6*(1), 2-14.

67. Mayer, G. A. (1964). Blood viscosity in healthy subjects and patients with coronary heart disease. *Canadian Medical Association Journal*, *91*(18), 951.

68. McDonald, D. A. (1974). *Blood flow in arteries*. 2nd edn. London: Edward Arnold.

69. Maton, A. (1997). *Human biology and health*. Prentice Hall. McGraw-Hill.

70. Morris, P. D., Ryan, D., Morton, A. C., Lycett, R., Lawford, P. V., Hose, D. R. and Gunn, J. P. (2013). Virtual fractional flow reserve from coronary angiography: modeling the significance of coronary lesions: results from the VIRTU-1 (VIRTUal Fractional Flow Reserve From Coronary Angiography) study. *JACC: Cardiovascular Interventions*, *6*(2), 149-157.

71. Muller, O., F. Mangiacapra, A. Ntalianis, K. M. Verhamme, C. Trana, M. Hamilos, J. Bartunek, M. Vanderheyden, E. Wyffels, G. R. Heyndrickx and F. J. van Rooij (2011). Long-term follow-up after fractional flow reserve-guided treatment strategy in patients with an isolated proximal left anterior descending coronary artery stenosis. JACC. *Cardiovascular interventions* 4(11), 1175–82.

72. Niyogi, P., Chakrabartty, S. K. and Laha, M. K. (2006). *Introduction to computational*. Pearson Education India. Bengaluru.

73. Nørgaard, B. L., J. Leipsic, S. Gaur, S. Seneviratne, B. S. Ko, H. Ito, J. M. Jensen, L. Mauri, B. De Bruyne, H. Bezerra, K. Osawa, M. Marwan, C. Naber, A. Erglis, Seung-Jung Park, E. H. Christiansen, A. Kaltoft, J. F. Lassen, H. E. Bøtker, S. Achenbach and NXT Trial Study Group (2014). Diagnostic performance of noninvasive fractional flow reserve derived from coronary computed tomography angiography in suspected coronary artery disease the NXT trial (analysis of coronary blood flow using CT angiography: next steps). *Journal of the American College of Cardiology* 63(12), 1145–55.

74. Nosovitsky, V. A., Ilegbusi, O. J., Jiang, J., Stone, P. H. and Feldman, C. L. (1997). Effects of curvature and stenosis-like narrowing on wall shear stress in a coronary artery model with phasic flow. *Computers and Biomedical Research*, *30*(1), 61-82.

75. Ntalianis, A., Sels, J. W., Davidavicius, G., Tanaka, N., Muller, O., Trana, C., Trana, C., Barbato, E., Hamilos, M., Mangiacapra, F., Heyndrickx, G.R., Wijns, M., Pijls, N.H.J., and De Bruyne, B. (2010). Fractional flow reserve for the assessment of nonculprit coronary artery stenoses in patients with acute myocardial infarction. *JACC: Cardiovascular Interventions*, *3*(12), 1274-1281.

76. Ojha, M., Cobbold, R. S., Johnston, K. W. and Hummel, R. L. (1989). Pulsatile flow through constricted tubes: an experimental investigation using photochromic tracer methods. *Journal of fluid mechanics*, *203*, 173-197.

77. Paszkowiak, J. J. and Dardik, A. (2003). Arterial wall shear stress: observations from the bench to the bedside. *Vascular and endovascular surgery*, *37*(1), 47-57.

78. Pedley, T. J., (1980). *The fluid mechanics of large blood vessels*. Cambridge University Press, Cambridge.

79. Phillips, T. N. and Roberts, G. W. (2011). Lattice Boltzmann models for non-Newtonian flows. *IMA journal of applied mathematics*, *76*(5), 790-816.

80. Pijls, N. H. and J. W. Sels (2012). Functional measurement of coronary stenosis. *Journal of the American College of Cardiology* 59, 1045–57.

81. Pyörälä, K., Laakso, M. and Uusitupa, M. (1987). Diabetes and atherosclerosis: an epidemiologic view. *Diabetes/metabolism reviews*, *3*(2), 463-524.

82. Reul, H., Schoenmackers, J., and Starke, W. (1972). Loss of pressure, energy and performance at simulated stenoses in pulsatile quasiphysiological flow. *Medical and biological engineering*, *10*(6), 711-718.

83. Richards, R. S. and Nwose, E. U. (2010). Blood viscosity at different stages of diabetes pathogenesis. *British journal of biomedical science*, *67*(2), 67-70.

84. Richardson, L. F. (1911). IX. The approximate arithmetical solution by finite differences of physical problems involving differential equations, with an application to the stresses in a masonry dam. *Philosophical Transactions of the Royal Society of London. Series A, Containing Papers of a Mathematical or Physical Character*, *210*(459-470), 307-357.

85. Richardson, L. F. and Gaunt, J. A. (1927). VIII. The deferred approach to the limit. *Philosophical Transactions of the Royal Society of London. Series A, containing papers of a mathematical or physical character*, *226*(636-646), 299-361.

86. Rosenblatt, G., Stokes, J. and Bassett, D. R. (1965). Whole blood viscosity, hematocrit, and serum lipid levels in normal subjects and patients with coronary heart disease. *The Journal of laboratory and clinical medicine*, *65*(2), 202-211.

87. Rosenson, R. S., Shott, S. and Tangney, C. C. (2002). Hypertriglyceridemia is associated with an elevated blood viscosity Rosenson: triglycerides and blood viscosity. *Atherosclerosis*, *161*(2), 433-439.

88. Ryval, J., Straatman, A. G. and Steinman, D. A. (2004). Two-equation turbulence modeling of pulsatile flow in a stenosed tube. *Journal of Biomechanical Engineering.*, *126*(5), 625-635.

89. Schlichting, H. (1968). *Boundary Layer Theory*. McGraw Hill Book Co. *New York*.

90. Siouffi, M., Deplano, V. and Pélissier, R. (1997). Experimental analysis of unsteady flows through a stenosis. *Journal of Biomechanics*, *31*(1), 11-19.

91. Sloop, G. D. and Garber, D. W. (1997). The effects of low-density lipoprotein and high-density lipoprotein on blood viscosity correlate with their association with risk of atherosclerosis in humans. *Clinical science*, *92*(5), 473-479.

92. Sloop, G., Holsworth Jr, R. E., Weidman, J. J. and St Cyr, J. A. (2015). The role of chronic hyperviscosity in vascular disease. *Therapeutic advances in cardiovascular disease*, *9*(1), 19-25.

93. Steiner, G. (1981). Diabetes and atherosclerosis: an overview. *Diabetes, 30(Supplement 2)*, 1-7.

94. Stone, P. H., Maehara, A., Coskun, A. U., Maynard, C. C., Zaromytidou, M., Siasos, G., Andreou, I., Fotiadis, D., Stefanou, K., Papafaklis, M., Michalis, L., Lansky, A.J., Mintz, G.S., Serruys, P.W., Feldman, C.L and Stone, G. W. (2018). Role of low endothelial shear stress and plaque characteristics in the prediction of nonculprit major adverse cardiac events: the PROSPECT study. *JACC: Cardiovascular Imaging*, *11*(3), 462-471.

95. Su, B., Huo, Y., Kassab, G. S., Kabinejadian, F., Kim, S., Leo, H. L. and Zhong, L. (2014). Numerical investigation of blood flow in three-dimensional porcine left

anterior descending artery with various stenoses. *Computers in biology and medicine*, *47*, 130-138.

96. Takiwaki, M., Tomoda, F., Koike, T., Taki, T., Inoue, H., Kigawa, M., Kitajima, I. and Uji, Y. (2014). Increased levels of small dense low-density lipoprotein cholesterol associated with hemorheological abnormalities in untreated, early-stage essential hypertensives. *Hypertension Research*, *37*(11), 1008-1013.

97. Tamariz, L. J., Young, J. H., Pankow, J. S., Yeh, H. C., Schmidt, M. I., Astor, B. and Brancati, F. L. (2008). Blood viscosity and hematocrit as risk factors for type 2 diabetes mellitus: the atherosclerosis risk in communities (ARIC) study. *American journal of epidemiology*, *168*(10), 1153-1160.

98. Tan, F. P. P., Soloperto, G., Bashford, S., Wood, N. B., Thom, S., Hughes, A. and Xu, X. Y. (2008). Analysis of flow disturbance in a stenosed carotid artery bifurcation using two-equation transitional and turbulence models. *Journal of biomechanical engineering*, *130*(6).

99. Tan, F. P. P., Wood, N. B., Tabor, G. and Xu, X. Y. (2011). Comparison of LES of steady transitional flow in an idealized stenosed axisymmetric artery model with a RANS transitional model. *Journal of biomechanical engineering*, *133*(5).

100. Thuesen, A. L., Riber, L. P., Veien, K. T., Christiansen, E. H., Jensen, S. E., Modrau, I., Andreasen, J.J., Junker, A., Mortensen, P.E. and Jensen, L. O. (2018). Fractional flow reserve versus angiographically-guided coronary artery bypass grafting. *Journal of the American College of Cardiology*, *72*(22), 2732-2743.

101. Tu, C., Deville, M., Dheur, L. and Vanderschuren, L. (1992). Finite element simulation of pulsatile flow through arterial stenosis. *Journal of Biomechanics*, *25*(10), 1141-1152.

102. van de Hoef, T. P., van Lavieren, M. A., Damman, P., Delewi, R., Piek, M. A., Chamuleau, S. A., Voskuil, M., Henriques, J.P.S, Koch, K.T., De Winter, R.J., Spaan, J.A.E, Siebes, M., Tijseen, J.D.P., Meuwissen, M. and Piek, J. J. (2014). Physiological basis and long-term clinical outcome of discordance between

fractional flow reserve and coronary flow velocity reserve in coronary stenoses of intermediate severity. *Circulation: Cardiovascular Interventions*, *7*(3), 301-311.

103. Varghese, S. S. and Frankel, S. H. (2003). Numerical modeling of pulsatile turbulent flow in stenotic vessels. *Journal of biomechanical engineering*, *125*(4), 445-460.

104. Varghese, S. S., Frankel, S. H. and Fischer, P. F. (2007a). Direct numerical simulation of stenotic flows. Part 1. Steady flow. *Journal of Fluid Mechanics*, *582*(1), 253-280.

105. Varghese, S. S., Frankel, S. H. and Fischer, P. F. (2007b). Direct numerical simulation of stenotic flows. Part 2. Pulsatile flow. *Journal of Fluid Mechanics*, *582*(1), 281-318.

106. Varghese, S. S., Frankel, S. H. and Fischer, P. F. (2008). Modeling transition to turbulence in eccentric stenotic flows. *Journal of biomechanical engineering*, *130*(1).

107. Weinstock, P. H., Bisgaier, C. L., Aalto-Setälä, K., Radner, H., Ramakrishnan, R., Levak-Frank, S. and Breslow, J. L. (1995). Severe hypertriglyceridemia, reduced high density lipoprotein, and neonatal death in lipoprotein lipase knockout mice. Mild hypertriglyceridemia with impaired very low density lipoprotein clearance in heterozygotes. *The Journal of clinical investigation*, *96*(6), 2555-2568.

108. World Health Organization, (2020) newsletter 9th December 2020 https://www.who.int/news-room/fact-sheets/detail/the-top-10-causes-of-death.

109. Wiwatanapataphee, B., Wu, Y. H., Siriapisith, T. and Nuntadilok, B. (2012). Effect of branchings on blood flow in the system of human coronary arteries. *Mathematical Biosciences and Engineering*, *9*(1), 199-214.

110. Womersley, J. R. (1955). Method for the calculation of velocity, rate of flow and viscous drag in arteries when the pressure gradient is known. *The Journal of physiology*, *127*(3), 553-563.

111. Wootton, D. M. and Ku, D. N. (1999). Fluid mechanics of vascular systems, diseases, and thrombosis. *Annual review of biomedical engineering*, *1*(1), 299-329.

112. Wu, J., Liu, G., Huang, W., Ghista, D. N. and Wong, K. K. (2015). Transient blood flow in elastic coronary arteries with varying degrees of stenosis and dilatations: CFD modelling and parametric study. *Computer Methods in Biomechanics and Biomedical Engineering*, *18*(16), 1835-1845.

113. Young, D. F. and Tsai, F. Y. (1973a). Flow characteristics in models of arterial stenoses I. Steady flow. *Journal of biomechanics*, *6*(4), 395-410.

114. Young, D. F. and Tsai, F. Y. (1973b). Flow characteristics in models of arterial stenoses II. Unsteady flow. *Journal of biomechanics*, *6*(5), 547-559.

115. Zarins, C. K., Giddens, D. P., Bharadvaj, B. K., Sottiurai, V. S., Mabon, R. F. and Glagov, S. (1983). Carotid bifurcation atherosclerosis. Quantitative correlation of plaque localization with flow velocity profiles and wall shear stress. *Circulation research*, *53*(4), 502-514.

116. Zeiher, A. M., Drexler, H., Saurbier, B. and Just, H. (1993). Endothelium-mediated coronary blood flow modulation in humans. Effects of age, atherosclerosis, hypercholesterolemia, and hypertension. *The Journal of clinical investigation*, *92*(2), 652-662.

LIST OF PUBLICATIONS

Papers Published/Communicated in peer reviewed International Journals

1. Blessy Thomas, Sumam K. S., and Sajikumar N. (2021). Patient Specific Modelling of Blood Flow in Coronary Artery. *Journal of Applied Fluid Mechanics*, 14(5), 1469-1482.

Publications in International and National Conferences

1. Blessy Thomas and Sumam K. S. (2016). Blood flow in human arterial system-A review. *Procedia Technology*, *24*, 339-346.

2. Blessy Thomas, Sumam K.S. and N. Sajikumar (2017) *Simulation of blood flow-an alternate approach*, 29th Kerala Science Congress 2017.